الجمهورية الجزائرية الديمقراطية الشعبية
People's Democratic Republic of Algeria
وزارة التعليم العالي والبحث العلمي
Ministry of Higher Education and Scientific Research

University of Larbi Ben M'hidi Oum-El-Bouaghi
Faculty of Sciences and Applied Sciences
Mechanical Engineering Department

Specialty: Mechanical Construction

A dissertation Submitted to the Faculty of Sciences and Applied Sciences, Department of Mechanical Engineering, in Partial Fulfillment of the 3rd Cycle Doctorate Diploma

By: Atif LAICHE

Title

Contribution to Structural Dynamic Modeling of Multiphysics Bodies:

Prediction of Loads in the Preliminary Design Phase of Flying Vehicles

Publicly defended, on ……., in front of the jury composed of:

BERKANI Oualid	MCA	Larbi Ben M'hidi Univ.	President
BOULAHIA Allaoua	MCA	Larbi Ben M'hidi Univ.	Supervisor
MECIBAH Med Salah	Professor	Frère Mentouri Constantine 1 Univ.	Examiner
AMOURI Ammar	MCA	Frère Mentouri Constantine 1 Univ.	Examiner
BOUZID Sihem	MCA	Larbi Ben M'hidi Univ.	Examiner

Acknowledgements

As an expression of gratitude, I'd like to thank Allah, the All-Powerful, for providing me with the power to endure, as well as the bravery and perseverance to get through all obstacles.

The work presented in this thesis was carried out at Larbi Ben M'hidi University, Pole of Sciences and Applied Sciences, Mechanical Engineering Department, **CMASMTF** Laboratory, Ain Beida, Oum El Bouaghi.

I express my deepest gratitude to my supervisor, Mr. **BOULAHIA ALLAOUA**, professor at Larbi Ben M'hidi University, for his crucial criticism, leading guidance, and supervision. It is my honor to study with him and grab a chance to be his Ph.D. student.

I wish to extend my special thanks to Mr. **BERKANI OUALID**, professor at Larbi Ben M'hidi University, and Oum El Bouaghi, for its acceptance to be the jury chair for this thesis.

Many thanks also go to Mr. **MECIBAH Med**. SALAH, Mr. **AMOURI AMMAR**, professors at the university of Brothers Mentouri, Constantine 1, and Mme. **BOUZID SIHEM**, professor at Larbi Ben M'hidi University, Oum El Bouaghi, who kindly agreed to be examiners for this thesis.

I also want to thank everyone in my lab who helped me finish the project, especially Mr. **DJEFFAL SELMAN**, Mr. **AISSAOUI ABDERAHMAN**, Mr. **BENDADA LARBI**, and Mr. **MEHALAINE ABD EL FATTEH.**

Dedication

I wish to extend my special thanks to my parents, Mr. **LAICHE LAKHDAR** and Mme. **KHENFER DJAMILA** for their prayers, love, and support throughout my life. Thank you both for giving me strength to reach my dream.

I would like to thank all my family members who have supported me from the beginning of this thesis to the end.

I'm also thankful to all of the **professors** and **staff** in the **Mechanical** Department and **Postgraduate**, who helped me get this research done.

It is impossible to forget thanking Mr. **MERZKANE FARID**, my great teacher of mechanical engineering at Ababsa Abd El'hamid High School, for his golden advices.

Abstract

In space vehicle structure design, the purpose on reducing weight is to minimize the gap of frequency concept between flight mechanics motion and structural vibration. Therefore, aircrafts are becoming more and more flexible. This necessitates the use of a flight mechanics model using aeroelasticity theory. The development try of this model is the main subject of this research. The aim of this last is eventually to be employed in disturbances and manoeuvre load prediction in the beginning conception phase. This in order to avoid unstable flight conditions, moreover, the flight mechanics model may be also used to design active load alleviation systems to decrease loads on the wing structure.

Various approaches and contributions were involved in the model of aeroelastic flight mechanics of which one can cite Modal approach in a linear time-invariant state-space system for Aeroelasticity, Summation of Forces (with multibody system dynamics) for Load Prediction in aerodynamics and Conventional Serial Staggered Partitioned approach for Fluid-Structure interaction. The totality of the multibody system dynamics model is designed on the basis of user input, so, it may be incorporated into a framework for design optimization. This gives us the ability to do various supplemental analyses.

Finally, several conclusions are reached. The response of static and dynamic behavior is checked, so it's likely that it can be applied to other classical, low aspect-ratio aircraft operating in the subsonic flying range.

Key words: Aeroelasticity, Dynamic modeling, Mode-superposition, Vibration, Quasi-steady models, Lumped-parameter method, Finite element method, Multibody system dynamics, Simscape Multibody.

Résumé

Dans la conception de structures de véhicules spatiaux, le but de la réduction du poids est de minimiser l'écart de concept de fréquence entre le mouvement de la mécanique de vol et la vibration structurelle. Par conséquent, les avions deviennent de plus en plus flexibles. Cela nécessite l'utilisation d'un modèle de mécanique de vol qui inclut l'aéroélasticité. Le développement d'un tel modèle est l'objet de cette recherche. Le but final est de l'utiliser pour la prédiction des charges de perturbations et de manœuvres au début de la phase de conception. Cela permettrait d'éviter des conditions de vol instables. De plus, le modèle de mécanique de vol peut également être utilisé pour concevoir des systèmes d'atténuation de charge actifs afin de réduire les charges sur la structure de l'aile.

Différentes approches et contributions ont été utilisées dans le modèle de mécanique de vol aéroélastique, notamment l'approche modale dans un système d'état-espace linéaire invariant dans le temps pour l'aéroélasticité, la sommation des forces (avec la dynamique du système à corps multiples) pour la prédiction de charge en aérodynamique et l'approche conventionnelle de partitionnement en série échelonnée pour l'interaction fluide-structure. La totalité du modèle de dynamique des systèmes à corps multiples est conçue sur la base de l'entrée de l'utilisateur, de sorte qu'elle peut être incluse dans un cadre d'optimisation de la conception. Cela nous donne la capacité de réaliser diverses analyses supplémentaires.

Enfin, plusieurs conclusions sont tirées. La réponse du comportement statique et dynamique est vérifiée, il est donc probable que cela puisse être appliqué à d'autres avions classiques à faible aspect ratio opérant dans la plage de vol subsonique.

Mots-clés : Aéroélasticité, Modélisation dynamique, Mode-superposition, Vibration, Modèles quasi-stationnaires, Méthode des paramètres concentrés, Méthode des éléments finis, Dynamique des systèmes à corps multiples, Simscape Multibody.

الملخص

يهدف التقليل من الوزن في تصميم هيكل مركبة الفضاء إلى تقليل الفجوة في مفهوم التردد بين حركة ميكانيكا الطيران والاهتزاز الهيكلي. لذلك، تصبح الطائرات أكثر مرونة. هذا يتطلب استدعاء نموذج لميكانيكا الطيران يتضمن الأيروإيلاستيكية. تطوير مثل هذا النموذج هو موضوع هذه الدراسة. الهدف النهائي هو استخدامه في توقع الأحمال و الاضطرابات الهوائية في مرحلة التصميم الأولى من أجل تجنب ظروف الطيران غير المستقرة. علاوة على ذلك، يمكن استخدام نموذج ميكانيكا الطيران أيضًا في تصميم أنظمة تخفيف الأحمال النشطة لتقليل الأحمال على هيكل الجناح.

شملت النماذج المختلفة والمساهمات في نموذج ميكانيكا الطيران الأيروإيلاستيكية، منها النهج النمطي في نظام الحالة الخطي الثابت الزمن للأيروإيلاستيكية، وجمع القوى (مع ديناميكا نظام الجسم المتعدد) لتوقع الحمل في الديناميكا الهوائية، والنهج التسلسلي المتدرج التقليدي للتفريق بين السوائل والهيكل. يتم تصميم نموذج ديناميكا نظام الجسم المتعدد على أساس إدخال المستخدم، لذلك يمكن إدراجه في إطار تحسين التصميم، مما يمنحنا القدرة على إجراء تحليلات إضافية متنوعة.

وأخيرًا، تم التوصل إلى عدة استنتاجات. تم التحقق من استجابة السلوك الثابت والديناميكي، لذلك من المحتمل أن يمكن تطبيقه على طائرات أخرى ذات نسبة جانبية منخفضة تعمل في نطاق الطيران دون الصوتي.

الكلمات المفتاحية: الأيروإيلاستيكية، التحليل الديناميكي، تجميع الأوضاع، الاهتزاز، نماذج نصف ثابتة، طريقة المعلمة المركزية، طريقة العنصر النهائي، ديناميكا الأنظمة المتعددة الجسم، سيمسكيب مولتيبودي.

Table of Contents

Acknowledgements ..... **i**

Dedication ..... **ii**

Abstract ..... **iii**

Table of Contents ..... **vi**

List of Figures ..... **ix**

List of Tables ..... **xii**

Glossary ..... **xiii**

List of Abbreviation xiii

List of Symbols xiv

Chapter 1: Introduction **1**

1.1 Background 1

1.1.1 Overview for Aeroelasticity 4

1.1.2 Overview for The Novelty of Flight Mechanics 6

1.2 Thesis Objectives, Scope, and Structure 7

1.2.1 Thesis Objective 7

1.2.2 Thesis Scope 8

1.2.3 Thesis Structure 9

Chapter 2: Aeroelastic Wing Theory **12**

2.1 Structures 12

2.1.1 Mode-Superposition Approach MSUP 12

2.1.2 Overview of LPM 18

2.1.3 Determination of Load Prediction 19

2.2 Aerodynamics 20

2.2.1 Choice of Linear on Nonlinear Study 20

2.2.2 Choice of Stable, Quasi-Stable or Unstable Aerodynamic Models 21
2.2.3 Study of Quasi-Stable Model 22
2.3 Fluid-Structure Interaction FSI 24
2.3.1 Choice of Partitioned or Monolithic Approaches 24
2.3.2 Partitioned Procedures 25
2.3.3 Benefits of Using Structures and Aerodynamics Combination 27
2.4 Lifting Surfaces 29
2.5 Summary 31

Chapter 3: Static and Dynamic Analysis of Flexible Wing Using LPM and FE 34
3.1 Overview of Modeling Methods 34
3.2 Modeling wing using Lumped-parameter Method 35
3.2.1 Description of the Simulink model 36
3.2.2 Simulated deflections according LPM 39
3.3 Modeling of a flexible rectangular wing using finite element import approach ... 43
3.3.1 Modeling methodology: 44
3.3.2 Subsystem explication 45
3.3.3 Simulated deflections according FE import Method 46
3.4 Ansys Simulations using Modal Analysis 50
3.5 General conclusions 54
3.6 Summary 55

Chapter 4: Modeling Aerodynamic Loads Using MATLAB Code and FEA 57
4.1 Aerodynamic Lift 57
4.2 Load due to the weight of the wing structure 58
4.3 Load Due to Fuel Stored in Wing 59
4.4 Overall Load 60
4.5 Aircraft Parameters 60
4.6 Verification of the Modeled Loads 61
4.7 Finite Element Analysis 62

4.8 Results and Discussion 63

4.9 Summary 64

Chapter 5: Aeroelastic Wing Methodology and Verification 66

5.1 General Concept 66

5.2 Explanation of the Simscape Multibody Model 67

5.2.1 General Environment 67

5.2.2 Aeroelastic Nodes 69

5.2.3 Special Nodes 73

5.2.4 Rigid Wing Basis 73

5.2.5 State-space Group 74

5.3 Ansys and Simscape Multibody Simulations 75

5.3.1 Aerodynamic Input 77

5.3.2 Qualitative evaluation 78

5.3.3 Dynamic Evaluation 83

5.4 Summary 87

Chapter 6: Conclusions and Recommendations 89

6.1 General conclusions 89

6.2 Recommendations 90

Annex A: Aerodynamic Coefficients of The Wing Model 92

Annex B: Structural Data Tables 94

Bibliography 98

Abstract…….. 104

List of Figures

Figure 1.1: Collar triangle of aeroelasticity [31]. 5

Figure 1.2: Friedmann hexahedron of aeroelasticity [32]. 6

Figure 1.3: Flowchart model of engineering design and analysis [44]. 9

Figure 2.1: First four mode shapes of wing simulated by finite element software [4]. 13

Figure 2.2: Lumped-beam representation [42]. 18

Figure 2.3: Prediction of the flutter speed index for various Mach numbers [57]. 21

Figure 2.4: Wake vortices decreases by the oscillating profile's effect [62]. 22

Figure 2.5: Moving wing parts freely to each other. 23

Figure 2.6: Scheme of conventional staggered procedures [65]. 26

Figure 2.7: Scheme of predictor-corrector serial staggered procedure. 26

Figure 2.8: Structural deformation modes connected with a lifting surface hinge spring [69]. 30

Figure 3.1: A flexible cantilever beam model according to the lumped-parameter method [73]. ... 35

Figure 3.2: top: Generic structure of the wing, down: Simscape Multibody model 36

Figure 3.3**:** Chain of four elements. 36

Figure 3.4**:** Simscape Multibody model of the complete system according to **LPM** [72]. 37

Figure 3.5: Simscape Multibody wing model according to the **LPM**. 37

Figure 3.6: Static vertical deflection [72]. 40

Figure 3.7**:** Vertical deflection of wing tip due to distributed gravitational loads [72]. 40

Figure 3.8: Vertical deflection of wing tip due to only an upward point force [72]. 41

Figure 3.9: Effect of increasing the number of flexible elements in **LPM** [72]. 42

Figure 3.10: First four mode shapes [72]. 43

Figure 3.11: Three interface frames and five interface frames, respectively, show how a beam is built in general [73]. 44

Figure 3.12: Flexible wing modeling workflow. 45

Figure 3.13: Simscape Multibody model of the complete system for 3 interface frames according FE import method. 46

Figure 3.14: Bushing joint subsystem. 46

Figure 3.15: Tip deflection due to a distributed gravitational load. 47

Figure 3.16: Tip deflection due to an upward point load. 47

Figure 3.17: Effect of increasing dynamic modes (3 interface frames). 48

Figure 3.18: Effect of increasing dynamic modes (5 interface frames). 48

Figure 3.19: Compare vertical deflection of wing with 3 interface frames, 5 interface frames. 49

Figure 3.20: Compare vertical deflection of wing using LPM and FE import method. 50

Figure 3.21**:** Upward and downward deflections of wing tip. 51

Figure 3.22: Comparison of mode shapes. 52

Figure 3.23: First four mode shapes obtained from finite element software. 53

Figure 4.1: Lift on the wing [27]. 57

Figure 4.2: Load due to wing structure weight [27]. 59

Figure 4.3: Load due to the weight of the fuel stored in the wing [27]. 60

Figure 4.4: Different profile of wing loads. 61

Figure 4.5: Finite element mesh of wing with tetrahedral elements. 62

Figure 4.6**:** Fixed wing from Face 2. 62

Figure 4.7: Analytical pressure load [22]. 63

Figure 4.8: Left: Displacement of the wing along Y axis; Right: Von mises stress and displacement [22]. 63

Figure 5.1: Flexible moving wing section overlaid on a rigid wing. 66

Figure 5.2: Representation of the Simscape Multibody wing model. 68

Figure 5.3: Simscape Multibody model of one aeroelastic node which contains one massless wing divided on two sections. 69

Figure 5.4: Representation of different reference frames and twist angles obtained from literature. 71

Figure 5.5: A 3D CAD model of the considered wing with aileron and flap. 74

Figure 5.6: Modes shapes: 1, 3, 7 and 9 obtained from FE software. 76

Figure 5.7**:** Response of Tip deflection for a forward-moving wing subjected to a "1-cos" vertical gust. 80

Figure 5.8: Response of Tip deflection for a forward-moving wing after a 10° downward flap deflection..... 81

Figure 5.9: Response of Tip deflection for a forward-moving wing after a 10° downward aileron deflection. 83

Figure 5.10: Modal damping $\zeta = 0.02$ for the 1st mode with structural loads. 85

Figure 5.11: Modal damping for the 1st mode $\zeta = 0.067$ with structural load and aerodynamic forces. 85

Figure 5.12: Amplitudes curves of modes 1-4 caused by period excitation using gusts..... 86

Figure A.1: Aerodynamic coefficients for the considered airfoil..... 92

Figure A.2: Aerodynamic forces coefficients of control surface: Flap element. 93

Figure A.3: Aerodynamic forces coefficients of control surface: Aileron element. 93

Figure B.1: Airfoil NACA0009 coordinates. 94

List of Tables

Table 2.1: The methods chosen for the multiple studies and the related hypotheses. 32

Table 3.1: Wing dimensions, moment of inertia and material properties [72]. 38

Table 3.2: Comparison study of the obtained deflection from analytic, Matlab and Ansys. 50

Table 3.3: Comparison study of mode shapes obtained from analytical theory, lumped parameter method and finite element analysis. 51

Table 4.1: Standard aircraft technical specifications. 61

Table 4.2: Materials properties. 62

Table 5.1: Modal damping ratios of the first ten modes. 84

Table B.1: Deformation of massless sections for mode shapes 1,2 and 3. 95

Table B.2: Deformation of massless sections for mode shapes 4, 5 and 6. 95

Table B.3: Dimensional characteristics of the considered wing. 95

Table B.4: Physical properties that describe the wing resistance to rotational motion. 96

Table B.5: Location of control surfaces : Flap and Aileron. 96

Glossary

List of Abbreviation

AFM	Aeroelastic Flight Mechanics
AoA	Angle of Attack
AWM	Aeroelastic Wing Model
CFD	Computational Fluid Dynamics
FEA	Finite Element Analysis
FSI	Fluid-Structure Interaction
GBE	Generalized Beam Elements
LE	Leading Edge
LPM	Lumped-Parameter Method
MSD	Multibody System Dynamics
MSUP	Mode-Superposition Method
TE	Trailing Edge
SOF	Summation of Forces
a.c.	aerodynamic center
a.p.	application point
c.g.	center of gravity
e.a.	elastic axis
mlb	massless body
2D	Two-dimensional
3D	Three-dimensional

List of Symbols

A	State matrix	N/A
B	Input matrix	N/A
$\boldsymbol{C}$	Damping matrix	$[Nm^{-1}s, Nm\ s]$
C_{aero}	Aerodynamic damping matrix	$[N\ s, Nm^{-1}s, Nm\ s]$
C	Output matrix	N/A
C_L	Lift coefficient	$[-]$
C_D	Drag coefficient	$[-]$
C_M	Pitching moment coefficient	$[-]$
C_{l0}	Lift coefficient at zero angle of attack	$[-]$
$C_{l\alpha}$	Lift curve gradient	$[-]$
$C_{V\ddot{\alpha}}$	Effect of angular acceleration on vertical force	$[Ns^2]$
$C_{V\dot{\alpha}}$	Effect of angular velocity on vertical force	$[Ns]$
$C_{V\alpha}$	Effect of angle of attack on vertical force	$[N\ ]$
$C_{V\ddot{h}}$	Effect of plunge acceleration on vertical force	$[Nm^{-1}s^2]$
$C_{V\dot{h}}$	Effect of plunge speed on vertical force	$[Nm^{-1}s]$
$C_{H\ddot{\alpha}}$	Effect of angular acceleration on horizontal force	$[Ns^2]$
$C_{H\dot{\alpha}}$	Effect of angular velocity on horizontal force	$[Ns]$
$C_{H\alpha}$	Effect of angle of attack on horizontal force	$[N]$
$C_{H\ddot{h}}$	Effect of plunge acceleration on horizontal force	$[Nm^{-1}s^2]$
$C_{H\dot{h}}$	Effect of plunge speed on horizontal force	$[Nm^{-1}s]$
$C_{M\ddot{\alpha}}$	Effect of angular acceleration on moment	$[Nm\ s^2]$
$C_{M\dot{\alpha}}$	Effect of angular velocity on moment	$[Nm\ s]$
$C_{M\alpha}$	Effect of angle of attack on moment	$[N\ m]$
$C_{M\ddot{h}}$	Effect of plunge acceleration on moment	$[Ns^2]$
$C_{M\dot{h}}$	Effect of plunge speed on moment	$[Ns]$
$C_{LV}(V)$	Effect of speed on lift	$[N]$
$\mathbf{C}(k)$	Theodorsen's function	$[-]$
C_O	Chord length at wing root	$[m]$
C_T	Chord length at wing tip	$[m]$
C_{OF}	Width of fuel tank at wing root	$[m]$
C_{TF}	Width of fuel tank at L_F	$[m]$
D	Feedthrough matrix	N/A
D_i	Drag force	$[N]$
$\mathbf{F}$	External force vector	$[N]$

$\boldsymbol{F_C}$	Idealized control force	$[N]$
$\boldsymbol{F_C^*}$	Idealized control coefficient	$[m^2]$
H	Forward force	$[N]$
$\boldsymbol{K}$	Stiffness matrix	$[Nm^{-1}s, Nm\ s]$
K_{aero}	Aerodynamic stiffness matrix	$[N, Nm]$
L	Wing's length	$[m]$
L_i	Lift force	$[N]$
L_g	Gust length	$[s]$
L_F	Fuel tank's length	$[m]$
$\boldsymbol{M}$	Mass Matrix	$[kg, kg\ m^2]$
M_{aero}	Aerodynamic mass matrix	$[Ns^2, N\ m^{-1}s^2, Nm\ s^2]$
M_i	Pitch-up moment	$[N\ m]$
$S_{\ i}$	Section surface area	$[\ m^2]$
V	Downward force	$[N]$
W_{total}	Aircraft's weight	$[N]$
W_{Wing}	Weight of the wing	$[N]$
W_{Fuel}	Fuel's weight	$[N]$
a	Distance between mid-chord and elastic axis in semi-chords	$[m]$
b	Semi-chord	$[m]$
c_i	Section mid-chord	$[m]$
g	Sweep deflection	$[m]$
h	Downward (plunge) deflection	$[m]$
ka	Lift profile coefficient	$[-]$
kw	Structural load coefficient	$[-]$
n	Load factor (Flight conditions)	$[-]$
$\boldsymbol{q}$	Vector of generalized coordinates	$[-]$
q	Dynamic pressure	$[kgm^{-1}s^{-2}]$
q	Uniformly distributed load	$[N/m]$
q_L	Lift profile	$[N/m]$
q_{wing}	Structural load	$[N/m]$
q_f	Fuel load	$[N/m]$
s	Vector of response coordinates	$[m, rad]$
u	Input vector	N/A
x	State vector	N/A
x	Arbitrary position along wing	$[m]$
y	Output vector	N/A
Φ	Matrix holding relevant mode shapes	$[m, rad]$

ξ	Pitch-up deflection	$[-]$
ϕ	Mode shape op eigenvector	$[m, rad]$
ω	Natural frequency	$[rad\ s^{-1}]$
δ_{ij}	Kronecker delta	$[-]$
I	Identity matrix	$[-]$
Γ	Modal damping matrix	$[rad\ s^{-1}]$
Λ	Spectral matrix	$[rad^2\ s^{-1}]$
ρ	Air density	$[kg\ m^{-3}]$
u	Airflow speed	$[m/s]$
α	Angle of attack	$[rad]$
α_{eff}	Effective angle of attack	$[rad]$
$\alpha_{fw,eff}$	Effective flexible wing angle of attack	$[rad]$
α_{rw}	Rigid wing angle of attack	$[rad]$
φ_g	Instantaneous gust vertical velocity	$[m\ s^{-1}]$
$\bar{\varphi}_g$	Maximum gust vertical velocity	$[m\ s^{-1}]$
ξ	Aeroelastic twist deflection	$[rad]$
ζ	Modal damping ratio	$[-]$
$c_{\dot{\xi}}$	Pitch velocity effect on effective angle of attack	$[rad]$
u_{rw}	Forward velocity in rigid-wing reference frame	$[m\ s^{-1}]$
w_{rw}	Downward velocity in rigid-wing reference frame	$[m\ s^{-1}]$
δ	Aileron deflection angle	$[rad]$
δ_a	Aileron deflection angle	$[rad]$
δ_f	Flap deflection angle	$[rad]$
η	Dimensionless semispan	$[-]$

Chapter 1:
Introduction

1.1 Background

Aeroelasticity and flight mechanics are frequently treated as separate fields, and simulations are analyzed using different models. This is a reasonable assumption to make when there is little connection between the two or when the frequencies of structural vibration are much higher than those related to flight mechanics. However, the current emphasis on reducing aircraft weight results in ever-more flexible conceptions [1]. As a result, the structure oscillates at a smaller frequency [2], which reduces the frequency gap between structural vibrations and motion caused by flight mechanics [3].

Due to this, a flight mechanics model that incorporates aeroelastic deformation is necessary for proper load anticipate (prediction). Structural stability can be guaranteed and unsteady flight circumstances can be prevented with accurate load prediction. Additionally, for the design of efficient control systems, a deeper comprehension of the linked aeroelastic and flight mechanics study is essential. Active load relief using these devices can result in improved customer satisfaction, lessened fatigue, and minimize loads on the wing structure [4]. As a result, the emphasis of aeroelastic research switches from the mitigation of negative consequences to the utilization of positive ones. An interesting detail is that the Wright brothers studied aeroelasticity for their wing-warp roll control system, which is where aeroelasticity research got its start [5]. In order to accomplish high-performance mission objectives, modern aircraft are being built with an increased emphasis on their great maneuverability. Modern aircraft have light-weight, flexible wings with a high aspect ratio as a means of achieving this goal. Design ideas for aircraft have been researched that make use of the wings' flexibility to improve maneuverability [6].

Flexibility is an important aspect to consider when designing mechanical structures that will be subjected to significant loads. Simscape Multibody and Simulink are commonly used tools in the modeling of flexible dynamics, with many researchers adopting these approaches to better understand a wide range of structures. For example, Victor et al. used both lumped parameters and finite element methods to model and predict beam deflection in a linear regime, ultimately finding that while the lumped parameter approach is user-friendly for flexible bodies, it has certain drawbacks when it comes to modeling high-dimensional structures [7]. Subedi et al. experimentally modeled a flexible beam using a camera to identify lumped parameters, and found that an increasing number of elements reduces deflection ratio [8]. Another study developed a model based on the port Hamiltonian formulation and applied it to a robotic system [9].

The lumped parameter method (LPM) has proven useful in modeling high-speed robots and machine tools in the field of robotics [10]. In one study, a new method was proposed to minimize the impact of vibration on rigid structures by subdividing them into separate elements [11]. Single-link flexible manipulators were modeled using a flexible fishing rod model and LPM-based Simscape Multibody [12].

A survey of literature related to dynamic analyses of flexible robotic manipulators was conducted in a study [13]. In another study, global shape functions for flexible multibody systems were obtained using isogeometric finite element models that aimed to discretize the geometry [14]. Held et al. developed a flexible multibody systems software, Dynmanto, in the Matlab toolbox, which incorporates flexible bodies in multibody simulations and allows for obtaining global shape functions [15]. The lumped parameter method was shown to be an effective method for predicting the contact force of elastic colliding bodies in studies [16] and [17]. The method's advantages lie in its simplification of mathematical formulation, computational efficiency, and better understanding of the coupling effect of excited modes on the occurrence of multiple impacts. In one study [18], an improved approximation was presented for calculating wing tip deflection that is well-suited for preliminary wing designs. Another study [19] aimed to practically explore different methods for constructing and representing dynamic mechanical models and develop a strong understanding of modal analysis, which involves constructing a system's total response by combining individual modes of vibration. The lumped parameter method has proven efficient in a wide range of

domains, including acoustics and mechanics [20]. In a separate study, Svoboda and Hromčík presented a finite element based structural model of a flexible wing that addressed the problem using Euler-Bernoulli, showing remarkable accuracy towards modeling [21]. Mathematical modeling and simulation analysis of aerodynamic loads acting on the wing structure, including aerodynamic lift, the weight of the wing, and fuel storage loads, were discussed in another study [22].

It is crucially important to identify the critical parameters which influence the aircraft wing structure during flying conditions. The aircraft's wing plays an important role towards the aircraft balance allowing it to dexterously perform graceful movement [23]. The main purpose of [23] is to provide an exhaustive analysis of a wide range of loads' types. The airfoil profiles reside in generating the aircraft's forward airspeed [24]. From a modeling point of view, in [24], the authors have performed a numerical validation on A300 wing model to determine the entire displacement, stress and deflection of the wing by adding the winglet or removing it. Wing is similar to a cantilever beam that transfers and collects all of the applied air load to the fuselage. It has a crucial structural role in ensuring a steady and functional flight.

When constructing a wing, it is important to meet certain criteria, such as high lifting force, low aerodynamic drag, and low mass [25]. In this study, the focus was on unmanned aerial vehicles (UAVs), specifically analyzing and optimizing the structure and topology of one of their UAV wings. A 3D model of the wing, based on its current dimensions, was created from scratch using ANSYS Mechanical APDL 18.1, a commercial software. XFLR5 software was then used to obtain the distributed lifting forces to be applied to the wing, assuming stationary flight conditions. MATLAB R2015a software, utilizing the DMS, was used for topology optimization. The wing supports the heaviest charges to which the aircraft structure is subjected. The wing's design is not randomly chosen but it strongly relied on different geometrical and physical parameters. Wing is the main source of producing the so-called lift-load in an aircraft [26]. Then, the finite element method is used to assume the stresses, strains, deformations and safety factors; it is concluded that the obtained pressure distribution is triggered by the various parameters acting on the wing. From [27], the authors have used two methods, namely modal method and kriging surrogate model. Both methods are coupled with the static equilibrium equation to perform a fast static aeroelastic analysis

for the sake of obtaining the deflection of the wing and modeling the generalized forces under different deformations, angles of attack and Mach numbers.

Structural analysis of a transport aircraft wing is done in [28] using a CAD software CATIA V5 and finite element software Ansys Workbench in order to obtain the total deformation, stress, strain and safety factor caused by the aerodynamic loads. A general aircraft is modeled and analyzed using RDS software and finite element software package COMSOL respectively in order to check the wing reliability. Simulation has been performed into three parts, namely takeoff, climb and cruise through Matlab code and Simulink taking into account the aerodynamic loads and pitching moment [29].

To this end, an investigation was carried out to model an aeroelastic wing model using both modal superposition and quasi-steady aerodynamic in the Simscape Multibody environment. Modeling wing using a modal approach is generally based on a state-space system that has accurate findings in the static and dynamic responses of the model. In the same context, coupling this approach with the quasi-steady aerodynamics approach in a partitioned manner paves the way to predict and calculate both structural and aerodynamic loads that act on the wing structure. Additionally, disturbances that have a direct impact on the wing, like aileron or flap deflection, especially affect wing loads. Furthermore, coupling the mentioned approaches forms an aeroelastic wing model, which is the most important object in this thesis. Another technique for modeling is the Lumped Parameter Method **LPM** which is used to model the static and dynamic behavior of simple flexible geometries. This approach could be more efficient in real experimental studies. Unfortunately, due to the absence of its experimental equipment, modeling of the considered wing using LPM will not be included in this report. According to the literature, the modal model (i.e., the aeroelastic wing modelled by the modal approach) that might be developed in the current study should be more accurate in comparison to the structural modeling, computing time, and precision required for the lumped-parameter wing model. Furthermore, the modal model outperforms the lumped parameter model because it requires less processing and can be efficient.

1.1.1 Overview for Aeroelasticity

The interaction between fluid materials and flexible solid objects is studied by the relatively new field of applied mechanics known as aeroelasticity. Aeroelasticity is typically used in the

field of aircraft engineering. Aeroelastic issues, however, also apply to transportation engineering (cars, ships, submarines) and civil engineering (slender structures, towers, smokestacks, suspension bridges, electric lines, and pipelines). Its uses in machine engineering (compressors, turbines) are also significant.

In the following sections, we will focus on aeroelasticity theory. Aeroelasticity is the branch of engineering that studies the phenomena that result from the interaction of aerodynamic, inertial, and elastic forces occurring during the relative motion of a fluid (air) and a flexible body (aircraft wings). Modeling the flexible flight mechanics of an aircraft's wing requires a solid understanding of aeroelasticity. Aeroelasticity is simply explained in the next sections, and this short introduction provides a clear understanding of the problem.

Figure 1.1 represents the interaction between solid mechanics, structural dynamics and fluid domain (i.e., elastic forces, inertial forces, and aerodynamic forces, respectively) which is at the core of aeroelasticity [30]. The change of the aerodynamic forces leads to a structural deformation. The complete fluid-structure interaction system must be simultaneously simulated due to this interaction.

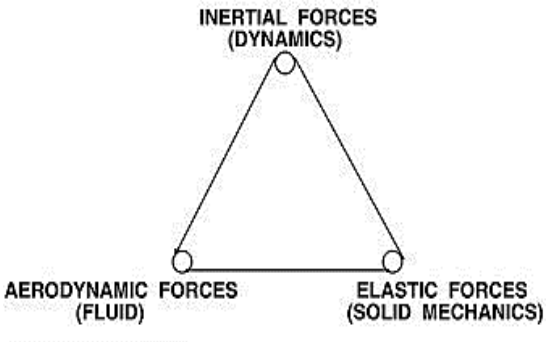

Figure 1.1: Collar triangle of aeroelasticity [31].

As seen in Figure 1.2 [32], Friedmann more recently contribute to improving the above triangle by including the effect of control elements such as flaps, ailerons, slates, and spoilers, and the effect of thrust force which is powered by the engine. The aeroservoelasticity that is the focus of this thesis is represented by the top half of the hexahedron. It covers the examination of control algorithms for things like trim or load alleviation as well as the analysis of the aircraft wing response to control input.

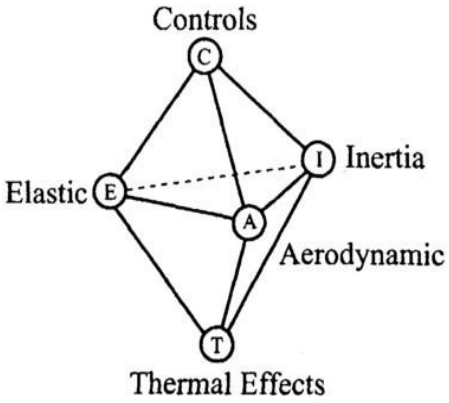

Figure 1.2:Friedmann hexahedron of aeroelasticity [32].

This research topic is growing more and more crucial because to the advancement of electronics, sensors, and autonomous control theories [33]. Aerothermoelasticity, in which heat effects are introduced to the conventional aeroelastic model, is represented by the lower half of the hexahedron. Aerothermoelasticity is essential in the transonic flight range [34]. Since it is not the focus of the current study, this will not be covered.

There are various approaches to treat the aero(servo)elastic problem. One can examine the dynamic reaction or the static (i.e., steady-state) response by including transitory effects. Additionally, one must decide whether to simulate the entire response or to merely look for limits of aeroelastic instability. The elastic instability of the air can take the form of flutter or divergence. Analysis of instability streamlines the process by essentially ignoring the majority of the deformations and focusing solely on motion that is negatively damped. The complete dynamic response of the structure must be modeled because the most recent study objective is about prediction of loads during flight domain. The most complex aeroelastic analysis that can be done is this one.

1.1.2 Overview for The Novelty of Flight Mechanics

From the current theory, the aeroelasticity of wings in steady state is regarded as a well-developed research field, and the majority of its results are considered to be timeless and valid [32]. However, aeroelasticity is still a relatively new discipline. Aeroelasticity in the regime of transonic flight [35], lightening loads using flexible structures [36], and the integration of aeroelasticity in flight mechanics are a few examples of topics where significant progress is currently being made [3].

The current study which is situated in an active research area, is focused on this challenge. An efficient Aeroelastic Flight Mechanics (AFM) model has already been attempted several times, but no agreed-upon modeling methodology has been established. Dedicated flight mechanics software, finite element analysis, and computational fluid dynamics. Although it takes days to complete the computation for a four-second maneuver, this method produces incredibly accurate results [37]. A dynamic of multi-physics systems is frequently used to connect various disciplines. A multi-physics systems has been integrated with a Computational Fluid Dynamic solver by something like a number of researchers [3], [38], [39]. These researchers reduced computational complexity by utilizing the multibody dynamics approach's inherent advantages. Chapters 2 and 5 discuss the precise modeling methods.

The used models during the preliminary design phase necessitate an additional performance improvement in the simulation time by using aerodynamic data inputs, such as a quasi-stable model or an unstable method (refer to part 2.2). In addition, through a multibody environment, some of these an aerodynamic model was combined with the lumped mass method. [40].

1.2 Thesis Objectives, Scope, and Structure

In the previous sections, the aeroelastic flight mechanics is covered. We will now discuss this thesis' particular context.

1.2.1 Thesis Objective

The primary purpose of this thesis project is to develop an Aeroelastic Wing Model **AWM** for disturbances (i.e., gust) and prediction of maneuver load. Furthermore, it makes designs safer and leads to reduced loads that act on the structure. The purpose of the research contribution can be summarized as follows:

Is it possible to quickly and accurately predict and calculate the load on a flexible aircraft wing in the subsonic flying range by combining the modal superpositioning method and quasi-steady aerodynamics in a partitioned way through a multibody system environment called " Simscape Multibody"?

The developed model is used to investigate the dynamic aeroelastic response of a small passenger aircraft's single moving wing. The created wing model predicts and captures the

whole aeroelastic problem, such as structural deformation, aerodynamic loads, and the influence of elements on wing deformation.

Comparatively speaking, it is estimated that this model can increase efficiency by potentially improving both accuracy and computing cost. Despite the seeming contradiction, literature implies that this is possible. Because of two factors, accuracy is increased. First, unlike modal superposition, the **LPM** is not suitable for prediction of loads and necessitates more hypothesis and experimental material, especially with complicated geometry like a wing [41], [42]. Additionally, provided that they behave linearly [43] (i.e., in a linear time-invariant manner), the Mode-Superposition approach **MSUP** can describe more complex and difficult systems than the lumped-parameter approach since the latter models only simple geometries through the Simscape Multibody environment. This then improves the accuracy of load prediction since the modal superposition approach is better suited to more complicated geometries.

1.2.2 Thesis Scope

The model developed by the current research can be performed using "Simscape Multibody analysis tools." It receives input from the desired model and other equipment for evaluation, such as structural or aerodynamic data. For this, the model must be developed using the Simscape Multibody toolbox, also known as Simscape Multibody, in a MATLAB environment. A multibody simulation environment is provided by Simscape Multibody, which is a component of Simulink.

Generally speaking, the purpose of the latest study is to develop a model that can simulate the graphs of small deflections of flexible aircraft wing structure, the evaluation of the dynamic response of flap and aileron elements, and the loads that effect the structure. This needs to be useful for a range of applications in flight mechanics, including the input of control elements and gust disturbances.

Unfortunately, due to the lack of complete DATA, the creation of the flight mechanics model, which combines the entire aircraft model parts using multibody system dynamics, is not part of the scope. However, it will be recommended for future studies.

The diagram in Figure 1.3 illustrates the iterative process of evaluating aircraft designs to arrive at a viable design solution based on the initial top-level requirements. The current research focuses on developing a model that fits within the category of "analysis tools." This model takes input data, such as structural or aerodynamic data, from the product model, which is represented by state-space blocks, and from other analysis tools.

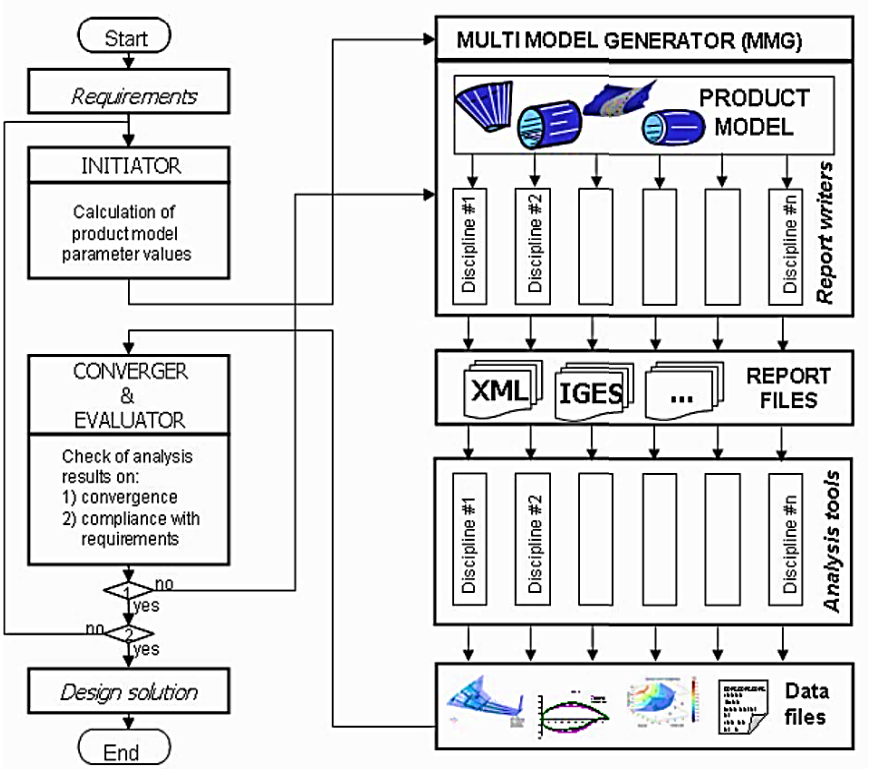

Figure 1.3: Flowchart model of engineering design and analysis [44].

1.2.3 Thesis Structure

This thesis is composed of 6 chapters. Firstly, chapter 1 covers the background of aeroelasticity and flight mechanics. Secondly, the aeroelastic wing theory is discussed in chapter 2 as is the theoretical background of a mathematical model of the modal approach, the lumped parameter approach (treated in detail in chapter 3), aerodynamic contribution, **FSI** study, and the influence of the inclusion of lifting surfaces such as flap and aileron.

Furthermore, a comparative study of a simple flexible wing using lumped-parameter and finite element methods is described in chapter 3 using Simscape Multibody environment and finite element software to solve the static and dynamic deflection of rectangular wing.

In addition, an application about how to model and simulate the aerodynamic loads by integrating some mathematical equations is performed using the MATLAB code in chapter 4. Moreover, chapter 5 represents the methodology of the Simscape Multibody model, i.e., how the discussed theory in chapter two was used to create the considered wing model.

Not least of all, the qualitative and dynamic evaluation of the considered wing structure is verified at the end of chapter 5 in order to validate the aeroelastic wing model. Finally, this report ends with general conclusions and additional proposals for future studies in chapter 6.

Chapter 2:

Aeroelastic Wing Theory

The following chapter covers the four disciplines that describe the AWM. The structural model is covered in section 2.1, while the aerodynamic model is covered in section 2.2. The above models are coupled in section 2.3 to create fluid-structure interactions. The impact of lifting surfaces on aerodynamics and wing response is briefly discussed in section 2.4. The chapter comes to an end with a brief summary in section 2.5.

2.1 Structures

The structural model will be explained now. The modal superposition method will be used for this model in order to capture both wing deformation and motion. In the next section, the modal method is discussed and a detailed explanation of the choice of this approach is given. After that, an overview of the **LPM** method is briefly treated in section 2.1.2 to obtain the best understanding of the modal model that necessitates an improvement. Finally, we end up with load prediction section 2.1.3.

2.1.1 Mode-Superposition Approach MSUP

Mode-Superposition is the fundamental concept of the modal method. First, this idea will be presented. Then there will be a detailed discussion of how it applies to our particular problem.

Modal superposition theory: The mode-superposition method involves using natural frequencies and mode shapes obtained from modal analysis to describe the static and dynamic response of a structure. In linear dynamics, it is often necessary to determine a system's response in the frequency or time domain. The mode-superposition method offers a computationally efficient way to do this, and in some types of linear dynamic analyses, it is the only way to obtain accurate results. The deflection of a structure can be expressed as a linear combination of a small number of vibration modes, with the amplitudes of these

modes forming the so-called generalized coordinates [45]. By using generalized coordinates, the structural model becomes more compact, as only the amplitudes of the mode shapes, rather than the deflections of every node, are needed to determine the system's state. This is in contrast to finite element methods where each node is modeled separately, resulting in much larger structural models [46].

Figure 2.1 provides examples of typical wing forms. Mode shape 1 (top-left) appears to be the first bending mode of a wing, also known as a flap-wise bending mode, in a minimal frequency response, while the fourth mode (bottom-right) shows the existence of a torsional mode with a higher natural frequency. Between these two are the other modes of bending and twisting, respectively. Due to their lower frequencies and typically higher amplitudes, the lower modes appear to be more dominant than the higher ones. Because of that, higher modes are typically ignored in the modal approach.

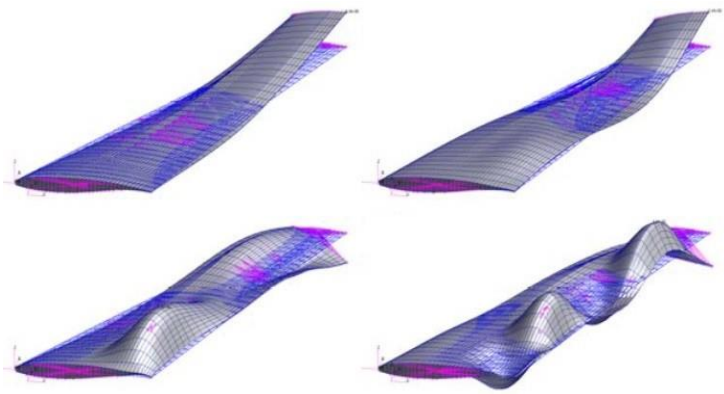

Figure 2.1: First four mode shapes of wing simulated by finite element software [4].

Be noted that twisting and bending typically occur in separate modes for simple, isotropic structures constructed of, for instance, metals, such as aluminum. Torsion and bending coupling frequently take place within mode forms for anisotropic structures constructed of, for instance, composites or for more complicated wings [47]. These linked mode forms can be employed to precisely reflect the structure, even if they could be a little more difficult to identify [47].

Theoretically, the governing equation for the modal approach is equation $(2-1)$. In this equation, s is the vector of response coordinates, which contain the degrees of freedom's

values, and the generalized coordinates vector q represents the amplitudes of the mode forms, Φ is the matrix that contains the lower mode shapes as its columns. Note that the used mode shapes can be normalized and orthogonal [48] and form the different values of DoF (i.e., capture the rotation and translation of each node, respectively). In addition, the coordinate transformation s is represented in equation $(2-1)$ from the physical coordinates to the modal coordinates. The transformation of these coordinates reduces the size of the structural problem elements.

$$\mathrm{s}(t) = \Phi \mathrm{q}(t) \qquad (2-1)$$

Application of the MSUP to Aeroelasticity: Modal approach is a potent method for speeding up computation time when performing dynamic response analyses of linear structures. With the help of this approach, the dynamic response of a structure can be approximately represented by the superposition of a few numbers of its eigenmodes. For aeroelastic problems, this coordinate of transformation is treated in this section. Equation $(2-2)$ depicts the general expression of a motion equation. In this known equation, M, C and K are the matrices of mass, damping and stiffness, respectively. Additionally, s is the vector of response coordinates which is represented in equation $(2-3)$, where g is the forward sweep bending, h is the plunge or the downward deflection and ξ is the twist or pitch-up deflection. The digits refer to the number of spanwise sections. In the side of this equation, **F** represents the applied force vector which is composed of: H is the forward force, V is the downward force, and M is the pitch-up moment, equation $(2-4)$.

$$M\ddot{\mathrm{s}} + C\dot{\mathrm{s}} + K\mathrm{s} = \mathbf{F} \qquad (2-2)$$

$$\mathrm{s} = [h_1\ \mathrm{g}_1\ \xi_1\ \ldots\ h_n\ \mathrm{g}_n\ \xi_n]^T \qquad (2-3)$$

$$\mathbf{F} = [V_1\ H_1\ M_1\ \ldots\ V_n\ H_n\ M_n]^T \qquad (2-4)$$

In modal analyses, mode shapes are usually obtained without damping and external forces, as it mentioned in equation $(2-5)$. The solution of this equation is discussed now. Structural damping and external forces will be discussed in more detail later in this section.

$$M\ddot{\mathrm{s}} + K\mathrm{s} = \mathbf{0} \qquad (2-5)$$

A solution for equation $(2-5)$ takes the form of $s(t) = \phi^{i\omega t}$, as described in the literature. Substituting this solution into $(2-5)$ yields equation $(2-6)$, which represents the general form of the eigenvalue problem. In this equation, ϕ refers to the number of eigenvectors that solve the eigenvalue problem for corresponding eigenvalues of ω^2. All of these eigenvectors represent the mode shapes of the structure, while ω represents a natural frequency related to a given mode shape.

$$K\phi = \omega^2 M\phi \qquad (2-6)$$

In relation to the stiffness and mass matrices, the mode shapes are orthogonal [48]. Equation $(2-7)$ is obtained using the property of orthogonality, it forms the generalized mass also called ''M-orthonormal'' [48]. δ_{ij} represents the Kronecker delta, which has a null value in each combination of i and j, except when $i = j$, in which case it is 1.

Including the matrix of the mode shapes, in order to rewrite equation $(2-7)$. M-orthonormality can also be written as is shown in equation $(2-8)$ such as I is the identity matrix.

$$\phi_i^T M\phi_j = \delta_{ij} \qquad (2-7)$$

$$\Phi^T M\Phi = I \qquad (2-8)$$

By applying the coordinate transformation of equation $(2-1)$ in equation $(2-2)$ and pre-multiplying all terms with Φ^T and equation $(2-8)$ is substituted, this gives equation $(2-9)$ [42].

$$I\ddot{q} + 2\Gamma\dot{q} + \Lambda q = \Phi^T \mathbf{F} \qquad (2-9)$$

Equation $(2-10)$ shows that Λ is the spectral matrix with the diagonal eigenvalues ω_i^2. The eigenvalue problem has this type of property [2]. The modal damping matrix Γ will be discussed in detail in the next sections.

$$\Lambda = \Phi^T K\Phi = \begin{bmatrix} \omega_1^2 & & \\ & \ddots & \\ & & \omega_m^2 \end{bmatrix} \qquad (2-10)$$

Since the matrices of I and Λ are diagonal, the system of vibration equations in $(2-9)$ could be uncoupled, so it is important to solve the modal damping Γ and the applied force **F**. Note that the given modes are not orthogonal to the damping matrix Γ, However, it can be useful when we use a common assumption in the form of "Rayleigh Damping" [49]. This case occurs when C is a linear combination of stiffness matrix K and mass matrix M. So, it is obvious in this case that the condition of orthogonality of the eigenmodes compared to the matrix C will be checked. Note that c_1 and c_2 are constant scalars.

The general form of Rayleigh damping is represented in equation $(2-11)$, where the damping matrix C appears to be a linear combination of the mass matrix M and the stiffness matrix K. Since the matrices of M and K are diagonal, the damping matrix Γ is also diagonal. If Rayleigh damping is considered, the modal damping matrix Γ in equations $(2-9)$ will take the form illustrated in equation $(2-12)$.

Because of its diagonal form, this sort of damping is also known as "proportional damping" because each mode is individually damped [42]. In equation $(2-12)$, ζ represents the modal damping ratio. This damping is intractable to identify for complex structures such as an aircraft wing [50].

$$C = c_1 M + c_2 K \tag{2-11}$$

$$2\Gamma = \Phi^T C \Phi = \begin{bmatrix} 2\zeta_1\omega_1 & & \\ & \ddots & \\ & & 2\zeta_m\omega_m \end{bmatrix} \tag{2-12}$$

In order to achieve the structural deformation, it is possible to create a structural state-space system that enables quick calculation of the whole deformation in Simscape Multibody environment[42]. The form of a state-space system is defined in equation $(2-13)$.

$$\begin{aligned} \dot{\mathbf{x}} &= \mathrm{A}\mathbf{x} + \mathrm{B}\mathbf{u} \\ \mathbf{y} &= \mathrm{C}\mathbf{x} + \mathrm{D}\mathbf{u} \end{aligned} \tag{2-13}$$

From the previous equation, **x** is the vector containing the state vector of variables, it is a function of time, **y** is the output variables and it is a function of time, **u** is the input variables also it is a function of time, A is the state constant matrix, B is the input matrix, also it is constant and C is the output matrix as well as D is the direct transition (or feedthrough) matrix, a constant matrix.

The output vector **y** is specified in equation $(2-15)$ and forms the vector of response coordinates s, the vector of modal coordinates q, and their first and second derivatives. The vector **x** is given by equation $(2-14)$, the applied force vector **F** from equation $(2-2)$ is considered as an input in **u**. Equation $(2-9)$ can now be used to produce the state space equation, resulting in equation $(2-16)$. Equation $(2-17)$ shows the output equation.

$$\mathbf{x} = \begin{bmatrix} \mathrm{q} \\ \dot{\mathrm{q}} \end{bmatrix} \tag{2-14}$$

$$\mathbf{y} = \begin{bmatrix} \mathrm{s} \\ \dot{\mathrm{s}} \\ \ddot{\mathrm{s}} \\ \mathrm{q} \\ \dot{\mathrm{q}} \\ \ddot{\mathrm{q}} \end{bmatrix} = \begin{bmatrix} \Phi\mathrm{q} \\ \Phi\dot{\mathrm{q}} \\ \Phi\ddot{\mathrm{q}} \\ \mathrm{q} \\ \dot{\mathrm{q}} \\ \ddot{\mathrm{q}} \end{bmatrix} \tag{2-15}$$

$$\begin{bmatrix} \mathrm{q} \\ \dot{\mathrm{q}} \end{bmatrix} = \begin{bmatrix} 0 & I \\ -\Lambda & -2\Gamma \end{bmatrix} \begin{bmatrix} \mathrm{q} \\ \dot{\mathrm{q}} \end{bmatrix} + \begin{bmatrix} 0 \\ \Phi^T \end{bmatrix} \mathbf{F} \tag{2-16}$$

$$\begin{bmatrix} \Phi\mathrm{q} \\ \Phi\dot{\mathrm{q}} \\ \Phi\ddot{\mathrm{q}} \\ \mathrm{q} \\ \dot{\mathrm{q}} \\ \ddot{\mathrm{q}} \end{bmatrix} = \begin{bmatrix} \Phi & 0 \\ 0 & \Phi \\ -\Phi\Lambda & -2\Phi\Gamma \\ I & 0 \\ 0 & I \\ -\Lambda & -2 \end{bmatrix} \begin{bmatrix} \mathrm{q} \\ \dot{\mathrm{q}} \end{bmatrix} + \begin{bmatrix} 0 \\ 0 \\ \Phi\Phi^T \\ 0 \\ 0 \\ \Phi^T \end{bmatrix} \mathbf{F} \tag{2-17}$$

The applicability of the modes determines how many must be used to obtain correct results for a wing. Theoretically, any collection of modes may be used to simulate structural response, but in practice, a large variety of modes would be needed to achieve a desired level of accuracy. Aeroelastic applications typically make use of a number of fixed-free vibration modes [43], [51]. In this context, the term "fixed-free" denotes the presence of forces and moments at one end. Given that the aircraft wing is in free-flight state, this is appropriate [52]. According to published researches [48], [46], between 15 and 25 modes should be considered for an accurate Aeroelastic Flight Mechanics **AFM** model.

Since the mode shapes represent the deflection from this equilibrium, they must be defined in relation to a fixed equilibrium position. Since mode shapes are established for a structure vibrating in a vacuum or without aerodynamic forces, the equilibrium position is the shape of the wing on the ground. The aircraft in which the wing root chord line is located will serve as the reference plane for the mode forms (the "rigid wing plane" treated in section 5.2.2). The elastic axis located in the middle of each wing section is represented by the mode as they form themselves in their forward, downward, and pitch up positions. Note that secondary motion is neglected, such as the inward translation of the wing tip caused by a plunge.

2.1.2 Overview of LPM

With the Lumped-parameter Method (LPM), which uses a group of rigid parts connected by springs and dampers, it is easy to model the continuous wing.

In the top part of this Figure 2.2, each beam element is linked to another beam element using a weld (W) in order to ensure the best connection between **GBE**, and each beam element comprises two massless bodies (B) linked by a joint (J). This last captures the deformation of each massless body.

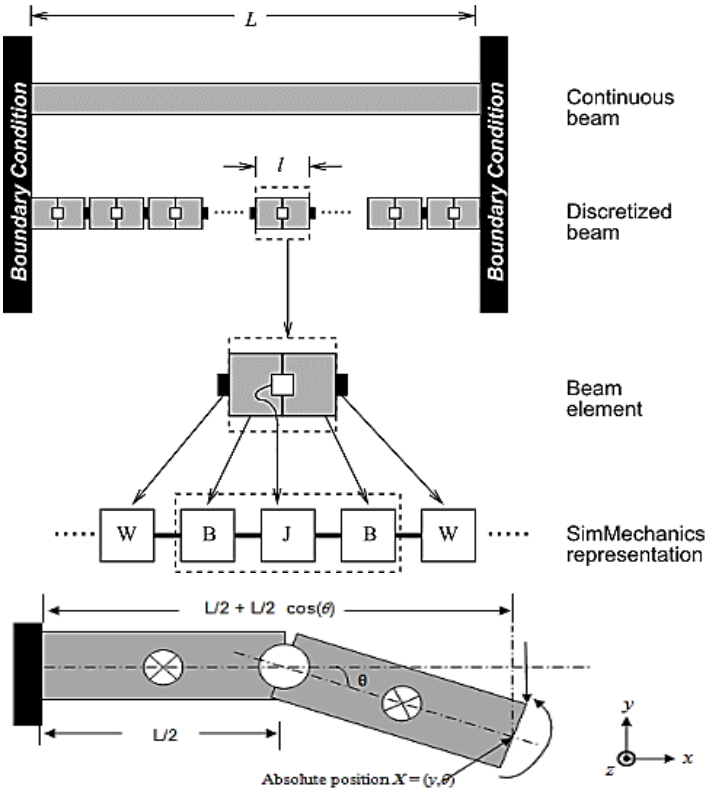

Figure 2.2: Lumped-beam representation [42].

The lower part of Figure 2.2 depicts an individual generalized beam element. The stiffness and damping coefficients of the joint are set to represent the properties of the section of the beam they describe [42].

Due to the usage of rigid parts, this method is easily adaptable to the Simscape Multibody dynamics environment [7]. Using the **LPM**, the structure is divided into a number of generalized beam elements that are all the same and each of them is a body-joint-body combination. The library of the Simscape Multibody environment creates the equations of motion automatically. The approach creates a compact model that can yet represent the structure's dynamic response because it does not model every node but instead makes use of generalized coordinates. These generalized coordinates indicate the degrees of freedom of the generalized beam elements.

Unfortunately, this approach can be difficult to extend and accurately describe for less computationally complex geometries such as airplane wings, even when including experimental data and materials. On the other hand, modeling using a modal approach based on finite element analyses are preferable [7]. Furthermore, the bending moment cannot be precisely defined as a function of beam bending angles because the bending moment at a particular beam element only depends on that beam element's deflection. In truth, the bending moment is also impacted by the adjacent deflection angle [42].

This problem could be resolved by creating a special joint that calculates the joint deflection and response force by taking into account the deflection angles of various elements. Unfortunately, this causes the beam elements to become connected, making it impossible to easily determine joint primitives. For these reasons, which are taken from several sources of literature, modeling aeroelastic wing deformation does not often employ the **LPM**.

2.1.3 Determination of Load Prediction

It is important to take into consideration the prediction of loads in order to minimize the effect of loads on the structure. Load reduction is intended to reduce severe wing deflection and wing tip deformation [53]. Peak loads, which can be significantly larger than those during normal flight, may happen during flight as a result of gusts or maneuvers [4]. To

reduce the dynamic response to winds and maneuvering actions, control mechanisms can be used. The summation of forces **(SOF)** approach bases loads on the addition of inertial and aerodynamic forces [54]. Inverse-Fourier transforms would often be used to determine these in the frequency domain before moving them into the time domain [54]. The forces have previously been obtained in the time domain for the Multibody System Dynamics **MSD** simulation that is being used in the current study [42]. The **MSD** environment can automatically integrate these forces. The **SOF** method will be employed in this instance even though, the **MD** method is better suited to handle load prediction [53] since it takes advantage of the Simscape Multibody framework used to create the model.

2.2 Aerodynamics

In an aeroelastic study, the aerodynamic analysis can be very difficult. 60% of the CPU time was used for fluids in a high-fidelity aeroelastic study using the Reynolds average and Navier-Stokes method, 38% was used for mesh deformation needed for the aerodynamic analysis, and only 2% was used for structures [55].

2.2.1 Choice of Linear on Nonlinear Study

If a linear model is adequate for the anticipated loads uses or if nonlinear aerodynamic effects need to be taken into account should be decided first. Examples of the foundations for nonlinear models are the Navier-Stokes equations or the Euler equations [56]. For example, a Doublet-Lattice Approach **DLM** or a quasi-steady method are the foundations of linear models, which are easier.

The relationship between the flutter speed index and Mach number is shown in Figure 2.3. The speed at which flutter instability only manifests itself is known as the flutter speed index. The flutter speed index for subsonic Mach numbers below about 0.75 can be accurately described by linear analysis, as this figure shows. Aeroelastic analysis becomes substantially more difficult in the transonic zone, as shown by Figure 2.3, which depicts highly nonlinear aerodynamic effects. As the airplane experiences structural bending in this domain, shock waves may arise and vanish. Furthermore, zones of separated flow may form as these shock waves grow and diminish [57]. Linear aerodynamic models are utilized since they are accurate enough, and the model is focused on aircraft traveling at subsonic speeds.

There is broad consensus among authors that linear models can adequately capture subsonic aeroelasticity with connected flow [32], [34], [58].

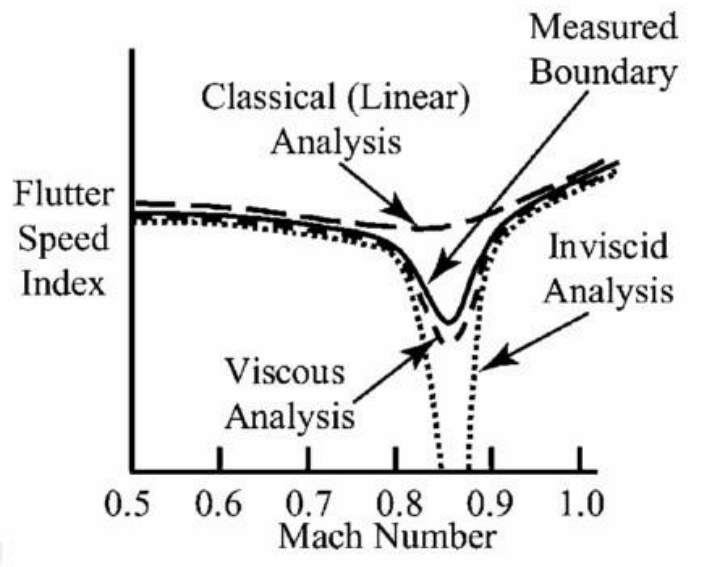

Figure 2.3: Prediction of the flutter speed index for various Mach numbers [57].

2.2.2 Choice of Stable, Quasi-Stable or Unstable Aerodynamic Models

The following decision to be taken is whether to utilize a stable, quasi-stable, or unstable aerodynamic model [31], which is covered in more detail in the following paragraphs.

- **Stable models:** The factors affecting aerodynamic forces and moments are the current position and orientation. They only rely on the angle of attack in real-world application. An algebraic equation or a look-up table can be used to model the considered case.

- **Quasi-stable models**: Instantaneous position, orientation, and motion provide an equally steady aerodynamic state that impacts aerodynamic forces and moments. This requires the assumption that motion occurs infrequently. Inertial and wake effects are not taking into account as it is mentioned in [59], [60]. In addition, a basic algebraic equation or look-up table is implemented.

- **Unstable models**: The entire flow must be determined in order to calculate aerodynamic forces and moments. As far as the unsteady effects is remarkably pointed out the oscillation profile takes place, as it is shown in Figure 2.4. Once the vortex of the same length occurs, the vorticity gives birth around the airfoil which triggers the

lift profile. The effective angle of attack changes as a result of the downward deflection h of an airstream u from this vortex, which alters the airflow that intrudes on the airfoil profile [61]. As the profile oscillates in a dynamic environment, Figure 2.4 depicts how the shed vortex varies over time in terms of its strength and orientation. The main things that cause instability are viscosity, thickness of the airfoil, flow separation, and being able to be compressed [61].

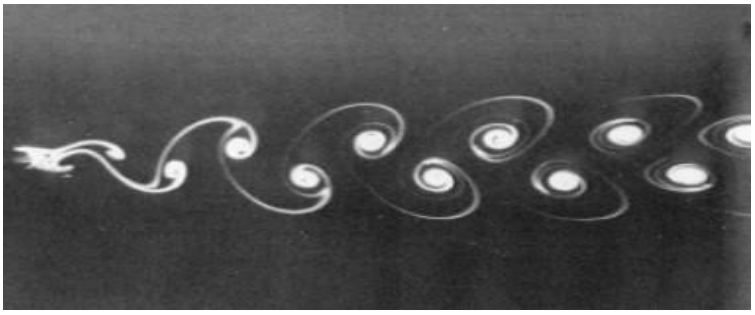

Figure 2.4: Wake vortices decreases by the oscillating profile's effect [62].

2.2.3 Study of Quasi-Stable Model

At this point, a more thorough examination of quasi-steady models is complete, where aerodynamic forces and moments are affected by position, orientation, and motion **POM**. Even though this assumption seems pretty simple, the quasi-steady approximation can be used in a number of situations [31].

Equation $(2-18)$ represents Theodorsen's formula for calculating lift [61]. L represents the lift load, C_{l0} is the coefficient of lift at 0° AoA, and $C_{l\alpha}$ is the gradient of the lift curve. Moreover, ρ is the air density, a is the distance between the mid-chord point and the elastic axis as a fraction of the semi-chord, b is the distance from leading edge or trailing edge to the mid-chord point, h is the downward deflection, $\mathbf{C}(k)$ is the Theodorsen's function, u is the airflow velocity and α is the local AoA.

$$L = \rho b u^2 C_{l0} + \pi\rho b^2\left(\ddot{h} - ba\ddot{\alpha} + u\dot{\alpha}\right) + C_{l\alpha}\rho b u^2\, \mathbf{C}(k)\left[\frac{\dot{h}}{u} + b\left(\frac{1}{2} - a\right)\frac{\dot{\alpha}}{u} + \alpha\right] \quad (2-18)$$

Equation $(2-18)$ can be utilized for the quasi-stable model with $\mathbf{C}(k)$ constant and equal to one, relating to a lower frequency k of zero [63]. The equations are then reduced to simple **POM** algebraic functions.

This quasi-stable model can also be used in conjunction with lift, drag, and moment using a look-up table. This approach must be used with the effective angle of attack α_{eff}. The three-quarter chord point should be used to calculate this α_{eff} [60]. The following will explain how to determine α_{eff} from equation $(2-18)$, observing that it is approximately the section between brackets as given in equation $(2-19)$. The terms depending on $\ddot{\alpha}$ and $\ddot{h}$ that are left out as a result of this method have a minor effect in comparison to other terms [31].

$$\alpha_{eff} \approx \left[\frac{\dot{h}}{u} + b\left(\frac{1}{2} - a\right)\frac{\dot{\alpha}}{u} + \alpha\right] \qquad (2-19)$$

According to what was mentioned in section 1, Figure 2.5 depicts a wing that can be described as a collection of spanwise parts that can move independently of one another. The deformation of multiple spanwise sections is determined by the state-space system. This leads to the assumption made by the strip theory. Each unit along the spanwise direction of a wing is represented here by being thought of as a piece of an endless wing with uniform spanwise elements (see Figure 2.5).

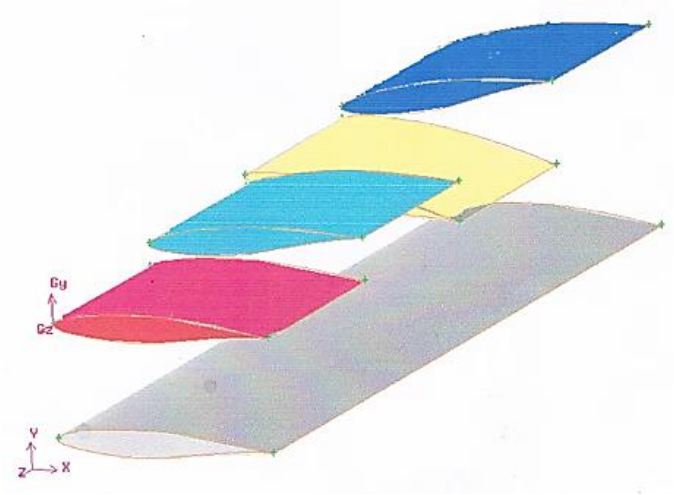

Figure 2.5: Moving wing parts freely to each other.

Strip theory and higher-fidelity models disagree on smaller aspect ratio wings due to three-dimensional phenomena. Nevertheless, as long as the motion frequency is low, strip theory reaches the precision of unsteady panel methods when the static lift slope at section areas closes the tip is adjusted to match higher-fidelity models[64]. In quasi-steady conditions, strip theory with a tip adjustment is correct.

In conclusion, the aerodynamic model that will be used is a quasi-stable aerodynamic model based on Theodorsen's theory, considering strip study with a wing tip correction. Also, it consists of look-up tables.

2.3 Fluid-Structure Interaction FSI

As was already said, this chapter talks about how the structural and aerodynamic models from the above sections are linked together.

In the **FSI** problem, 03 domains are involved: the fluid domain, the structural domain, and the fluid mesh domain [65]. The fluid mesh domain looks at how the structural deformation changes when the mesh domain changes. The rules that define fluid dynamics and structural mechanics are coupled through a multi-physics process known as fluid-structure interaction. A fluid flow in the region or inside the wing interacts in a stable or oscillating manner with a flexible or moving wing to produce this phenomenon. Stresses and strains are applied to the solid object when a fluid flow comes into contact with a structure, which may cause deformations. Based on the flow's velocity, pressure, and material characteristics of the structure, these changes can be very big or very small.

2.3.1 Choice of Partitioned or Monolithic Approaches

To model FSI, there exist two different methods that can be employed. The so-called "partitioned approach" involves asynchronously enforcing the interface criteria while alternately integrating the aerodynamic and structural equations over time. The so-called monolithic approach treats FSI synchronously, which means that at every time step, all associated equations agree [66]. Due to the modularity of the framework, various models may be employed in the partitioned method [55]. During the analysis, the data is exchanged between the two models. Due to the flexibility of the framework, the partitioned method has many advantages over the monolithic approach in terms of integration [55]. Furthermore, it has a lower computing cost than the monolithic approach [66]. A new strategy is needed for the monolithic approach. This can be done if a linear aerodynamic model is used by implementing the equations of aerodynamic into the structural model to create an aeroelastic state space system. There are two possibilities for the monolithic method for non-linear aerodynamic models.

First, depending on the superposition of the aerodynamic effects due to step deformations, using integral operations, a nonlinear equation can be fitted into a state-space system [67], [68]. Second, until a unique convergent solution is found, several **FSI**s can be carried out in the same time step.

Generally, the monolithic approach has the limitation of being accurate only for constant velocity of airflow, which cannot be guaranteed in flight dynamics. As indicated in the lift equation $(2-20)$ the influence of the two cannot be easily decoupled. From equation $(2-20)$, C', C'' and C''' are constant and $C_{LV}(V)$ indicates the velocity influence on lift. The effect of α_{eff} and V cannot be dissociated into different terms, consequently decoupling is not possible. Moreover, $C_{LV}(V)$ will be a parabolic function rather than a linear function. As a result, when speed is not constant, the state-space of an aeroelastic system cannot be linear and time-invariant.

$$L = \frac{1}{2}\,\rho V^2\, S C_L\left(\alpha_{eff}\right) = C' V^2\;\; C_L\left(\alpha_{eff}\right) \neq C''\, C_{LV}(V) + C'''\;\; C_L\;\left(\alpha_{eff}\right) \quad (2-20)$$

The partitioned strategy is selected for the model due to the aforementioned reasons.

2.3.2 Partitioned Procedures

An adequate approach of solution exchange must be defined to ensure the time accuracy of a partitioned approach, i.e., consistency between aerodynamic loads and structural deformation [55]. There are several procedures, which are described here. The first approach, represented in Figure 2.6 (a), is the so-called conventional serial staggered procedure. The structural state at time n (Un in the figure) is transmitted to the aerodynamic discipline (1) in this approach, which progresses the aerodynamic solution from time n to time $n + 1$ (2). Therefore, at time $n + 1$ ($Pn + 1$ in the figure), the aerodynamic forces and moments are transmitted to the structural discipline (3), which progresses the structural solution from time n to time $n + 1$ (4). This approach is interesting due to its simplicity, and it is the most common of the partitioned procedures [65]. The aerodynamic solution is refreshed before structural solution in the provided procedure (a) Serial. This can be reversed as well. Figure 2.6 (b) depicts the second approach (b) Parallel, which is the so-called conventional parallel staggered method. At first, the structural state at time n (Un in the

Figure) and the aerodynamic forces at time n (Pn in the figure) are transferred to the aerodynamic discipline and the structural discipline, respectively (1). Second, the aerodynamic and structural solutions are both increased from time n to time $n+1$ (2). This is a parallel process since it takes place concurrently. When the aerodynamic and structural models are executed on different processors, this approach is more efficient, but it has lower stability features [55].

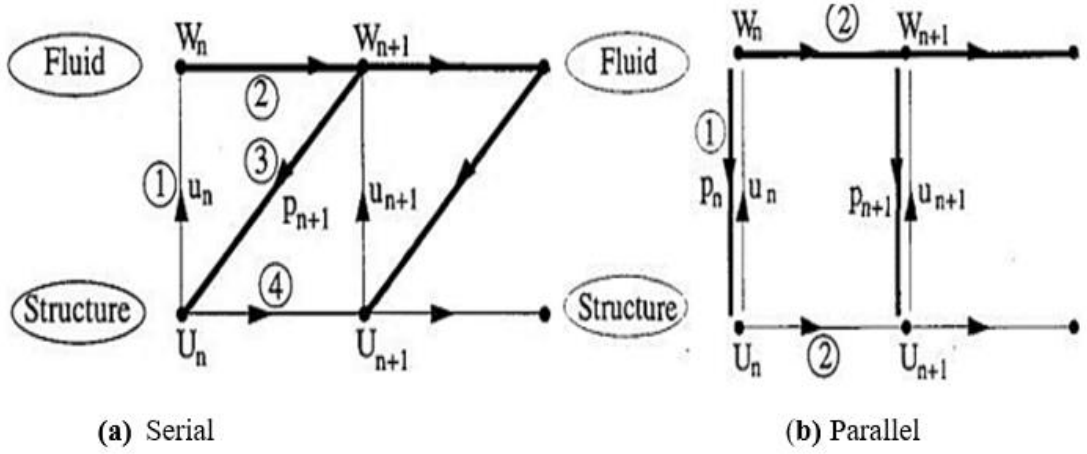

Figure 2.6: Scheme of conventional staggered procedures [65].

Figure 2.7 illustrates the predictor-corrector inclusion to the conventional serial staggered approach. In this method, the structural deformation at time $n+1$ is predicted (U_{n+1}^{p} in the figure). The aerodynamic state is then progressed from time n to time $n+1$ (3) by transferring this predicted structural state to the aerodynamic model (2). The structural model (4) serves as the corrector step, receiving the forces obtained from the aerodynamic model at time $n+1$. The structural model is also time-advanced (5). The accuracy of the model is improved by using a predictor-corrector system, at a relatively low additional computing cost [55].

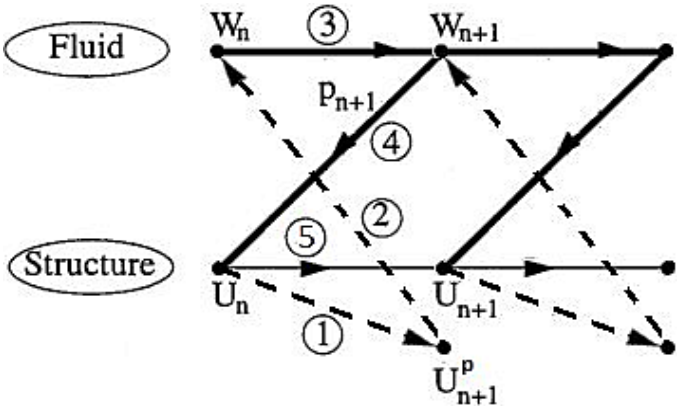

Figure 2.7: Scheme of predictor-corrector serial staggered procedure.

2.3.3 Benefits of Using Structures and Aerodynamics Combination

Note that the discussed partitioned method is included in the model. This section investigates the connection of structural and aerodynamic equations by coupling equations $(2-2)$, $(2-3)$ and $(2-4)$ in order to construct the final equation of vibration stated in equation $(2-21)$.

$$M\begin{bmatrix}\ddot{h}_1\\ \ddot{g}_1\\ \ddot{\xi}_1\\ .\\ .\\ .\\ \ddot{h}_n\\ \ddot{g}_n\\ \ddot{\xi}_n\end{bmatrix}+C\begin{bmatrix}\dot{h}_1\\ \dot{g}_1\\ \dot{\xi}_1\\ .\\ .\\ .\\ \dot{h}_n\\ \dot{g}_n\\ \dot{\xi}_n\end{bmatrix}+K\begin{bmatrix}h_1\\ g_1\\ \xi_1\\ .\\ .\\ .\\ h_n\\ g_n\\ \xi_n\end{bmatrix}=\boldsymbol{F}=\begin{bmatrix}V_1\\ H_1\\ M_1\\ .\\ .\\ .\\ V_n\\ H_n\\ M_n\end{bmatrix} \qquad (2-21)$$

The force vector **F** covers forces from control surfaces, gravity, and aerodynamics. To detect the position, orientation, and motion **POM** of each wing section. The forces acting on that section are added to the model using the aerodynamic strip theory. The effects of position, orientation, and motion **POM** on the forces V, H, and the moment M are represented in equations $(2-22)\ -\ (2-24)$ for a single spanwise section.

$$V = C_{V\ddot{\alpha}}\ddot{\alpha} + C_{V\dot{\alpha}}\dot{\alpha} + C_{V\alpha}\alpha + C_{V\ddot{h}}\ddot{h} + C_{V\dot{h}}\dot{h} + C_{V0} \qquad (2-22)$$

$$H = C_{H\ddot{\alpha}}\ddot{\alpha} + C_{H\dot{\alpha}}\dot{\alpha} + C_{H\alpha}\alpha + C_{H\ddot{h}}\ddot{h} + C_{H\dot{h}}\dot{h} + C_{H0} \qquad (2-23)$$

$$M = C_{M\ddot{\alpha}}\ddot{\alpha} + C_{M\dot{\alpha}}\dot{\alpha} + C_{M\alpha}\alpha + C_{M\ddot{h}}\ddot{h} + C_{M\dot{h}}\dot{h} + C_{M0} \qquad (2-24)$$

These equations use coefficients called $C_{V\ddot{\alpha}}, C_{V\dot{\alpha}}, C_{V\alpha}, C_{V\ddot{h}}, C_{V\dot{h}}$ to describe how angular acceleration $\ddot{\alpha}$, angular velocity $\dot{\alpha}$, angle of attack α, plunge acceleration $\ddot{h}$, and plunge speed $\dot{h}$ influence the vertical force. The coefficients $C_{H\ddot{\alpha}}, C_{H\dot{\alpha}}, C_{H\alpha}, C_{H\ddot{h}}, C_{H\dot{h}}$ indicate the effects of these variables on the horizontal force, while $C_{M\ddot{\alpha}}, C_{M\dot{\alpha}}, C_{M\alpha}, C_{M\ddot{h}}, C_{M\dot{h}}$represent the effects of these variables on the section pitching moment. The forces and moment are unaffected by the vertical position h, however, there is an influence that is unaffected by the location and orientation factors (for example, gravitational force), which are recorded in variables C_{V0}, C_{H0} and C_{M0}.

Replacing equations $(2-22)\ -\ (2-24)$ in equation $(2-21)$ to form equation $(2-25)$. This formula represents the vibrational aeroelastic equation.

$$M\begin{bmatrix}\ddot{h}_1\\ \ddot{g}_1\\ \ddot{\xi}_1\\ .\\ .\\ .\\ \ddot{h}_n\\ \ddot{g}_n\\ \ddot{\xi}_n\end{bmatrix}+C\begin{bmatrix}\dot{h}_1\\ \dot{g}_1\\ \dot{\xi}_1\\ .\\ .\\ .\\ \dot{h}_n\\ \dot{g}_n\\ \dot{\xi}_n\end{bmatrix}+K\begin{bmatrix}h_1\\ g_1\\ \xi_1\\ .\\ .\\ .\\ h_n\\ g_n\\ \xi_n\end{bmatrix}=$$

$$\begin{bmatrix}C_{V\ddot{h},1} & C_{V\ddot{g},1} & C_{V\ddot{\xi},1} & \cdots & 0 & 0 & 0\\ C_{H\ddot{h},1} & C_{H\ddot{g},1} & C_{H\ddot{\xi},1} & \cdots & 0 & 0 & 0\\ C_{M\ddot{h},1} & C_{M\ddot{g},1} & C_{M\ddot{\xi},1} & & . & . & .\\ . & . & . & & . & . & .\\ . & . & . & & . & . & .\\ . & . & . & & . & . & .\\ 0 & 0 & 0 & \cdots & C_{V\ddot{h},n} & C_{V\ddot{g},n} & C_{V\ddot{\xi},n}\\ 0 & 0 & 0 & \cdots & C_{H\ddot{h},n} & C_{H\ddot{g},n} & C_{H\ddot{\xi},n}\\ 0 & 0 & 0 & \cdots & C_{M\ddot{h},n} & C_{M\ddot{g},n} & C_{M\ddot{\xi},n}\end{bmatrix}\begin{bmatrix}\ddot{h}_1\\ \ddot{g}_1\\ \ddot{\xi}_1\\ .\\ .\\ .\\ \ddot{h}_n\\ \ddot{g}_n\\ \ddot{\xi}_n\end{bmatrix}$$

$$+\begin{bmatrix}C_{V\dot{h},1} & C_{V\dot{g},1} & C_{V\dot{\xi},1} & \cdots & 0 & 0 & 0\\ C_{H\dot{h},1} & C_{H\dot{g},1} & C_{H\dot{\xi},1} & \cdots & 0 & 0 & 0\\ C_{M\dot{h},1} & C_{M\dot{g},1} & C_{M\dot{\xi},1} & & . & . & .\\ . & . & . & & . & . & .\\ . & . & . & & . & . & .\\ . & . & . & & . & . & .\\ 0 & 0 & 0 & \cdots & C_{V\dot{h},n} & C_{V\dot{g},n} & C_{V\dot{\xi},n}\\ 0 & 0 & 0 & \cdots & C_{H\dot{h},n} & C_{H\dot{g},n} & C_{H\dot{\xi},n}\\ 0 & 0 & 0 & \cdots & C_{M\dot{h},n} & C_{M\dot{g},n} & C_{M\dot{\xi},n}\end{bmatrix}\begin{bmatrix}\dot{h}_1\\ \dot{g}_1\\ \dot{\xi}_1\\ .\\ .\\ .\\ \dot{h}_n\\ \dot{g}_n\\ \dot{\xi}_n\end{bmatrix}$$

$$+\begin{bmatrix}C_{Vh,1} & C_{Vg,1} & C_{V\xi,1} & \cdots & 0 & 0 & 0\\ C_{Hh,1} & C_{Hg,1} & C_{H\xi,1} & \cdots & 0 & 0 & 0\\ C_{Mh,1} & C_{Mg,1} & C_{M\xi,1} & & . & . & .\\ . & . & . & & . & . & .\\ . & . & . & & . & . & .\\ . & . & . & & . & . & .\\ 0 & 0 & 0 & \cdots & C_{Vh,n} & C_{Vg,n} & C_{V\xi,n}\\ 0 & 0 & 0 & \cdots & C_{Hh,n} & C_{Hg,n} & C_{H\xi,n}\\ 0 & 0 & 0 & \cdots & C_{Mh,n} & C_{Mg,n} & C_{M\xi,n}\end{bmatrix}\begin{bmatrix}h_1\\ g_1\\ \xi_1\\ .\\ .\\ .\\ h_n\\ g_n\\ \xi_n\end{bmatrix}+\begin{bmatrix}C_{V0,1}\\ C_{H0,1}\\ C_{M0,1}\\ .\\ .\\ .\\ C_{V0,1}\\ C_{H0,1}\\ C_{M0,1}\end{bmatrix}$$

$$= M_{aero}\begin{bmatrix}\ddot{h}_1\\ \ddot{g}_1\\ \ddot{\xi}_1\\ .\\ .\\ .\\ \ddot{h}_n\\ \ddot{g}_n\\ \ddot{\xi}_n\end{bmatrix} + C_{aero}\begin{bmatrix}\dot{h}_1\\ \dot{g}_1\\ \dot{\xi}_1\\ .\\ .\\ .\\ \dot{h}_n\\ \dot{g}_n\\ \dot{\xi}_n\end{bmatrix} + K_{aero}\begin{bmatrix}h_1\\ g_1\\ \xi_1\\ .\\ .\\ .\\ h_n\\ g_n\\ \xi_n\end{bmatrix} + \mathbf{F_0} \qquad (2-25)$$

It is evident from this equation that the vector of response coordinates s and its first and second derivatives are necessary and sufficient to determine the aerodynamic force terms.

The aerodynamic matrices in the equation are known as the aerodynamic mass matrix M_{aero}, the aerodynamic damping matrix C_{aero}, and the aerodynamic stiffness matrix K_{aero} because of their similarity to the mass, damping, and stiffness matrices (M, C, and K), respectively.

It should be noted that the modes become coupled since these matrices contain off-diagonal elements, although this is a characteristic of all aeroelastic systems [31]. Equation $(2-25)$ clearly illustrates the benefit of utilizing aerodynamic strip theory: the forces and moments impacting on a spanwise section are entirely depending on that the deformation of only that section**.**

2.4 Lifting Surfaces

The addition of lifting surfaces to the model will be explained in the following section. Control or lifting surfaces should be taken into account since they are a crucial input for the aeroelastic wing model. A crucial step that shouldn't be overlooked is including flaps and ailerons' deflections. Unfortunately, the engine, slats, and spoilers will not be included because the required modal data are not available.

There are various ways to integrate control surfaces in an aeroelastic model. In the first stages of designing an aircraft wing, it is typical to assume that the presence of control surfaces can be accurately represented by their aerodynamic contribution [3]. By supposing this, one ignores the dynamics, actuation systems, and inertia related to the control surface. Based on this supposition,

a control surface is governed by an infinitely rigid and powerful linear servo actuator that can regulate both the feedback and the position of the control surface. Figure 2.8 shows a parameterized spring connecting a flap element to the wing model. A flapping control surface influences on the modal analysis.

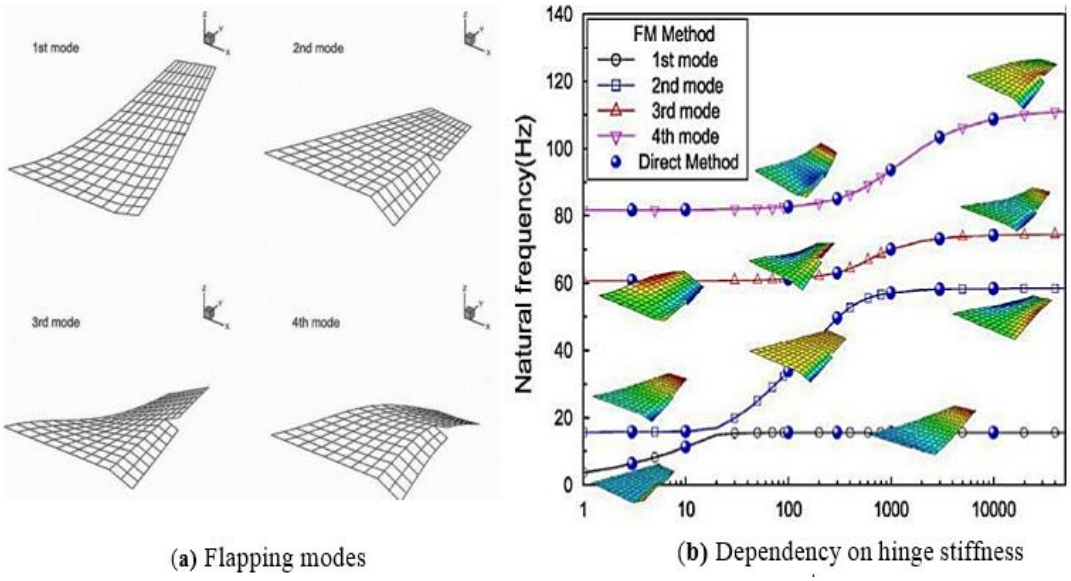

Figure 2.8: Structural deformation modes connected with a lifting surface hinge spring [69].

Figure 2.8a represents the various modes caused by flap deflection mode. The first mode seems to be a clear bending mode, similar to that of a wing with no lifting surface. The second is a flapping mode. The rest mode shapes indicate a twist-flapping mode and a bending-flapping mode, respectively.

The presence of a control surface, as shown in Figure 2.8b, has an effect on the natural frequencies of the mode shapes. Each line in this graphic defines a natural frequency and its accompanying mode shape. The mode form is unaffected by the hinge stiffness if the straight line is horizontal, indicating that no flapping mode happens. Flapping occurs in the sloping line parts. The figure shows that flapping happens in various modes when the hinge stiffness changes. When only the aerodynamic contribution is considered, these effects are neglected. As a result, this hypothesis is therefore frequently used mostly to stable or lower frequencies aeroelastic situations[1].

To make the lifting surface work, it is assumed that when a control surface is moved, an idealized point force will operate at the trailing edge of the wing in order to capture the movement of the flapping mode. The discussed point force is determined using equation (2 − 24) [70] where, $\boldsymbol{F_C}$ is the idealized control force, $\mathbf{q}$ is the dynamic pressure and $\boldsymbol{F_C^*}$ is the control coefficient. According to the slender-wing theory, adjusting the control coefficient $\boldsymbol{F_C^*}$ will not change the dynamic pressure $\mathbf{q}$ throughout the rest of the wing but will change the control force $\boldsymbol{F_C}$ [70].

$$\boldsymbol{F_C = qF_C^*} \qquad (2-24)$$

Considering that the control force $\boldsymbol{F_C^*}$ is unchanging throughout a perturbed motion. However, as the control force is also influenced by the dynamic pressure $\mathbf{q}$, this does not inevitably lead to a constant control force. Even though this approach is straightforward, it accurately simulates a flapping control that is located at the **TE** of a wing [70]. Algebraic equations such as Theodorsen's function model [71] or a look-up table that uses the input of lifting surface deflection angle δ and the effective AoA α_{eff} could be used to determine the value of the control coefficient $\boldsymbol{F_C^*}$ (see Annex A). It is still possible to employ the mode shapes that were discovered using the methods described in section 2.1, i.e., without a moving lifting surface.

2.5 Summary

The previous chapter treated the background theory for an aeroelastic wing, and by taking this into consideration, many decisions about the study of an aeroelastic wing model were made.

Table 2.1 summarizes the methodologies utilized for the multiple studies, as well as the hypotheses behind them.

Table 2.1: The methods chosen for the multiple studies and the related hypotheses.

Discipline	**Approach & hypotheses**
Structures	Structural modal superposition method in a linear time-invariant state-space system ➢ *Free-free in vacuo mode shapes* ➢ *Neglect high frequency modes* ➢ *Small deformation* ➢ *Modal damping ratio*
Aerodynamics	Look-up tables utilizing the quasi-stable α_{eff} ➢ *Subsonic flight regime* ➢ *Neglect the mode shapes with high frequencies* ➢ *Low frequency motion* ➢ *Strip theory* ➢ *Corrected aerodynamic coefficients near wing tip*
Lifting surfaces	Inclusion of lifting surfaces ➢ *Ignore lifting surface dynamics, inertia, and actuation* ➢ *Idealized lifting force at TE*
Load prediction	Summation of structural and aerodynamic loads fitted into Simscape Multibody environment
Fluid-structure interaction	Conventional serial staggered partitioned approach

Chapter 3:
Static and Dynamic Analysis of Flexible Wing Using LPM and FEA

In this chapter, an overview of modeling methods is described in section 3.1. Then, an application of modeling a rectangular-shaped wing using **LPM** is discussed in section 3.2. For comparison, the same wing is also treated using finite element import method (see section 3.3). Thereafter, verification of the validity of the obtained results from the two methods is carried out using modal analysis through Ansys Workbench software, as described in section 3.4. In addition, general conclusions that clarify the advantages and disadvantages of each method are discussed in section 3.5. Lastly, a short summary is provided in section 3.6. Note that the analytical modeling used in both methods is referred in [42], [73] in order to model a flexible body through Simscape Multibody environment.

3.1 Overview of Modeling Methods

There are multiple methods for modeling flexible structures. **LPM** and FE import method are one of the most widely used. However, these can be computationally expensive and frequently necessitate special treatment when applied to large multibody models, particularly those with several physical domains and complex control systems. For extremely detailed discretization and large numbers of degrees of freedom (many **GBE**s and joints in the **LPM** case, many states in the **FEA** case), the dynamics become difficult to solve analytically and numerically.

This study looks at two effective methods for capturing small, linear, and elastic deformations of a prototype of rectangular wing in Simscape Multibody models.

3.2 Modeling wing using Lumped-parameter Method

The behavior of flexible bodies has been studied using a variety of methods, and Simscape Multibody is one of the useful ways for understanding this behavior. In the present study, a rectangular wing is modelled using an adaptation of the Lumped parameter method.

In **LPM**, the structure is divided into smaller parts a number of generalized beam elements that are all identical. Each of the aforementioned beam elements is composed of a body-joint-body combination, as seen in Figure 3.1. The **LPM** essentially entails modeling the structure as a collection of components. The stiffness and damping characteristics of each flexible element are captured by internal springs (k) and dampers (b), which are used to derive the static and dynamic response [7]. Each flexible unit (element) is composed of two rigid body elements named (m1, m2) that are connected through a revolving joint block.

In order to achieve the strongest liaison among units, the **LPM** wing is more precisely approximated as a group of discrete flexible pieces joined together through welding (W). Actually, the ribs of the wing are replaced by the welding (W) [72]. The coupled unit effect has an impact on the stability. Each flexible wing unit offers one internal degree of freedom to the body for each type of bending it represents.

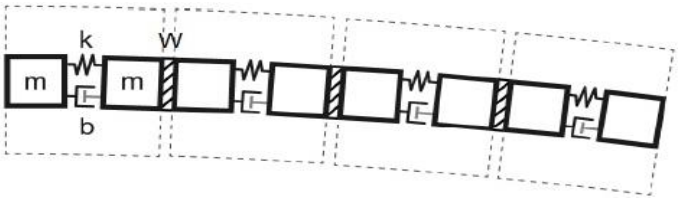

Figure 3.1: A flexible cantilever beam model according to the lumped-parameter method [73].

Additionally, the representation in Figure 3.2 (top) depicts the suggested generic wing construction. The frames Base (B) and Follower (F), which serve as the block's ports, are linked via a series of flexible elements. The flexible joint in this situation, as depicted by the Simscape Multibody model in Figure 3.2 (down), tries to combine two bodies with a single degree of freedom of rotation. This joint, in turn, moves the base (B) and follower (F) in accordance with a single time-varying transformation. The reciprocity movements of the

base (B) and follower (F) ensure that the origins of the frame correspond throughout the simulation. One of the revolutionary primitives' primary functions is to provide a degree of freedom for rotation. The primitive Pz performs this transition, causing the follower frame to rotate in accordance with the base frame. Moreover, the variation in the element number is possible, as it shown in Figure 3.3. This last describes the chain of four element connect together in order to construct the **LPM** wing.

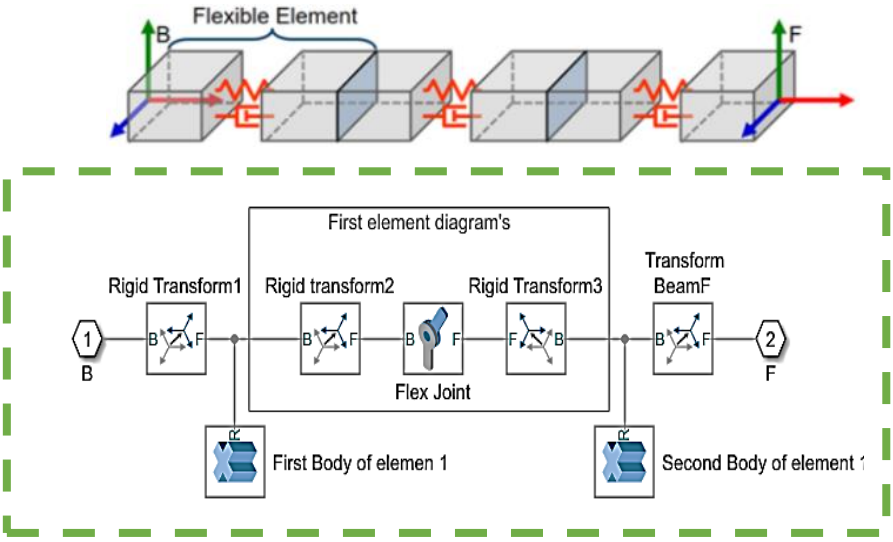

Figure 3.2: top: Generic structure of the wing, down: Simscape Multibody model of a flexible element [72],[73].

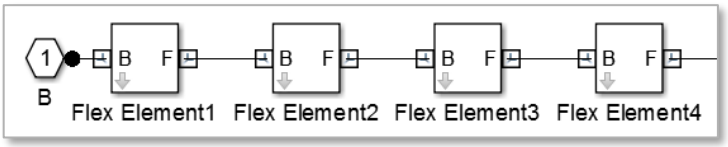

Figure 3.3**:** Chain of four elements.

3.2.1 Description of the Simulink model

The body's boundary conditions, which are enforced by joints, kinematic constraints, or explicit forces and torques, complete the model. A flexible wing is depicted in Figure 3.4 utilizing the **LPM** model. The numerous blocks are connected to the world frame and to one another. The flexible wing block includes all the components required to construct the **LPM**, including the flexibility type, number of components, geometry, damping factor, and material properties.

We are able to apply an external force and torque on the attached frame from the load's block. The physical signal inputs define the force and torque. The deflections of the interface frames relative to the frames of the flexible body model are detected using a sensor block. As inputs to the deformation model, the sensor signals (position, velocity, and acceleration) are crucial [72].

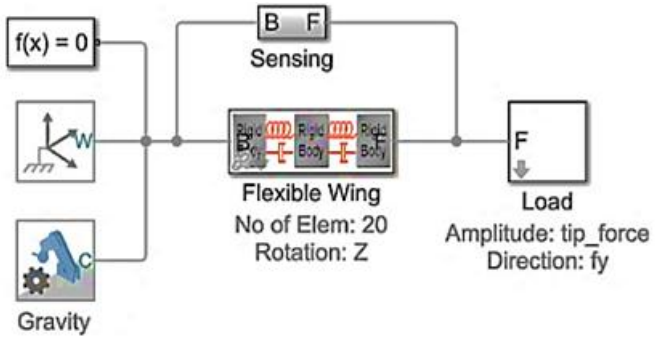

Figure 3.4**:** Simscape Multibody model of the complete system according to **LPM** [72].

Several results can be obtained to verify the static and dynamic deflection of the structure. This model is set up to allow the identification of the various natural frequencies of the wing at various modes through the application of linearization techniques [73]. Figure 3.5 describes a lumped-wing with 10 flexible elements.

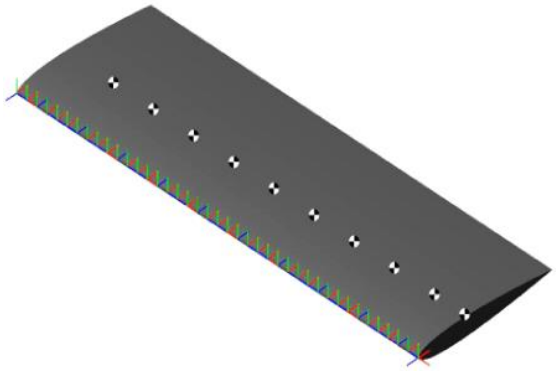

Figure 3.5: Simscape Multibody wing model according to the **LPM**.

Spring coefficient: The following mathematical formula can be used to determine the stiffness of the revolute joint:

$$k = \frac{E.I}{l}\left[\frac{N.m}{rad}\right] \qquad (3-1)$$

From equation $(3-2)$ we can determine the length l of an undeformed flexible wing unit:

$$l = \frac{L}{n}[m] \qquad (3-2)$$

Damping coefficient: Two damping factors define the wing's dampening. These two elements allow the damping to adjust to the wing's size and material. Literally, when the characteristic of material such as density ρ increases, the damping ratio ζ also increases, and the natural frequency ω_n decreases.

- ✓ Elastic damping factor ($f_{elastic}$): Damping factor for bending and elongation.
- ✓ Shear damping factor (f_{shear}): Damping factor for torsion.

The damping coefficient C used in the flexible elements is calculated according to the following formulas [42]:

$$C_{a_{bending}} = f_{elastic}.\frac{E.I}{l}\left[\frac{Nm}{(rad\ sec^{-1})}\right] \qquad (3-3)$$

$$C_{b_{bending}} = f_{elastic}.\frac{E.A}{l}\left[\frac{Nm}{(rad\ sec^{-1})}\right] \qquad (3-4)$$

$$C_{torsion} = f_{shear}.\frac{E.J}{l}\left[\frac{Nm}{(rad\ sec^{-1})}\right] \qquad (3-5)$$

Table 3.1: Wing dimensions, moment of inertia and material properties [72].

Length (L)		0.3 $[m]$
Chord length at wing root (C)		0.1 $[m]$
Area cross-section (A)		$8.217.10^{-4}$ $[m^4]$
Area moment of inertia (Ixx)		$6.803.10^{-9}$ $[m^4]$
Area moment of inertia (Iyy)		$1.906.10^{-6}$ $[m^4]$
Torsion J		2.6710^{-8} $[m^4]$
Aluminum Material	Density (ρ)	2800 $[kg/m^3]$
	Young Modulus (E)	70.10^3 $[MPa]$
	Shear Modulus (G)	27.10^3 $[MPa]$

3.2.2 Simulated deflections according LPM

In the MATLAB environment, simulations of the model under consideration are run, and the results are talked about in the sections that follow.

3.2.2.1 Simulation of Static Deflection versus Number of Elements

In this study, it is not required to be restricted to a set of elements fewer than 10, since it is also important to consider topic optimizations and understand how far an element may be taken in order to reduce the vibrations' amplitudes [72]. The static deflection of a cantilever wing can be calculated using Euler-Bernoulli beam theory [72]. The bending moment, shear force, and wing deflection can be figured out using mathematical axioms dedicated to engineering beam applications [73]. In this case, a rectangular wing can be regarded as a cantilever beam, so the analytical deflection has been calculated using equation $(3-6)$.

$$\delta = \frac{\mathrm{q}.L^4}{8.E.I} = 0.0048[m] \qquad (3-6)$$

$$\mathbf{q} = \rho.A.g = 2.2573\ 10^3 \left[\frac{N}{m}\right] \qquad (3-7)$$

where, $\mathbf{q}$ is the uniformly distributed load on the wing. Because gravity has negligible values, we multiplied it by 100 to clearly show the wing's deflection in the simulation. By substituting the value of q into the equation $(3-6)$ the value of analytical deflection is $\delta = 0.0048\ [m]$. The remaining parameters used in equation $(3-6)$ were previously defined in Table 3.1. The value is determined by the simulated model is equal to $\delta = 0.0047\ [m]$.

In Figure 3.6 the comparison between the tip deflection of the wing versus the variation of element number modeled is graphically presented. In the beginning of the simulation, more specifically in the case of 5 elements the deflection of the wing gives approximately the same analytical value's deflection. When the number of elements increases (more than 5 elements), the results of transient simulations closely match theory, especially as the number of elements grows [72].

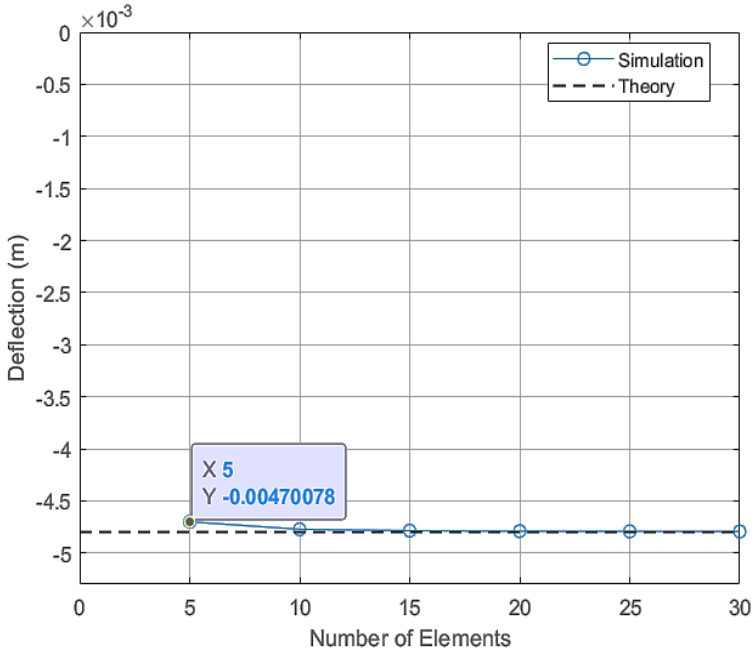

Figure 3.6: Static vertical deflection [72].

3.2.2.2 Case I: Distributed Gravitational Load

The wing is just susceptible to its own weight in this section [72]. The vertical deflection of the wing tip is displayed versus time in Figure 3.7. The tip of the wing lightly oscillates between $[0, 0.095\ m]$ for around 1.5 seconds before reaching equilibrium.

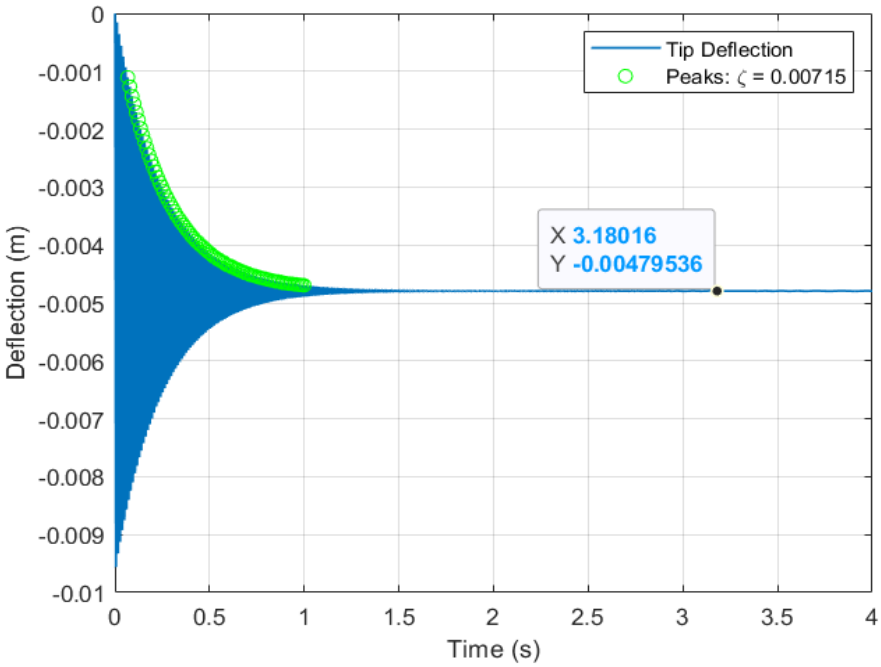

Figure 3.7**:** Vertical deflection of wing tip due to distributed gravitational loads [72].

3.2.2.3 Case II: Upward Point Force

In this case, as shown in Figure 3.8, the wing structure is subjected to only an upward point load of 230 $[N]$ during 4 seconds. The point force is removed after 4 seconds allowing the wing to vibrate lightly between the range of $[0\ 0.0075\ m]$ and to return to its state of equilibrium. The damping ratio ζ is determined using the peaks. The analytical deflection at the free end of the wing is calculated using equation $(3-8)$.

$$\delta = \frac{F.L^3}{3.E.I} = 0.0043[m] \qquad (3-8)$$

Using equation $(3-8)$, where $F = 230\ [N]$, the obtained value from the simulation of vertical deflection is: $\delta = 0.0043\ [m]$. The damping ratio ζ can be found from the logarithmic decrement [73].

$$\zeta = \frac{1}{\sqrt{1+(\frac{2.\pi}{\delta})^2}} \qquad (3-9)$$

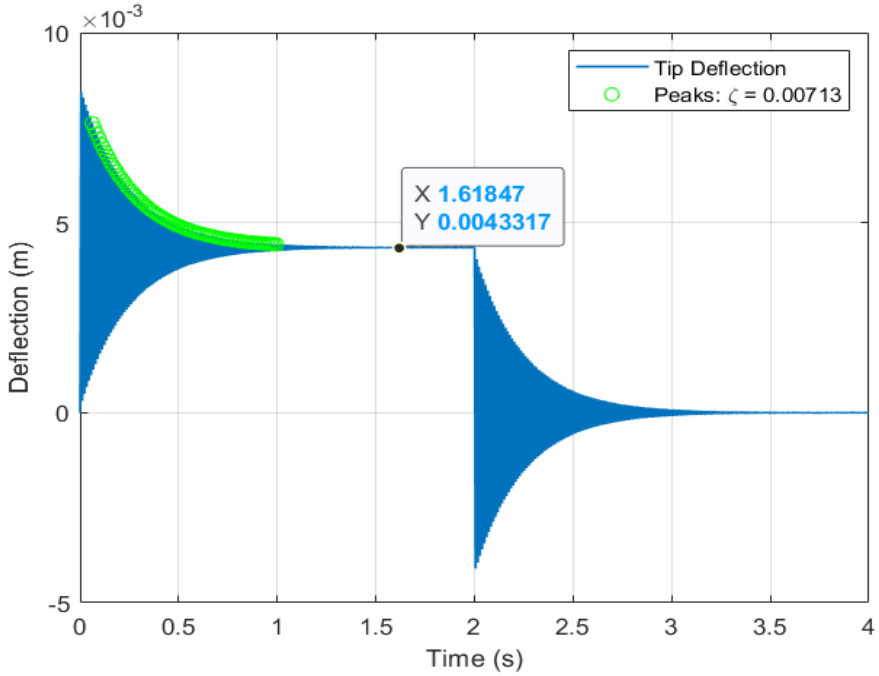

Figure 3.8: Vertical deflection of wing tip due to only an upward point force [72].

3.2.2.4 Comparison of elements' deflection

In this simulation example, different elements are utilized to define the bending of the wing. For example, the wing is constructed of 10, 20, and 30 elements to show what happens as the number of elements increases [72].

Number of elements: In terms of oscillation values, the three graphs in Figure 3.9, representing 10, 20, and 30 elements, respectively, are comparable. Increasing the number of elements makes it possible to reduce the wing's deflection. The number of elements and the deflection of the wing have an inverse relationship.

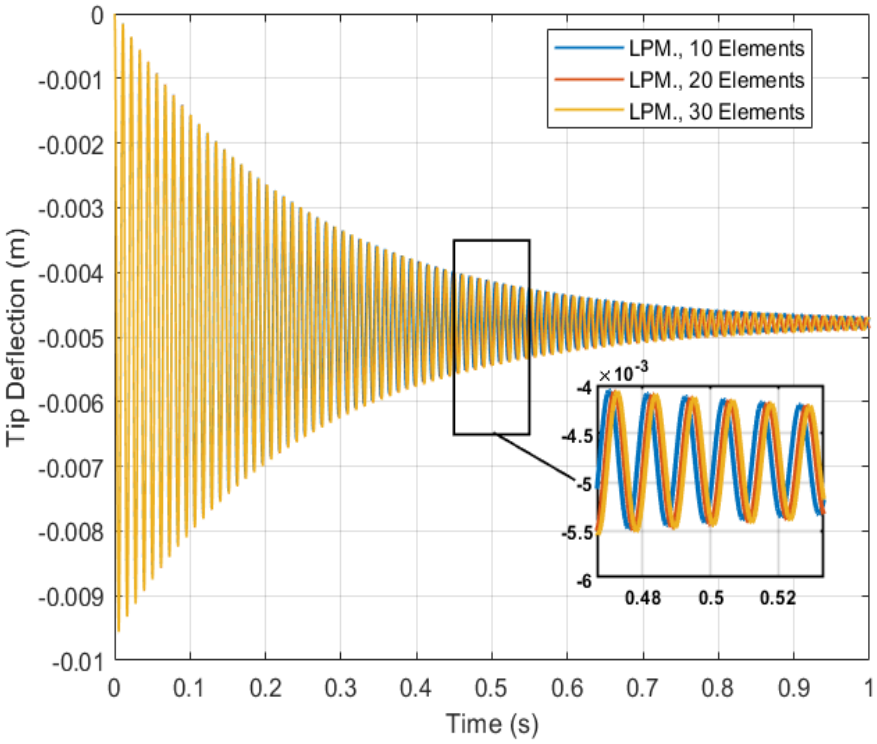

Figure 3.9: Effect of increasing the number of flexible elements in **LPM** [72].

As a result, it can be observed from Figure 3.9 that the wing almost oscillates as the number of elements grows. Increasing the number of elements by more than 10 is generally the most effective way to reduce the deflection of the wing.

3.2.2.5 Mode shapes

Linearization is used to determine the various natural frequencies ω_n of the mode shapes. The natural frequencies ω_n can be predicted using equation $(3-10)$. For the boundary conditions in this model (fixed-free), $\beta_n = [3.52\ 22\ 61.7\ 121]^{\mathrm{T}}$.

$$\omega_n = \frac{\beta_n . \sqrt{(\frac{E.I}{\rho.A})}}{L^2} \ , f_n = \frac{1}{2\pi}\sqrt{\frac{k}{m}} \qquad (3-10)$$

The first four mode shapes of the wing, which were produced via LPM in Matlab code, are shown in Figure 3.10. In this last, mode shape 1 describes the first pure bending mode of the wing with a lower natural frequency. Surprisingly, mode shape 4 has a greater natural frequency and it represents the pure torsional mode. The rest of the modes have lower frequencies and greater amplitudes; thus, the lower modes are more dominant than the higher modes. For this reason, in **LPM** and modal approach we should neglect the higher modes.

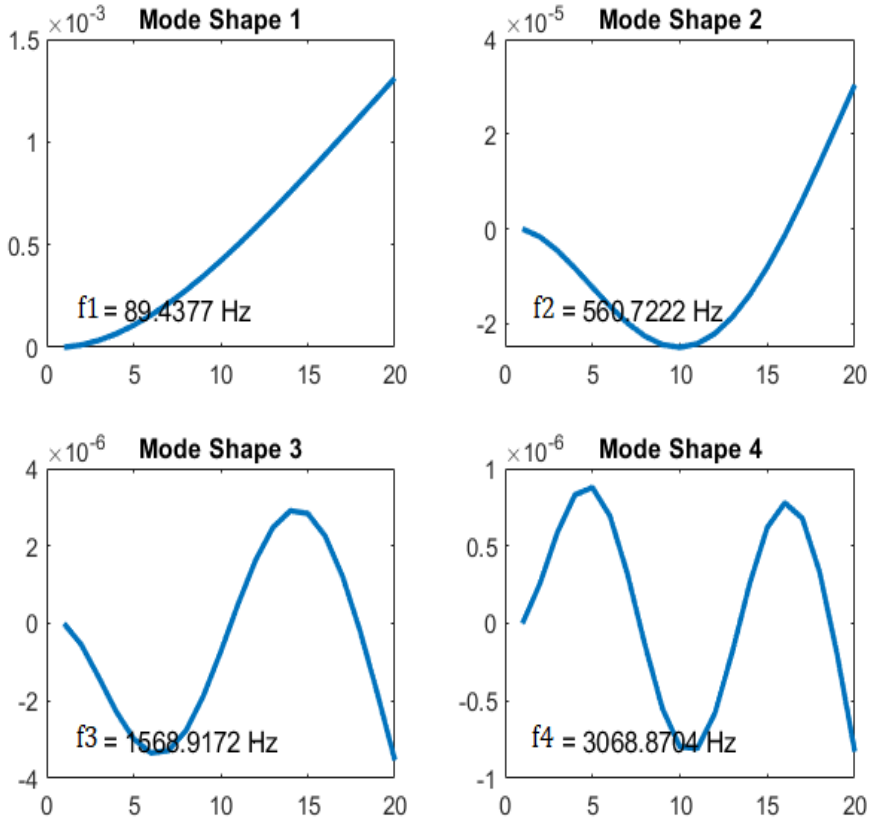

Figure 3.10: First four mode shapes [72].

It is important to note that the current deflection formulas correspond well to the simulated wing model. thus, the numerical simulation of the wing's deflection and the analytical deflection values correspond fairly well [72].

3.3 Modeling of a flexible rectangular wing using finite element import approach

In this section, the same wing structure is modeled using another powerful approach of flexibility by superimposing deflection on rigid wing motion. Figure 3.11 shows the generic structure of the body represented by these blocks. Each frame (represented by the triad) can

move along six degrees of freedom with respect to the rigid body. The deflection is calculated using data supplied by finite element software and entered in the block mask. The rigid body is given additional degrees of freedom, and the force controlling that deflection is determined using stiffness and mass matrices obtained from finite element software, namely Ansys Workbench, or by applying the Graig-Bampton method through Matlab code in order to reduce the size of the finite element model (i.e., the size of mass and stiffness matrices).

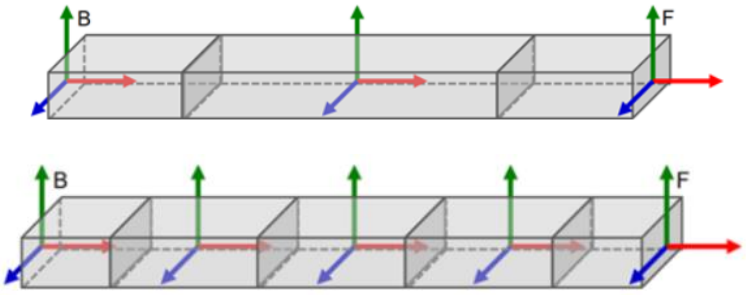

Figure 3.11: Three interface frames and five interface frames, respectively, show how a beam is built in general [73].

The finite element import method models a flexible wing structure using a deflection model that relies on data imported from finite element software. Wing deflection is superimposed on rigid wing motion. The mass of the structure can be assigned to the rigid wing or distributed across each interface frame.

3.3.1 Modeling methodology:

1- Create CAD and FE model in FEA software, step 1 and 2 in Figure 3.12.

2- Define part interface frame step 2 in Figure 3.12.

3- Import data (Mass matrix $[M]$ and Stiffness matrix $[K]$ into Simscape Multibody, these matrices are obtained from FEA models via modal reduction techniques. This leads to combine a multibody **FEA** (one from ANSYS the other from MATLAB). Refer to steps 3 and 4 in Figure 3.12.

4- Connect joints, forces Figure 3.13.

5- Simulate.

3.3.2 Subsystem explication

State-space model: From Figure 3.12, data exported from finite element software is used within the state-space block to calculate the force resisting the deformation of the rigid body. One interface frame has no degrees of freedom associated with it so that the rigid body modes of the flexible body are not added twice.

Rigid Body Frame: As it shows from Figure 3.12**,** the index of the interface frame to which the rigid body part of the subsystem is rigidly attached. At that point, there are no deformations because the rigid body is used as a point of reference to measure deformations.

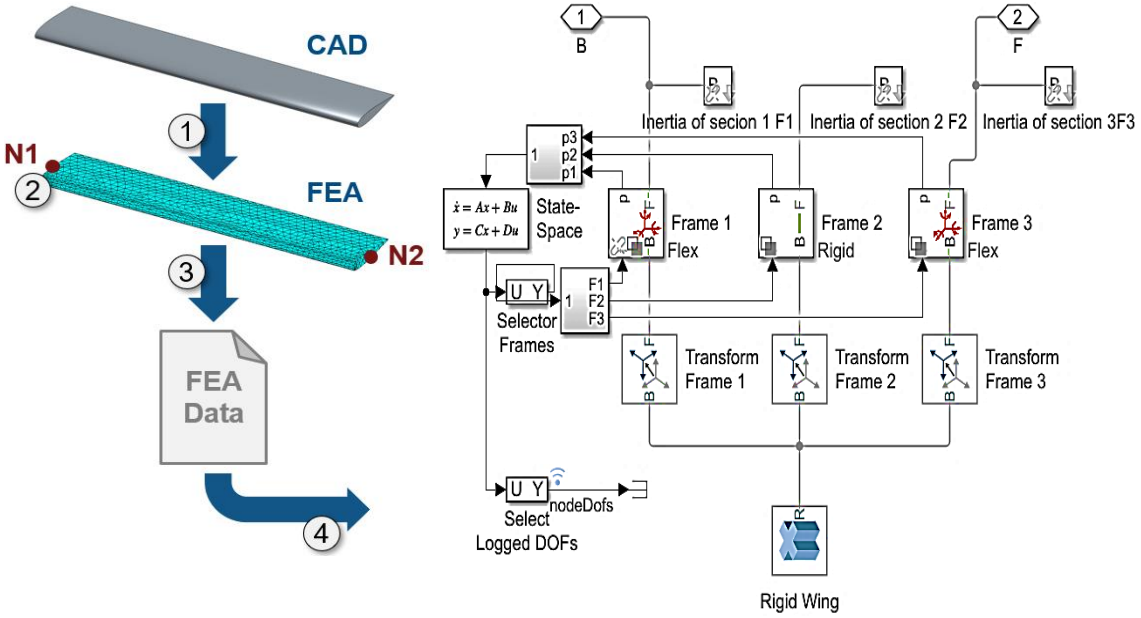

Figure 3.12: Flexible wing modeling workflow.

Interface frame degrees of freedom: In the same figure, an array of size n x 3, where n is the number of interface frames, containing the locations relative to the reference frame of the body in its undeformed configuration and with components resolved into that same frame. These coordinates must match up with where the boundary nodes were placed when the Craig-Bampton reduced model was made in the FEA software.

Generally, the subsystem shown in Figure 3.13 models the flexible wing. It consists of a rigid wing and a number of interface frames. In our case, we used two types of modeling:

flexible wing with three interface frames and flexible wing with five interface frames. All interface frames except one have six degrees of freedom between them and the rigid body.

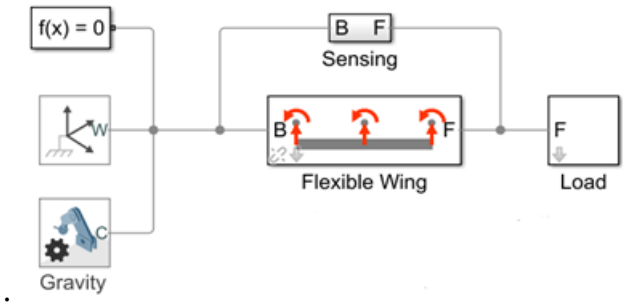

Figure 3.13: Simscape Multibody model of the complete system for 3 interface frames according FE import method.

Bushing joint subsystem: A bushing joint shown in Figure 3.14 models the degrees of freedom for the interface frames. Each degree of freedom's position, velocity, and acceleration are measured and fed into the state-space block equation. The forces and torques calculated by the state-space block are applied to this joint in order to capture the deformation response of the structure. A filter is required to break the algebraic loop.

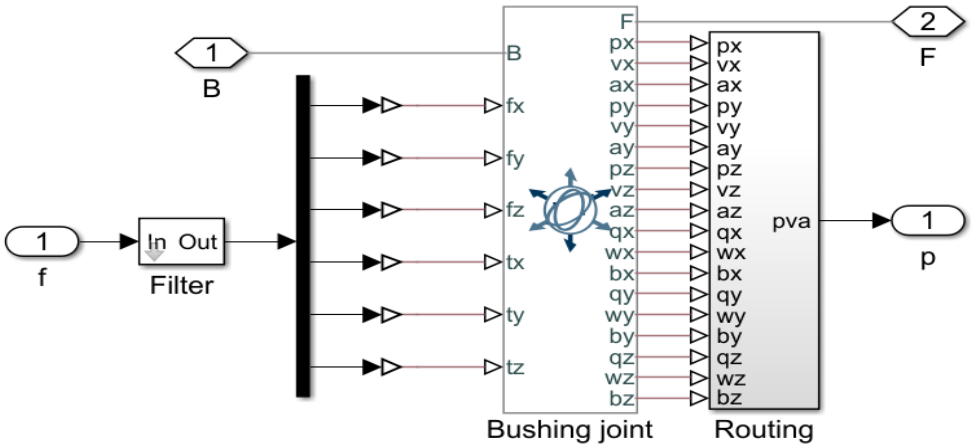

Figure 3.14: Bushing joint subsystem.

3.3.3 Simulated deflections according FE import Method

Referring to section 3.2.2, Figure 3.15 and Figure 3.16 show the time versus deflections of the tip of the wing under a distributed gravitational load and an upward point force which is applied at the free end of the wing (**Case II**). In each example, the wing is lightly damped and achieves stability after about four seconds. After four seconds, the point force

is eliminated, enabling the wing back to its original position of zero deflection. Only the internal spring and damping torques of the wing have influence on the return to equilibrium.

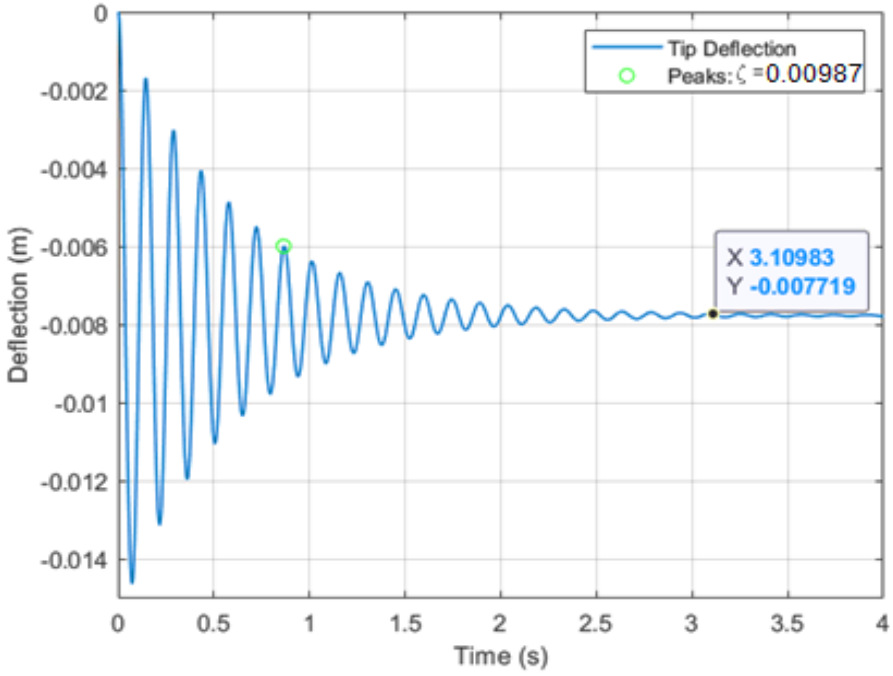

Figure 3.15: Tip deflection due to a distributed gravitational load.

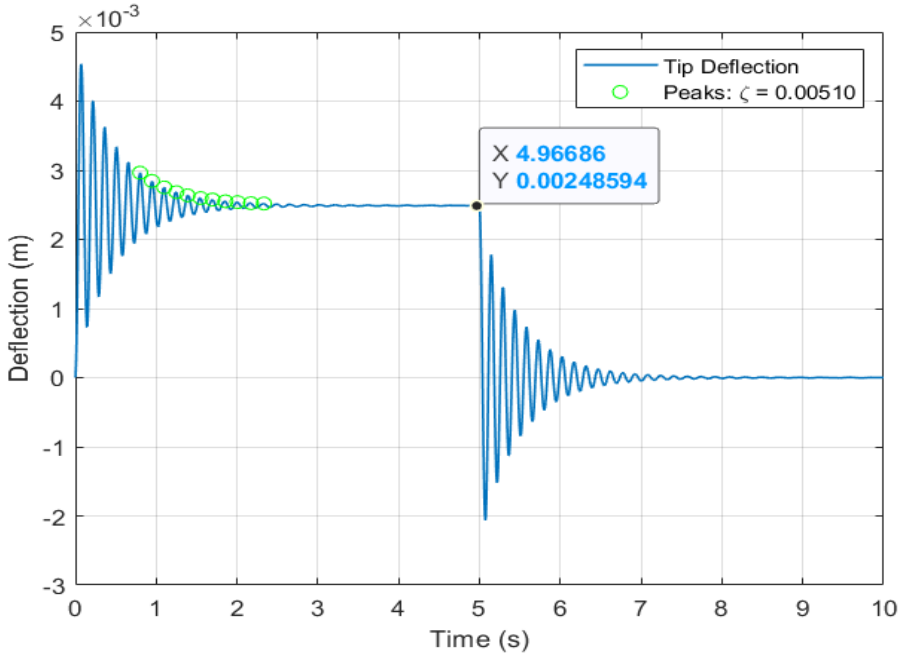

Figure 3.16: Tip deflection due to an upward point load.

According to the simulation's results, the tip of the wing attains a state of equilibrium deflection of $\delta = -0.007719\ [m]$ under a uniform gravitational load and

$\delta = 0.004285\ [m]$ under an upward point load. Comparing these values to the results of the analytical computations, $\delta = -0.0048\ [m]$ for a uniform gravitational load and $0.0043\ [m]$ for a tip load, respectively.

Dynamic modes: The main goal in Figure 3.17 and Figure 3.18 is to validate the damping deflection of the wing and to determine the effect of increasing the number of the dynamic modes in FE import method.

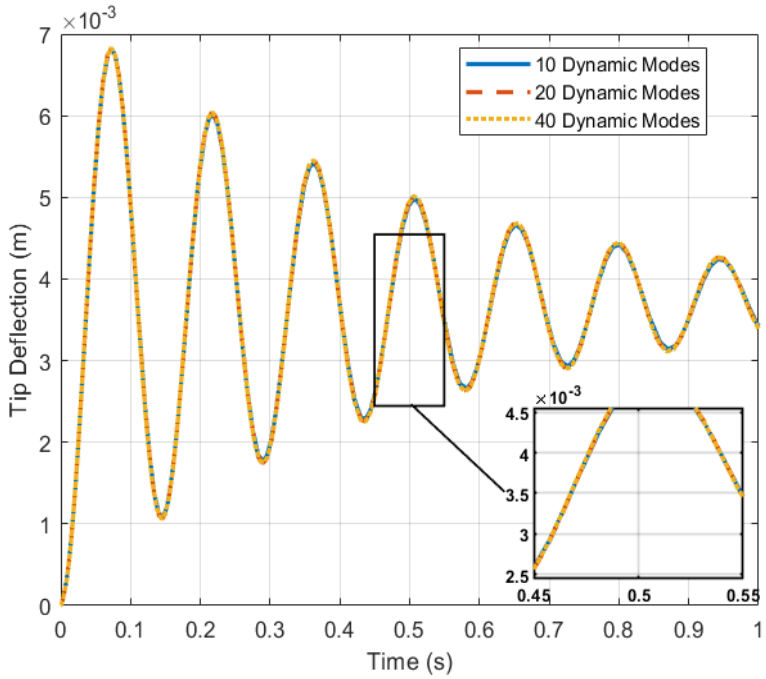

Figure 3.17: Effect of increasing dynamic modes (3 interface frames).

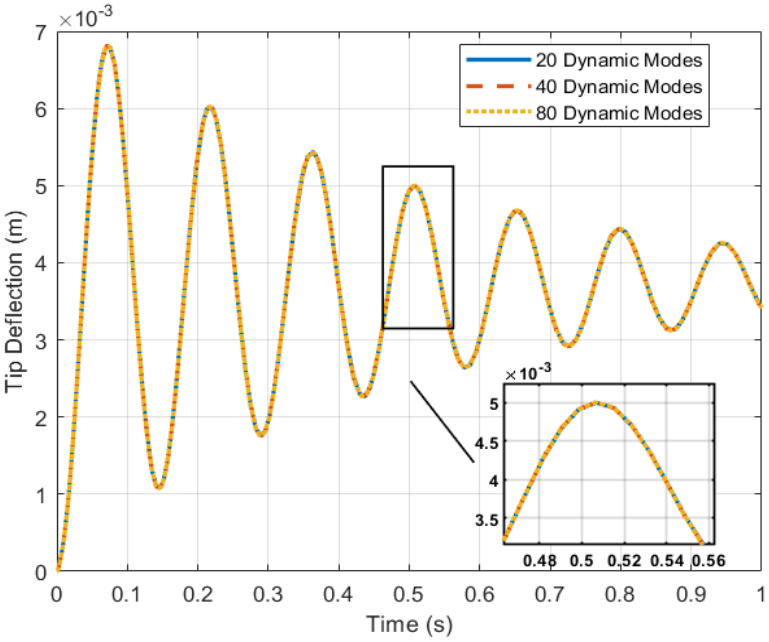

Figure 3.18: Effect of increasing dynamic modes (5 interface frames).

The plot in figures Figure 3.17 and Figure 3.18, respectively, shows the effect of increasing the number of dynamic modes included in the imported data from finite element software for a model with 3 interface frames and 5 interface frames, respectively. The **LPM** gives accurate results for both static and dynamic bending when the number of discrete elements changes. Similar for the second method, when adding more dynamic modes and changing the interface frames leads to an accurate result.

As shown in Figure 3.19, this plot compares the vertical deflection of a wing due to an upward point force. Three (03) interface frames and five (05) interface frames are compared in order to validate the change of the interface frames.

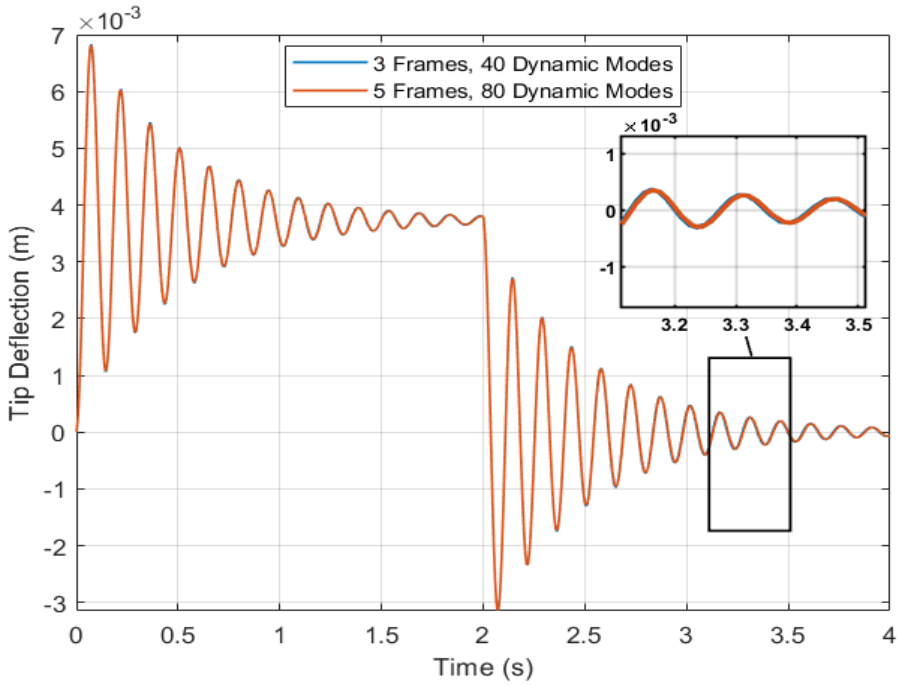

Figure 3.19: Compare vertical deflection of wing with 3 interface frames, 5 interface frames.

The plot shown in Figure 3.20 compares the simulation results of both wing models. Approximatively, the wing deflection in both methods is roughly the same. This step was performed to set the damping factor, which is most reliably set using measured data. The elastic damping factor in the lumped parameter model was tuned until the simulation results matched the results from the FE import beam model. It should be noted that all the obtained simulations of comparison study are done using case II.

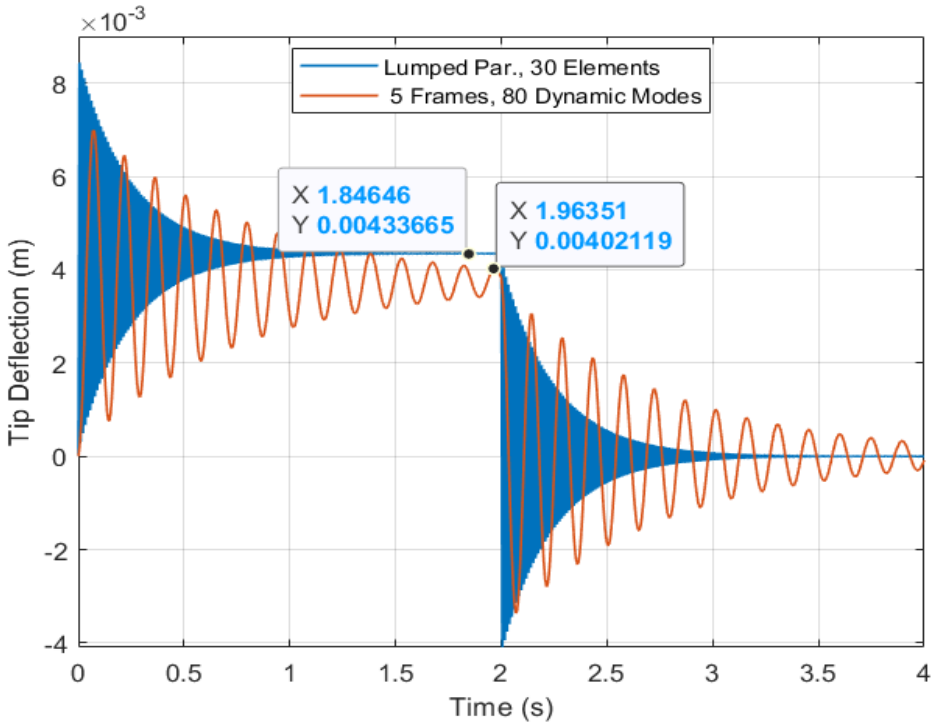

Figure 3.20: Compare vertical deflection of wing using LPM and FE import method.

3.4 Ansys Simulations using Modal Analysis

In comparison, a third method was developed using Ansys workbench software to validate the model used in sections 3.2 and 3.3 once more. The overall deflection and various modes of the wing are determined by structural and modal analysis using the finite element method. These software programs have automatic algorithms that automatically extract the data needed for pre- and post-processing. To confirm once more the minimal deflection of the wing structure, a comparative evaluation of the resulting deflection using analytical calculation, **LPM**, FE import method, and **FEA** in ANSYS software is carried out in Table 3.2.

Table 3.2: Comparison study of the obtained deflection from analytic, Matlab and Ansys.

	Equilibrium deflection (analytic)	**LPM**	**FE import method**	**Ansys software simulations**
Self-weight	$0.0048\ [m]$	$0.0047\ [m]$	$0.0077\ [m]$	$0.00456\ [m]$
Tip load	$0.0043[m]$	$0.0043\ [m]$	$0.0042\ [m]$	$0.00428[m]$

For comparison, Table 3.3 summarizes the different values of the vibration frequencies of mode shapes, which are obtained from analytical theory, the lumped parameter method, the finite element import method, and finite element analysis in Ansys software. To obtain a similar value of vibration frequencies, we combined 30 elements of the wing structure in the **LPM** and 5 frames with 80 dynamic modes in the FE import method.

Table 3.3: Comparison study of mode shapes obtained from analytical theory, lumped parameter method and finite element analysis.

Approaches	**Vibration frequency [Hz]**			
Analytical Calculations	89.54	560.72	535.2	2866.9
LPM (30 elements)	89.43	560.72	1568.91	3068.87
Ansys software	91.54	562.02	1535.2	2866.9

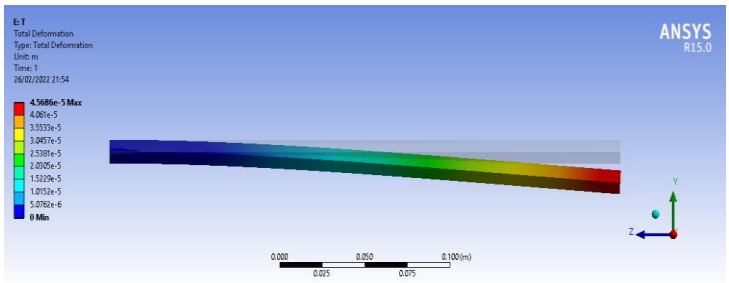

(a) Self-weight, $\delta = 0.00456\ m$

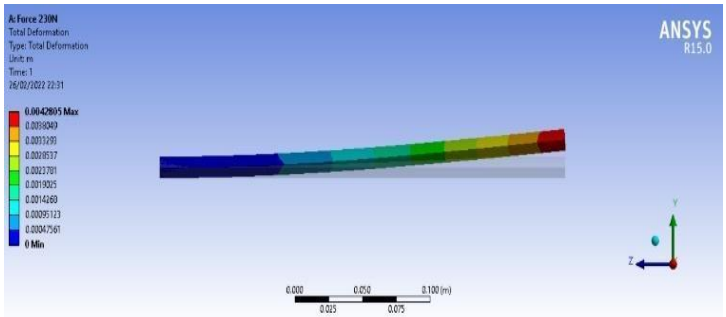

(b) Tip load, $\delta = 0.00428\ m$

Figure 3.21**:** Upward and downward deflections of wing tip.

Obviously, as it is shown in Figure 3.21, the first case depicts the bending of the wing when it is subjected to its own weight. The second case is returned to the tip load. Logically, the most influenced zone (red color) exists in the free end of the wing and it defines the bending of this last. In a comparable way, Figure 3.22 shows a comparative examination of the various natural frequencies using both methods. The similarity of the different natural frequencies derived from the Matlab code and the Ansys program is demonstrated by both curves.

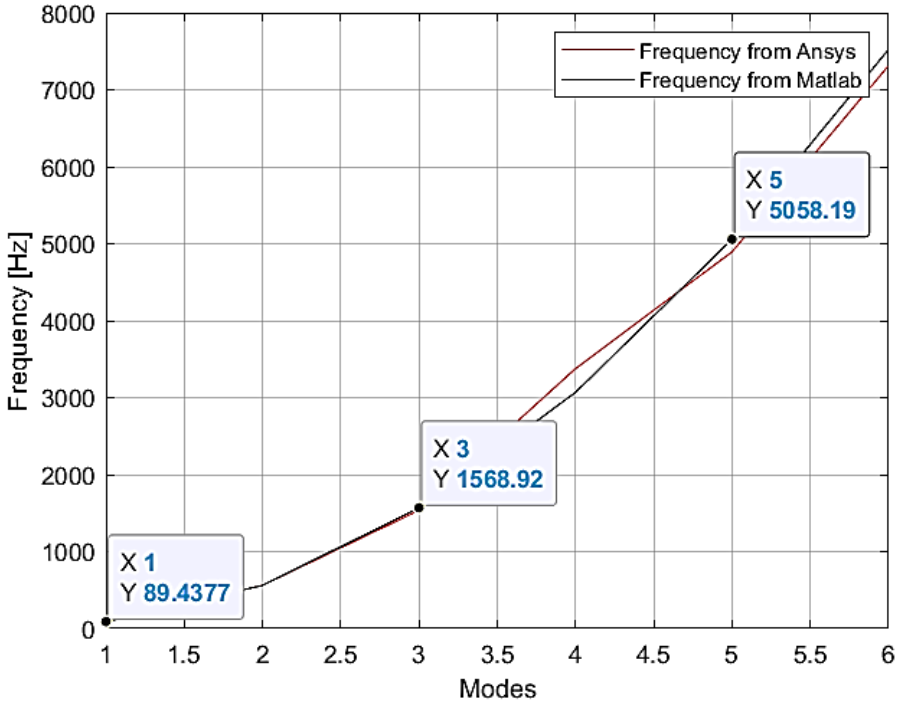

Figure 3.22: Comparison of mode shapes.

Figure 3.23 (a-d) depicts the first four mode shapes acquired from the finite element software, similar to Figure 3.10, where the mode shapes were derived using Matlab. To be clear, the mode shapes that were previously obtained using **LPM** exactly match the results of the finite element method in terms of natural frequencies and mode shapes.

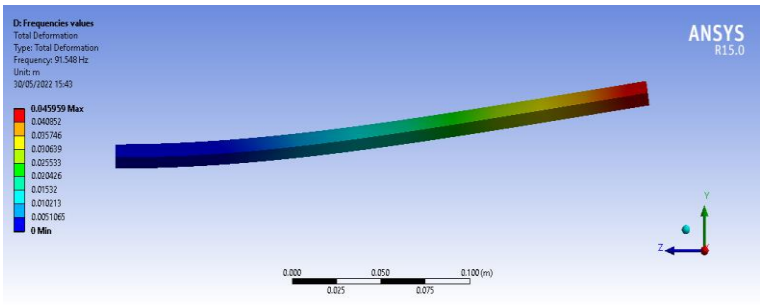

(a) First mode shape

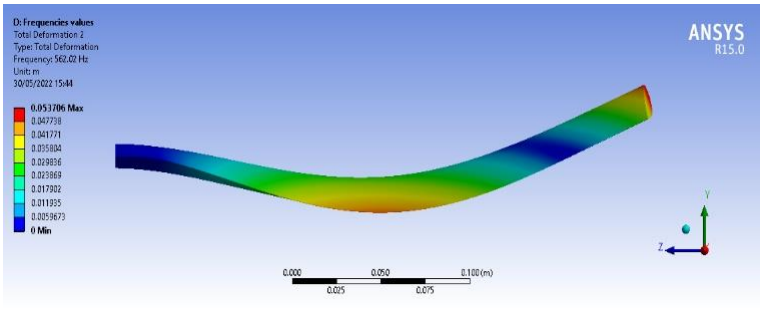

(b) Second mode shape

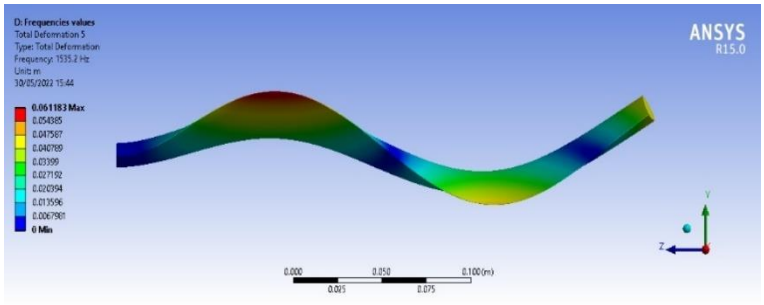

(c) Third mode shape

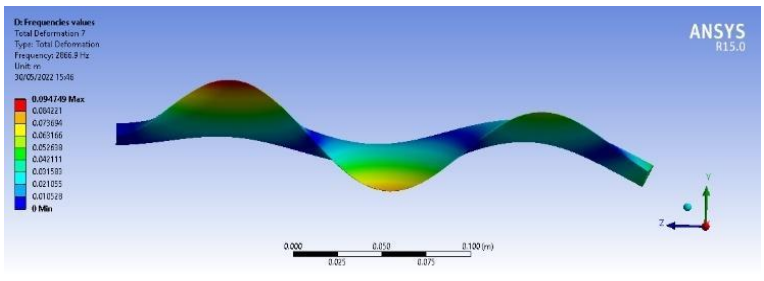

(d) Fourth mode shape

Figure 3.23: First four mode shapes obtained from finite element software.

3.5 General conclusions

Each approach has benefits and drawbacks [42]. For modeling flexible bodies with chain-like geometries, **LPM** is simple and rapid in term of implementation given that it takes a place in Simscape Multibody' toolbox, but it is more complex, ambiguous, and hence less helpful for modeling bodies with great dimensional geometries, such as wing structures with variable cross-section. The curvature bending moment is also represented by the reduction to independent GBEs. It seems to be difficult to apply the moment on each joint as a function of its own and neighboring joints' deflections in order to accurately estimate the curvature moment.

Hence, implementing the **FEA** approach is simple for any geometry as well as any number of degrees of freedom. Additionally, it is better suited to issues with control design and analysis. Once your FEA is integrated into a Simscape Multibody environment, this method introduces algebraic loops while Simulink searches for an appropriate solution for the acceleration of the massless bodies [42].

The **LPM** can be developed to represent more complicated geometries, such as airplane wings, as mentioned in section 2.1.2, although other method, such as the modal approach, is more suited for modeling these types of geometries [42]. Moreover, the **LPM** also becomes more accurate when it is used with a real experimental equipment.

To this end, the above comparative study can be extended to model a flexible aeroelastic wing using a developed modal superposition model based on state-space systems. Because the concept of the wing by FE import method into Simscape Multibody appears to be a close match to the modal approach, particularly in behavior response. Additionally, in both methods, the state-space system is the most important part to determine the structure’s position, motion and orientation. The use of this approach paves the way to predict the structural and aerodynamic forces and overall deformation of the moving wing section in different aeroelastic nodes (treated in next chapter). For this reason, the methodology of the aeroelastic wing model will be detailed and validated using structural modal approach in chapter 5.

3.6 Summary

In this chapter, a comparative study was made using **LPM**, the FE Import method, and **FEA** in Ansys Workbench. The two first approaches are provided in MATLAB code and the Simscape Multibody environment, also called "Simscape Multibody," while the third method is created in ANSYS and it is used to confirm the obtained results of the wing's deflection from the Simscape Multibody model.

Approximatively, both methods are a perfect match when it comes to modeling the dynamics of simple flexible structures that have a constant cross-section. Furthermore, the obtained results from both methods provide nearly the same results as in the third approach, namely the upward and downward deflection as well as mode shapes from the conventional formulas that fit in with the deflection obtained from the discussed model in Simscape Multibody. Thus, the analytical deflection values are a good match with the simulation wing's deflection.

The lumped parameter approach and the finite element import method in Matlab and Simscape Multibody can be used to describe the static and dynamic behavior of simple flexible geometries in a reliable way.

Chapter 4:

Modeling Aerodynamic Loads Using MATLAB Code and FEA

In this chapter, a static study is performed on a standard aircraft passenger. Firstly, the analytical study of structural and aerodynamic loads is presented through Matlab environment. Secondly, the different aerodynamic loads such as Aerodynamic lift, weight of the wing structure and weight of fuel stored in wing are defined in [75] and discussed in the following sections. Thirdly, the total load profile is derived by coupling the three components previously mentioned. Finally, the aircraft's parameters are implemented in the model in order to provide results for the standard aircraft.

4.1 Aerodynamic Lift

As it is show in Figure 4.1, the distribution of lift density q_L is defined. Then, the lift coefficient ka including units and express lift as a function of the aircraft weight W_{total} is solved.

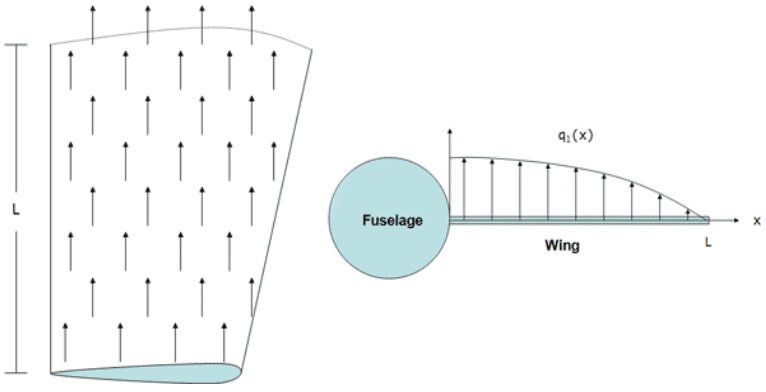

Figure 4.1: Lift on the wing [27].

From Figure 4.1, seemingly, the lift profile has the following elliptical equation:

$$q_L(x) = ka\sqrt{L^2 - x^2} \qquad (4-1)$$

Integrating along the length of the wing to obtain a lift load.

$$LiftLoad = \int_0^L ka\sqrt{L^2 - x^2}dx \quad (4-2)$$

$$LiftLoad = \frac{\pi L^2 ka}{4} \quad (4-3)$$

For our axisymmetric model of half the plane of the aircraft load factor (n) that leads to mathematically writing:

$$n/2 = LiftLoad/W_{total}$$

From [27], the load factor (n) takes a value of 1 when straight and level flight are concerned, while it exceeds the value of 1 during other conditions. Precisely, the lift surpasses the aircraft weight. The lift profile coefficient ka is figured out. Then, the resulting ka term is substituted into q_L, the expression of $q_L(x)$ is:

$$q_L(x) = \frac{2\ W_{total}\ n\ \sqrt{L^2 - x^2}}{\pi\ L^2} \quad (4-4)$$

This analytical model paves the way to understanding the various parameters effect on the lift load. For straight flight, equation $(4-2)$ becomes: The lift occurs at the base of the wing when $(x = 0)$.

$$q_L(x) = 2W_{total}/\pi L \quad (4-5)$$

4.2 Load due to the weight of the wing structure

The weight of the wing structure is shown in Figure 4.2. Assuming that the load is proportional to chord length (L), which is greatest near the root (C_O) of the wing and tapers off linearly, it is getting closer to the wing's tip (C_T). The equation $(4-6)$ is then used to calculate the weight of the wing structure.

$$q_{Wing} = kw\left(\frac{C_T - C_O}{L}x + C_O\right) \quad (4-6)$$

Integrating q_{Wing} along the length of the wing to obtain the total load due to the weight of the wing structure.

$$\text{structLoad}_{\text{total}} = \int_0^L kw\left(\frac{C_T - C_O}{L}x + C_O\right)dx \qquad (4-7)$$

$$\text{structLoad}_{\text{total}} = \left(\frac{C_O\, L\, kw}{2} + \frac{C_T\, L\, kw}{2}\right) \qquad (4-8)$$

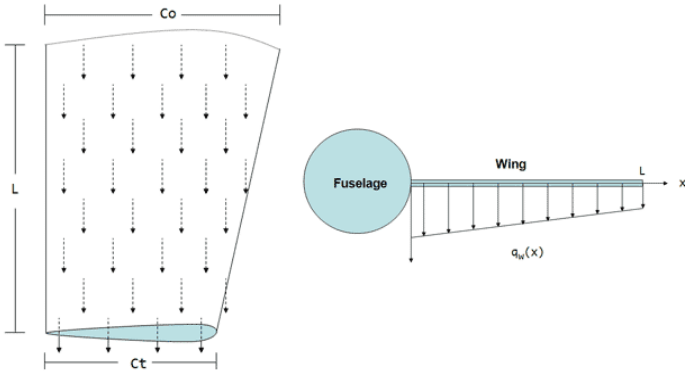

Figure 4.2: Load due to wing structure weight [27].

The structural load can be expressed in terms of load factor n and weight of the wing W_{Wing}, then the load factor n is calculated and substituted into equation $(4-10)$.

$$\frac{n}{2} = -\frac{\frac{C_O\, L\, kw}{2} + \frac{C_T\, L\, kw}{2}}{W_{Wing}} \qquad (4-9)$$

$$q_{wing}\,(x) = -\frac{W_{Wing}\, n\,(Co\, L - Co\, X + C_T\, X)}{L^2(Co + C_T)} \qquad (4-10)$$

4.3 Load Due to Fuel Stored in Wing

As shown in Figure 4.3, the fuel tank is placed inside the wing to amplify the lift load while reducing the net load on the wing. The fuel load is illustrated in Figure 4.3.

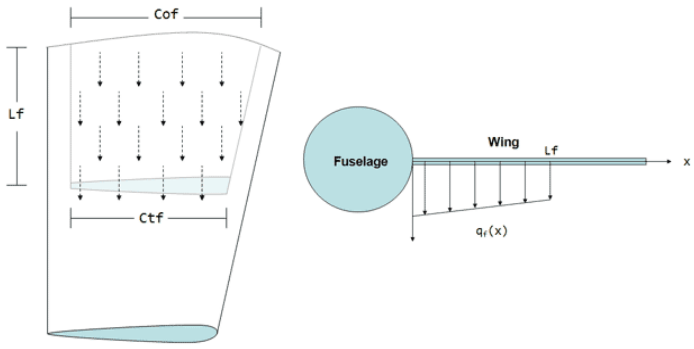

Figure 4.3: Load due to the weight of the fuel stored in the wing [27].

The magnitude of this load is calculated similarly to the structural load, which results in a solution accordingly. However, since the fuel storage does not reach out to the wing tip, the load profile is exclusively located in the middle of the wing.

$$q_f\ (x) = \begin{cases} -\dfrac{W_{\text{Fuel}}\, n\, (C_{\text{OF}}\, L_F - C_{\text{OF}}\, X + C_{\text{TF}}\, X)}{{L_F}^2\, (C_{\text{OF}} + C_{\text{TF}})} & \text{if } X \le L_F \\ 0 & \text{otherwise} \end{cases} \qquad (4-10)$$

4.4 Overall Load

To calculate the total load, add the aerodynamic lift, structural load, and fuel load. The equation $(4-11)$ is the overall load.

$$q_T\ = q_L\ +\ q_W\ +\ q_f \qquad (4-11)$$

$$q_T\ = \begin{cases} \sigma_2 - \sigma_1 - \dfrac{W_{\text{Fuel}}\, n\, (C_{\text{OF}}\, L_F - C_{\text{OF}}\, X + C_{\text{TF}}\, X)}{{L_F}^2\, (C_{\text{OF}} + C_{\text{TF}})} & \text{if } X \le L_F \\ \sigma_2 - \sigma_1 & \text{otherwise} \end{cases} \qquad (4-12)$$

Where

$$\sigma_1 = \frac{W_{Wing}\, n\, (C_O\, L - C_O\, X + C_T\, X)}{L^2\, (C_O + C_T)},\ \sigma_2 = \frac{2\, W_{Total}\, n\, \sqrt{L^2 - X^2}}{L^2\, \pi}$$

4.5 Aircraft Parameters

Once the mathematical model is built up for the wing loads, it is used to assess the physical and geometrical parameters of the aircraft. The studied model of aircraft has the following parameters in Table 4.1.

Table 4.1: Standard aircraft technical specifications.

W_{total}	6325 [N]
W_{Wing}	780 [N]
W_{Fuel}	823 [N]
L	15.24 [m]
L_F	2.4 [m]
C_O	2.15 [m]
C_T	1.07 [m]
C_{OF}	1.5 [m]
C_{TF}	1 [m]
n	1.5

4.6 Verification of the Modeled Loads

As it can be seen in Figure 4.4, aerodynamic lift contributes the most to the total load, knowing that the maximum load resides at the end of the fuel tank. The weight of the wing has a lessened effect on the entire load, while the fuel load is significant.

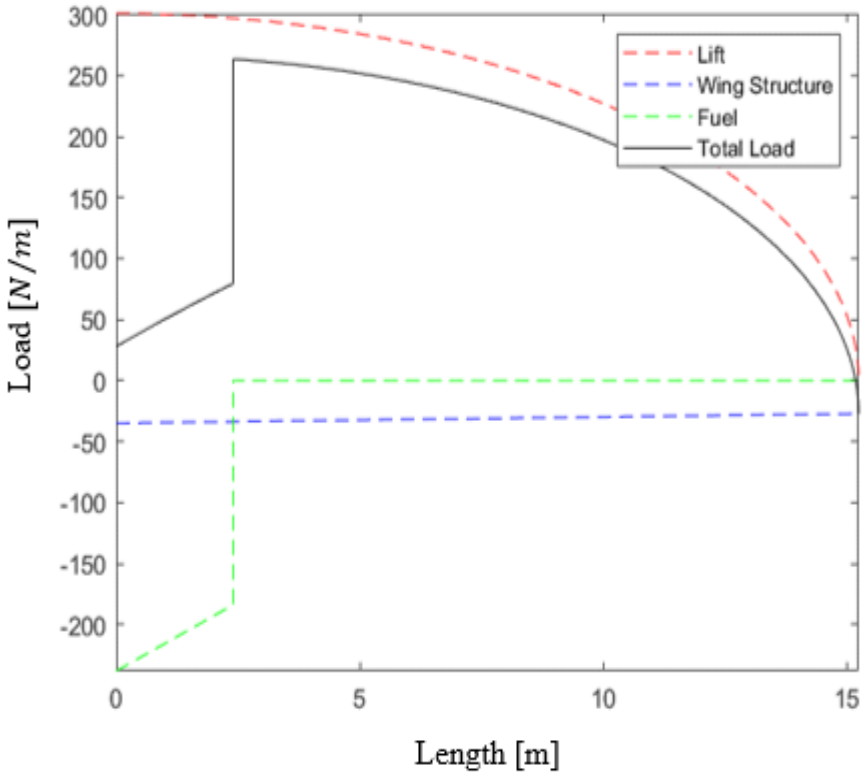

Figure 4.4: Different profile of wing loads.

4.7 Finite Element Analysis

This study is based on a finite element analysis of the considered wing [22]. Firstly, a static stress analysis of an aircraft wing is done in order to obtain wing deflection. Furthermore, the obtained results are graphically represented by a 3D view. Note that the wing structure is considered a rectangular shape to simplify the mathematical model. The general steps for this analysis are outlined below:

1- Importing the CAD model in STL format.

2- Meshing the CAD model of the Wing, Figure 4.5.

3- Defining material properties. Table 4.2.

4- Boundary conditions, Figure 4.6.

Table 4.2: Materials properties

Material Designation	**Aluminum Alloy**
Young's modulus	7.3 10^{10} [N/m²]
Poisson's Ratio	0.33

Figure 4.5: Finite element mesh of wing with tetrahedral elements.

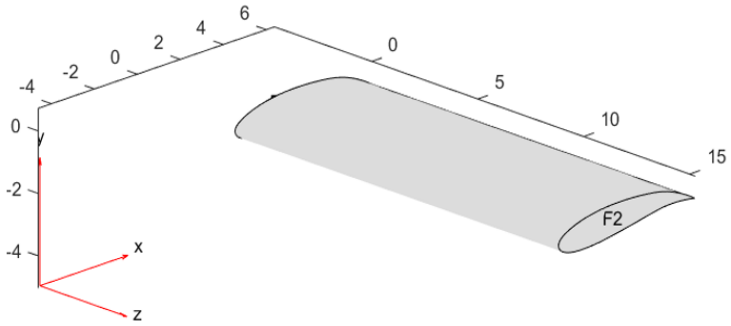

Figure 4.6**:** Fixed wing from Face 2.

4.8 Results and Discussion

The analytical pressure load is established to determine the total load with the appropriate 3D Model of the wing. From Figure 4.7, since the lift load is most contributor comparing to the other loads, the resulting lift load at the bottom surface of the wing is shown below and disseminated uniformly. The lift load produced by the wing is corresponding to the area of the wing. Given that the wing is rectangular in this instance, lift distributes uniformly. As shown in Figure 4.8 (left), the most displacement is located on the wing's tip along the Y axis, while the maximum von mises stress is found at the wing's root Figure 4.8 (right). Concludingly, both deformation criteria are caused by the effect of the pressure load.

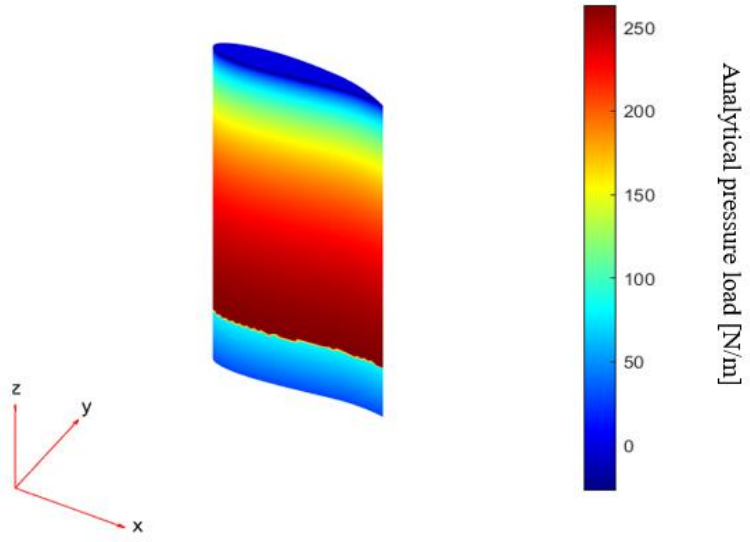

Figure 4.7: Analytical pressure load [22].

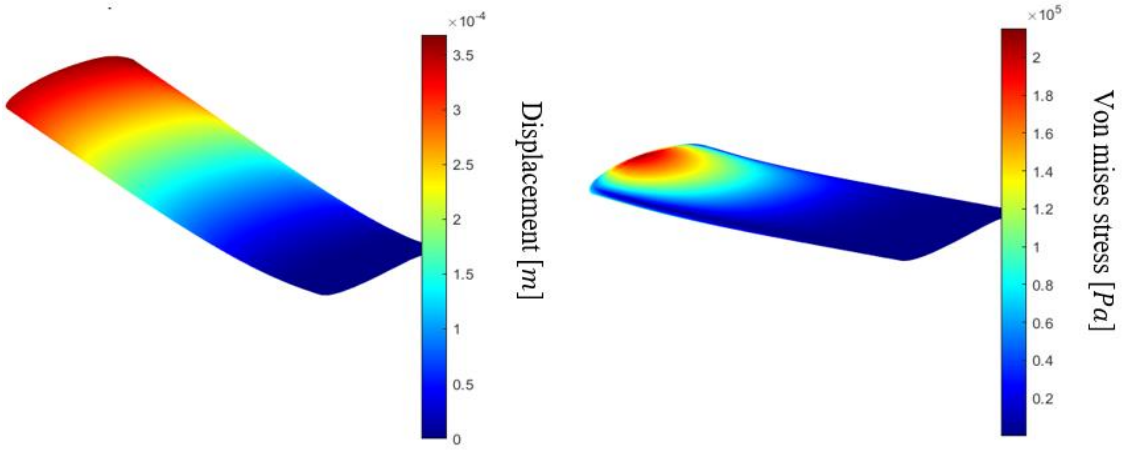

Figure 4.8: Left: Displacement of the wing along Y axis; Right: Von mises stress and displacement [22].

4.9 Summary

The analytical modeling of wing load for a standard aircraft was treated in details in this chapter. The integration and simplification of many mathematical equations was also established, in the sake of determining each load acting on the wing structure and to obtain the overall load profile. Additionally, the lift load, wing, and fuel weights that affect the wing were combined with other physical and geometrical characteristics. The most significant phenomenon to analyze is aerodynamic loads, hence the constructed model analytically identifies the key factors that affect how the system behaves. Furthermore, finite element analysis was performed using a callable MATLAB function to determine pressure distribution, von Mises stress, and displacement. Finally, the obtained results were graphically represented and discussed.

Chapter 5:
Aeroelastic Wing Methodology and Verification

This chapter examines the application and testing of the AWM, which depends on the theory that was discussed in chapter 2.

In the following, section 5.1 explains the general concept of the model. The Simscape Multibody model description will next be discussed in section 5.2. Section 5.3 included a qualitative and dynamic evaluation of the response. Finally, a brief summary is presented in section 5.4.

5.1 General Concept

According to this concept, a flexible wing is made up of a number of separate wing sections that are capable of moving freely of one another. This idea is shown in Figure 5.1, where the grey body is the rigid wing and the blue sections are the parts of the flexible wing.

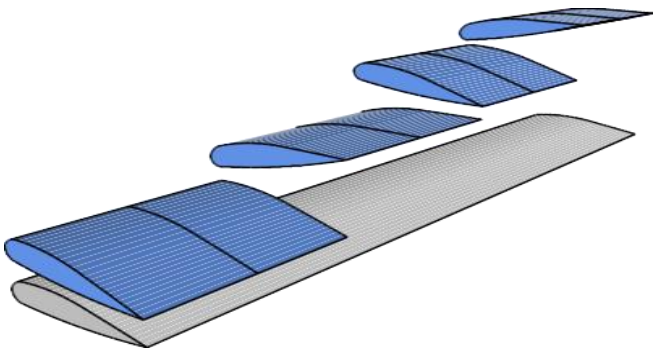

Figure 5.1: Flexible moving wing section overlaid on a rigid wing.

A rigid and a flexible wing coexist side by side in the model. The aeroelastic wing's actual location is represented by the flexible wing. Each aeroelastic node's vertical, horizontal, and pitch-up deflections are determined by the state-space system. The e.a. point in the spanwise

center of a section is described by the aeroelastic node of that section. Gravitational forces and the aerodynamic that applied on the wing structure are considered as an input for the state-space model. However, the rigid wing (grey wing) permits both rotation and translation of the wing root (the part embedded in the fuselage). Furthermore, it allows the calculation of the root forces and moment using the **SOF** (see equation $2-25$).

5.2 Explanation of the Simscape Multibody Model

In what follows, a description of a wing model through Simulink and Simscape Multibody in the Matlab package is given, based on the organigram design of the model given in the figure below.

The important blocks shown in Figure 5.3 can be created and treated as follows:

- The blue blocks describe the environment in general.
- The white blocks represent the aeroelastic and the special nodes (flexible wing parts).
- A rigid wing is represented by grey color.
- A state-space block is defined by orange color.

5.2.1 General Environment

Different functions are performed through the general domain blocks.

Time: In order to create figures, the "Time" block saves the time to the MATLAB workspace.

Atmosphere: For the specified flight altitude, the air density is defined using the "Atmosphere" block.

Gust: The gust that is implemented in the aeroelastic node blocks is produced by the "Gust" block. With a "1 - cos" profile, the block is capable of producing a vertical gust speed. This kind of gust is referenced extensively in literature [53], [54], [76] as well as in laws like Certification Specifications 23, [77] and Certification Specifications 25, [78]. The gust form

is defined in equation $(5-1)$, where φ_g is the simultaneous gust vertical velocity, $\bar{\varphi}_g$ is the highest gust velocity value in vertical direction and L_g is the gust length in terms of the time required for a point on an airplane traverse it [53].

$$\varphi_g(t) = \frac{\bar{\varphi}_g}{2}\left(1 - \cos\frac{2\pi}{L_g}\right) \qquad (5-1)$$

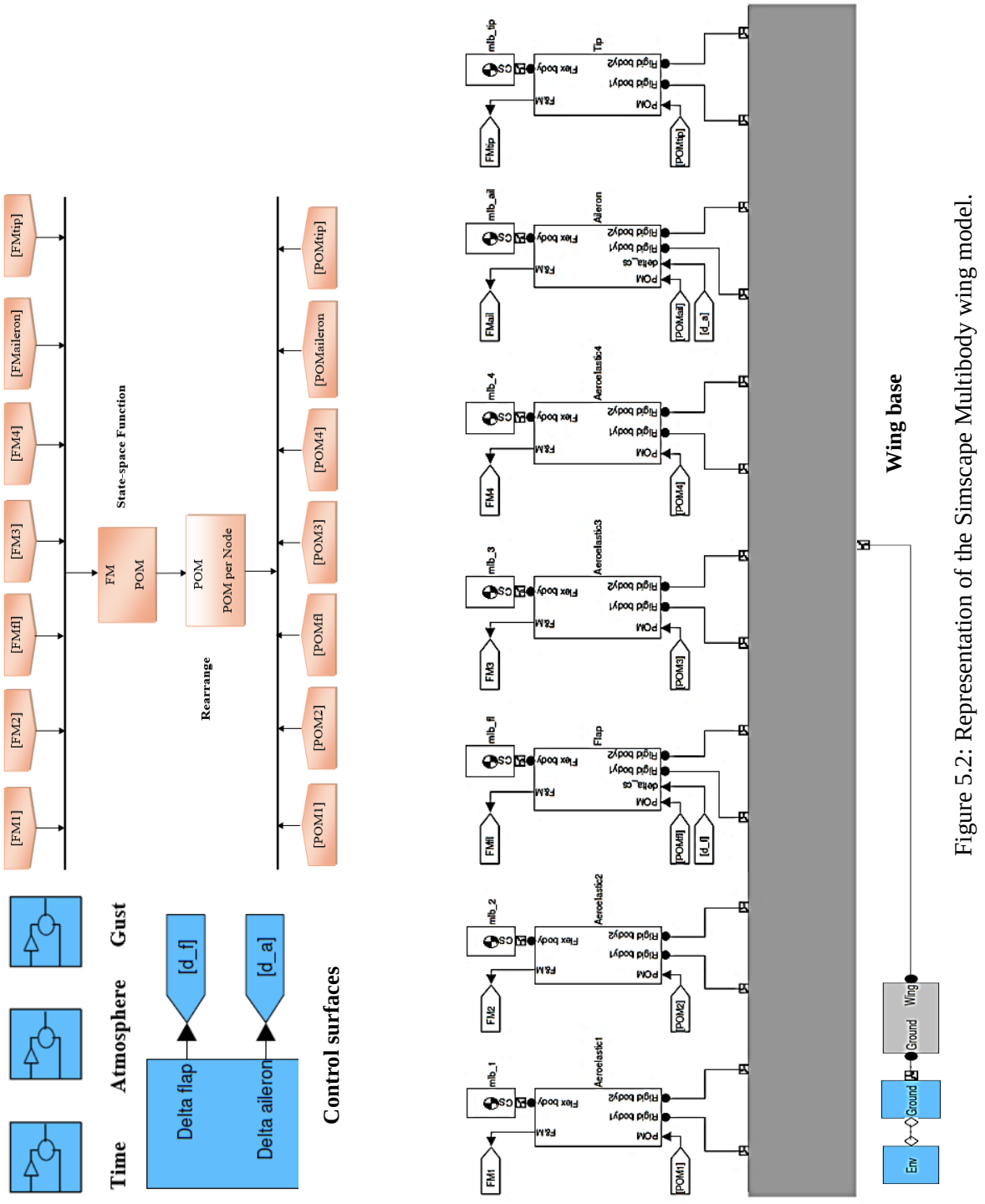

Figure 5.2: Representation of the Simscape Multibody wing model.

Controls: The "Controls" block is utilized to configure a certain magnitude of control parameters of the wing: flap element deflection (δ_f, α) and aileron element deflection (δ_a, α). It should be noted that the user defines the deviation angles of both elements (flap and aileron) directly and **not via pilot action** (see Annex A)**.**

Machine Environment: This block is used to define the different simulations of deflection response for the model. Also, it defines the gravity vector as having a value of zero. Gravity should not be included in this model; instead, gravity should be specified as a parameter input through the state-space system block [42]. As a result, weights are integred in the aeroelastic node blocks.

The **"Ground"** block connects the model to the **"Mach Env"** block.

5.2.2 Aeroelastic Nodes

The backbone of the aeroelastic wing is the aeroelastic nodes. Consider Figure 5.3, which illustrates how various blocks interact. Although there are just two wing sections shown in this figure, it's possible to add multiple sections to the model [42],[73]

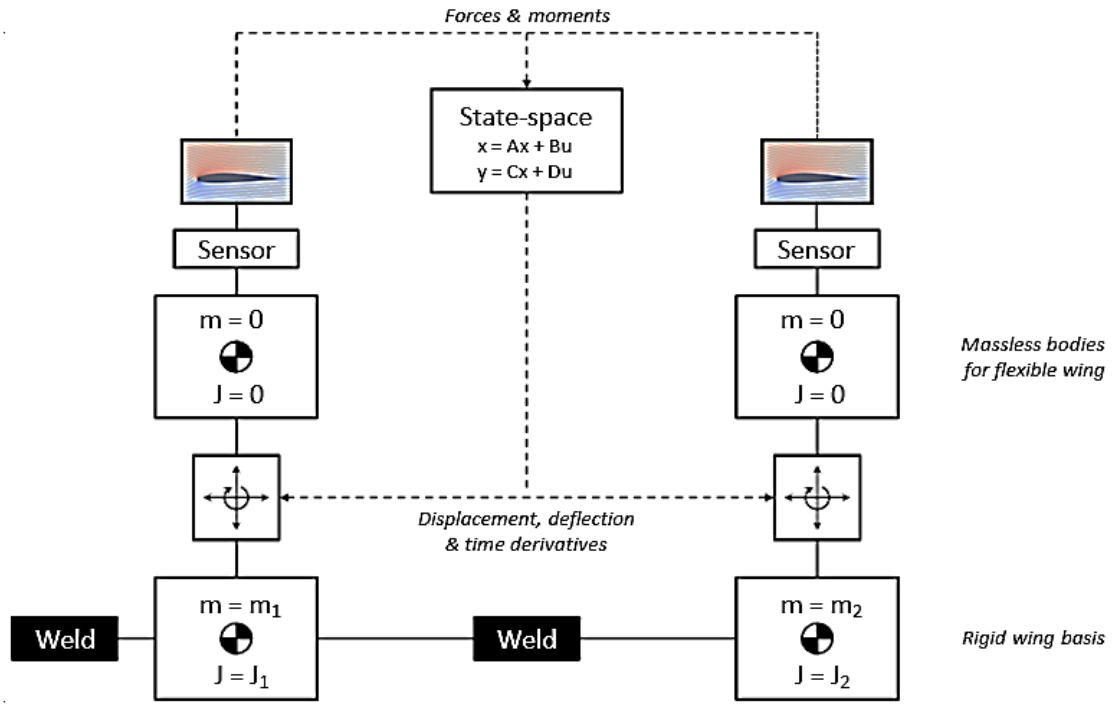

Figure 5.3: Simscape Multibody model of one aeroelastic node which contains one massless wing divided on two sections.

The rigid wing base is at the bottom and is made up of bodies that are joined together by welding in order to form a rigid wing structure. In addition, the rigid wing sections represent the mass and moment of inertia of the wing sections. An actuatable joint that may move vertically, horizontally, and pitch up is attached to each rigid body section. The massless bodies that represent the flexible wing position are joined to these joints. Furthermore, sensors are used to detect the movement of each mass of the wing sections, such as position, orientation, and motion **POM**. Then, using aerodynamic analysis, the moments, gravitational forces, and force applied to the section are determined. Finally, a state-space system determines the **POM** of the massless bodies after receiving these forces and moments. The system is finished when this data is used to operate the joints mentioned earlier. By using this method, you can simulate a flexible wing in the Simscape Multibody environment. Since Simscape Multibody can only simulate rigid bodies, this solution is required [42]. Aeroelastic node blocks are responsible for determining forces and moments and actuating massless sections.

Definition of forces and moments: A state-space system transmits position, orientation, and motion (**POM**) to each "Aeroelastic" block by a "**From**" tag, which is used to define the moments and forces. After that, it uses a "**Goto**" tag to transfer the forces and moments (**FM**) to the state-space block. Aerodynamic forces and moments are calculated using look-up tables, as was mentioned in section 2.2. The effective AoA serves as the input for these look-up tables.

One must first understand the various reference frames that are used in order to fully grasp how this angle of attack is determined. The X-axes for the used reference frames are represented as lines in the vertical plane in Figure 5.4. Names of coordinate systems, angles between them on the left, and how to use them on the right are all given in the box. Every one of these reference frames was chosen for the analysis for various reasons.

First, Earth reference frame F_E is used to determine the weight W, the airplane wing advance speed u, and the airplane wing descent speed w. (It's crucial to remember that the impact of the gust velocity φ_g impact is included in the effective aircraft wing downward velocity). Second, the lift force L and drag force D are defined using the aerodynamic reference frame F_a. Third, there is the body-fixed reference frame F_b. Fourth, the rigid-wing

reference frame F_{rw} is utilized to define the mode shapes. Note that the forces and mode shapes are defined in F_{rw}. (Refer to section 2.2). These two forces are the forward force H which is parallel to F_{rw} and the downward force V which is orthogonal to the F_{rw} , also the pitching moment M_i is included in this model. Now, we can use the effective flexible-wing reference frame $F_{fw,eff}$ in the sake of defining the effective AoA. Since the data of thrust force are absent F_{fw} will not include in the model calculations.

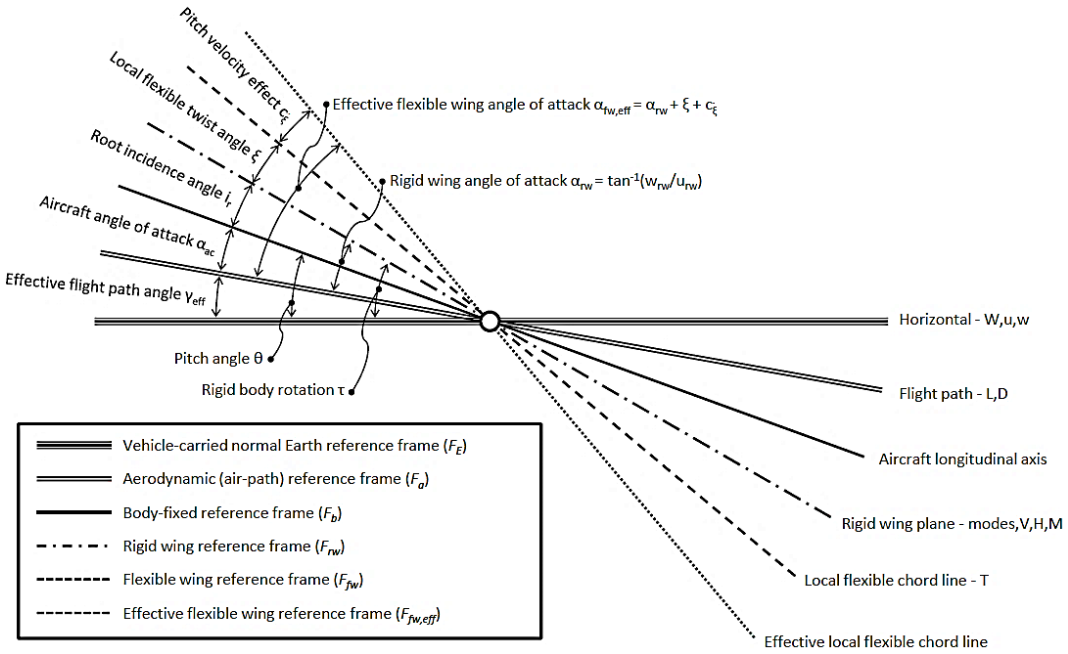

Figure 5.4: Representation of different reference frames and twist angles obtained from literature.

Given that the preceding reference frames have been found, the angles between these references can be addressed. Several of the angles, namely V, H, S and M, are needed to identify the parameters input for the state-space system, which is in the F_{rw} frame.

The first angle that should be defined is the angle τ, which is a component of the rotation matrix for rigid bodies. It is the matrix of transformation between F_E and F_{rw}. This may be determined in Simscape Multibody using a body sensor. It is used to convert the section weight W from F_E to F_{rw}. The next angle that needs to be calculated is the effective AoA of the flexible wing $\alpha_{fw,eff}$. The coefficients of aerodynamic forces and moments are computed using this effective angle of attack. Equation $(5-2)$ can be used to determine it, where, b is the semi-chord, $c_{\dot{\xi}}$ is the effect of the pitch speed on the effective AoA. In

addition, α_{rw} is the rigid wing AoA, a is the distance between mid-chord and elastic axis in semi-chords, u_{rw} is the forward velocity in the F_{rw}, ξ is the aeroelastic twist deflection, w_{rw} is the downward speed in the F_{rw} and ξ is the aeroelastic twist deflection.

$$\alpha_{fw,eff} = \alpha_{rw} + \xi + c_{\dot{\xi}} = \tan^{-1}\left(\frac{w_{rw}}{u_{rw}}\right) + \xi + \tan^{-1}\left(\frac{b\left(\frac{1}{2} - a\right)cos\,\xi\dot{\xi}}{u_{rw}}\right) \quad (5-2)$$

We remember ξ and $\dot{\xi}$ and from the state-space system, where the dot indicates a derivative with regard to time. Additionally, u_{rw} and w_{rw} can be computed using the rigid wing body's speed in the F_E frame (covered in section 5.2.4). Once that is done, it should be converted from F_E to F_{rw} using the rotation matrix that contains angle τ. A body sensor can detect the rotation matrix as well as the velocities. The user-input gust velocity w_g and the aeroelastic plunge and sweep speed, which are defined from the state-space system, should be added to these velocities. User input for the final two parameters, a and b, enables the computation of $\alpha_{fw,eff}$ and hence the calculation of the coefficients of moments and forces.

The rigid-wing AoA α_{rw}, described in equation $(5-2)$, is the final angle. The lift and drag forces are transformed from F_a to F_{rw} using this angle. Assuming that these forces and moments are determined in the F_{rw} frame, the aerodynamic forces and gravitational forces are transferred from the a.c. to the e.a. and from the c.g. to the e.a. The forces and moments as they work on the elastic axis and in the F_{rw} frame is determined at this moment (i.e., V, H, S and M). The "Aeroelastic" block's output is delivered to the state-space group through a "**Goto**" label.

Determination of mlb motion: The massless body **mlb** is found in the "Aeroelastic" block, which is used to determine the motion of it by a joint actuator. The means of actuation (three aeroelastic degrees of freedom) are simple "Joint Actuator" blocks attached to a planar joint that allows for pitching rotation, plunging, and sweeping translation. Motion (in the opposite direction from the forces) that arrives from the state-space group via a "**From**" tag is used for actuation. The **mlb** has zero weight and inertia for the sake of avoiding other forces than those given to the state-space block from working on the multibody system. As previously stated, the mass and inertia of an **mlb** are ignored in order to avoid incorrect forces when the bodies are moved.

5.2.3 Special Nodes

In this section, special nodes represent the control surfaces, such as flaps and ailerons. They send the forces and moments to the state-space block in order to compute them; on the other hand, they receive the **POM** from it. They also activate an **(mlb)**. Note that an **mlb** represents an object on the wing instead of a section of the wing. These could be ailerons and flaps. A tip node is always included as well. We will now talk about these three unique node types.

Special Lifting Surface Node -Flap: The "**Flap**" block demonstrates the aerodynamic impact of flap deviation. The influence of flap deviation is described as an idealized point load acting on the **TE** of the spanwise center of the flap, as it is mentioned in section 2.4. Applying downward flap deflection at the trailing edge leads the wing to twist downward, closely simulating reality [70]. Using the assumption of look-up tables in order to calculate the aerodynamic coefficients based on the flap deflection angle δ_f from the "**Controls**" block and the effective AoA $\alpha_{fw,eff}$ of the local flexible wing section. There are two options: δ_f come from the "**Controls**" block and $\alpha_{fw,eff}$ are calculated similarly to aeroelastic nodes. Furthermore, the forces are then translated to the F_{rw} frame, similarly to how it was with the aeroelastic nodes.

Special Lifting Surface Node-Aileron: The "**Aileron**" block functions similarly to the "**Flap**" block, but uses different input parameter values.

Special Tip Node: It is necessary to include the "**Tip**" block to compute the data for tip deflection. In the same way, this is done by the state space block, which sends the **POM** to the tip node and measures the **mlb** that shows the aeroelastic tip node.

5.2.4 Rigid Wing Basis

Wing root: The wing structure is joined to the "**Ground**" block by the "**Wing Base**" subsystem. In Simscape Multibody, we can set the wing root's translation, rotation, and time derivatives by utilizing a bushing joint, which has six degrees of freedom. Examples include the wing's forward speed and setting angle. At this bushing joint, the root moments and

forces are measured. (The same concept applies to the bushing joint discussed in section 3.3.2).

Rigid wing nodes: Each aeroelastic and special node has its own body block in the "**Rigid Wing**" subsystem. These body blocks are joined together by welds to provide the appearance of a rigid wing. The collection of body blocks depicts the wing's physical geometry, such as its sweep and dihedral, i.e., a clean wing (see Figure 5.5). This enables the connections between the rigid wing and the aeroelastic special node to be placed where they should be, specifically on the elastic axis of the wing. As a result, rigid body velocity measurements are correct for each node, even in situations like yawing motion, when outboard nodes move more quickly than inboard nodes. It should be noted that the wing under consideration in Figure 5.5 is a rigid wing with control surfaces (flap and aileron).

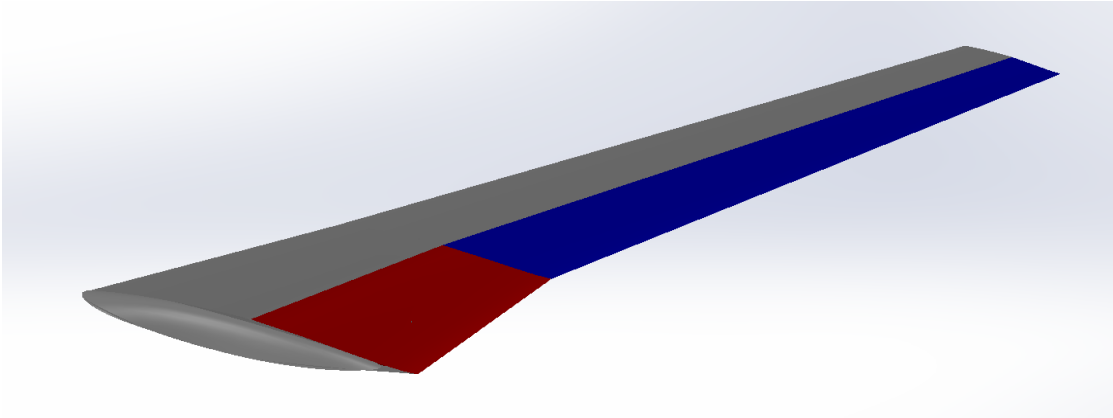

Figure 5.5: A 3D CAD model of the considered wing with aileron and flap.

The forces and moments obtained in the aeroelastic and special nodes must be applied to the system at some point in order to execute the Summation of Forces **SOF**. This cannot apply to massless bodies because they are already actuated by motion. Because of this, the rigid wing is subjected to the forces and moments.

5.2.5 State-space Group

This system is represented in Figure 5.3 by the orange blocks. This group is comprised of four components. This collection of blocks is responsible for determining the **POM** of the nodes according to the forces and moments acting on them.

From tags: In the aeroelastic and special node blocks, the forces and moments acting on each node were calculated. For transmitting data, "Goto" and "From" labels were employed. Each node's forces and moments vector [$V\ H\ S\ M$] is delivered via "From" labels, and a "Mux" block is used to assemble them into a sizable input vector.

State-space Function: As it was previously mentioned, the state-space group is the fundamental part of the model (refer to section 2.1), and it is also included in the "State-space with Delay" block. First, the input vector is changed to contain a series of [$V\ H\ M$] for each node rather than [$V\ H\ S\ M$]. Then, this changed input vector is sent to a state-space unit, which makes an output vector with the position, orientation and motion of the nodes, the amplitude of the modes, and time derivatives related to them.

This model incorporates a partitioned method, as was mentioned in section 2.3. From Simscape Multibody' toolbox, a block called "Unit Delay External IC" was used in Simscape Multibody for this purpose. This indicates that the state-space system's output is postponed by a one-time step in order to synchronize the prediction and the computation of the aerodynamic forces, moments with those of **POM** at the same time inside the state-space unit. Thus, model treatment does not take a long time. Initial conditions for the delayed state-space block can be provided by the programmer in the manner of an initial state vector and an output vector. The output vector is modified in the final phase to ensure just the nodal information **POM** and not the modal data is transmitted to the following blocks.

Rearrange: The components in the **"State-space Function"** block's output vector will then be rearranged using the **"Rearrange"** block. It enables the output to be separated into discrete sections for the various aeroelastic and special nodes via **"Goto"** tags.

Goto tags: Lastly, the output is then divided via a "Demux" block, and the various output vectors that contain the **POM** for the various nodes are transmitted to the "**Goto**" labels for the aeroelastic and special node blocks.

5.3 Ansys and Simscape Multibody Simulations

The finite element software Ansys Workbench is employed to establish the mode shapes for the wing. Figure 5.6 depicts the wing's first, third, seventh and ninth modes. Greater

modes are more complicated than lower modes, and, as a result of their greater stiffness, i.e., natural frequency, they often have a smaller amplitude. Annex B covers all the data obtained by performing a modal analysis for the first six modes.

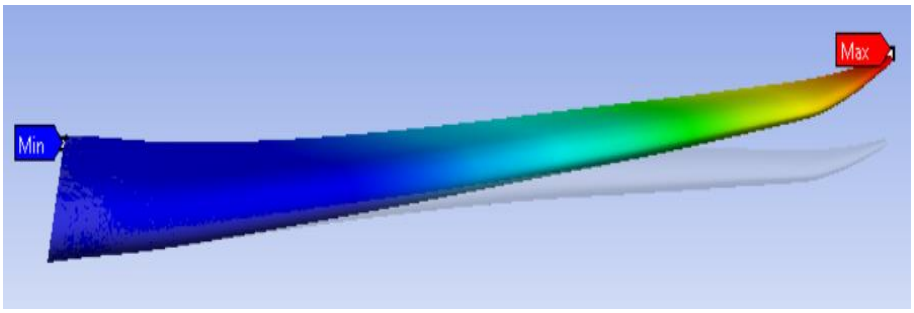

Mode 1 – 1.685 Hz. First bending mode shape: Upwards vertical deflection + Small pitch-down twist moment.

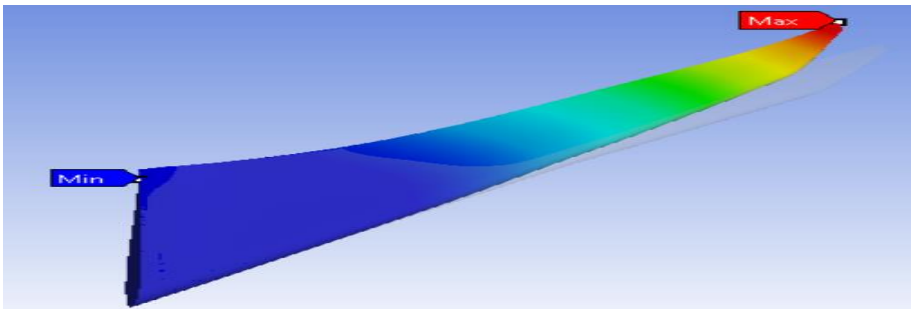

Mode 3 - 5.024 Hz. First sweeping mode shape: Forwards and backwards deflection.

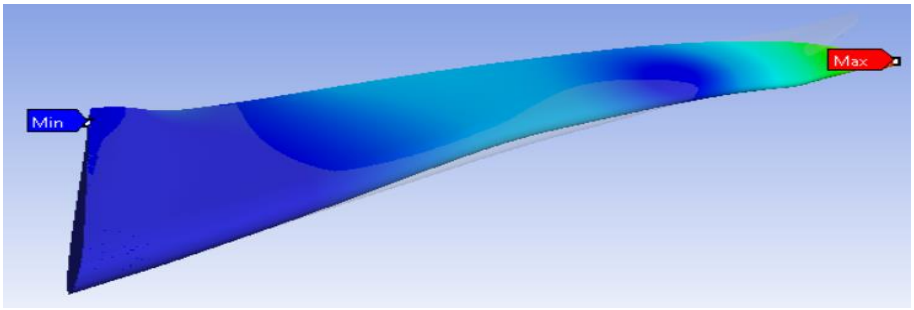

Mode 7 – 15.018 Hz. Second bending and twisting mode.

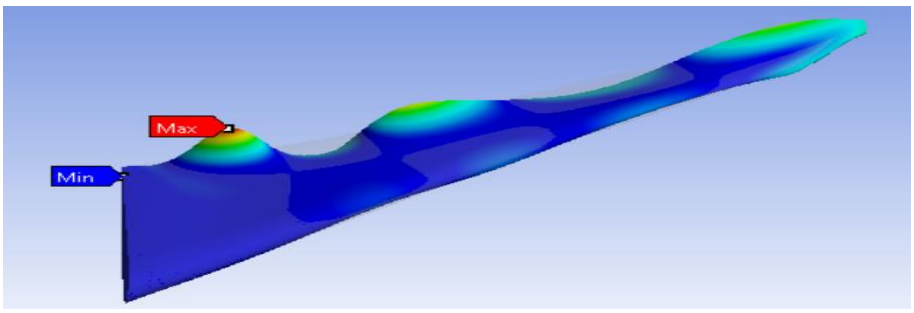

Mode 9 - 22.113 Hz. A higher mode.

Figure 5.6: Modes shapes: 1, 3, 7 and 9 obtained from FE software.

5.3.1 Aerodynamic Input

Simscape Multibody uses aerodynamic data to construct look-up tables. Note that look-up tables are integred in Simscape Multibody toolbox. Firstly, the programmer should enter the following inputs: vector of angles of attack α, as well as drag coefficient C_D, lift coefficient C_L and moment coefficient C_M vectors. Different coefficient values can be defined using the model at various spanwise sections. This makes it possible to use a tip correction, in which the aerodynamic coefficients are decreased close to the wing's tip (described in section 2.2.3). Secondly, equations $(5-3)$ can then be used to calculate the section lift force L_i , drag force D_i , and pitching moment M_i . Thus, the section surface area S_i, the section mid-chord c_i, and q is the dynamic pressure.

$$L_i = \mathrm{q}S_i C_L(\alpha), \qquad D_i = \mathrm{q}S_i C_D(\alpha), \qquad M_i = \mathrm{q}S_i c_i C_M(\alpha) \qquad (5-3)$$

Furthermore, as it mentioned in section 2.4, elements of control surfaces flap and aileron are integred in the wing model. Thus, their parameter inputs must be also included in the model. In other part, the discussed assumption of neglecting dynamics, inertia and actuation of flap and aileron and idealizing control force coefficient C_D, force coefficient C_L at the **TE** of the wing, these force coefficients must be represented on matrix form. In equation $(5-4)$, the force coefficients are in function of the control surface deflection angle δ and the AoA α. Equation $(5-4)$ demonstrates how to get forces and moments from their coefficients. Keep in mind that the control coefficient equation $(2-24)$ was used to derive these equations.

$$L = \mathrm{q}C_L(\alpha, \delta), \qquad D = \mathrm{q}C_D(\alpha, \delta) \qquad (5-4)$$

Final step is about the input of aerodynamic forces and moments for calculations, these forces should also be calculated in a pre-processing phase. Annex A contains all of the important aerodynamic data for the wing. These data were obtained directly from a DATCOM model. For more information, this DATCOM is a sizable collection of equations used in the modeling and construction of aircraft, more specifically aircraft wings. The DATCOM output contained wing aerodynamic data that was immediately useful, however the aerodynamic data for the control surfaces needed some MATLAB processing.

5.3.2 Qualitative evaluation

The initial essential examination of the model is a qualitative evaluation of the reaction to gust, lifting surfaces inputs. This provides an overview of the model's functionality and capacities. The wing model is discussed in section 5.1 and covered in detail in Annexes A and B. In the boundary condition inputs, all analyses assume that the wing is traveling (i.e., moving) forward at a constant speed of $133\,m/s$ and with zero AoA, therefore the local AoA of wing parts is determined by the wing twist and wing setting angle.

Refer to gust's equation $(5-1)$, beginning after of one second $[1s]$ with the values of gust length $L_g = 1s$ and maximum gust speed $\bar{\varphi}_g = 11.15\ \mathrm{m/s}$. Figure 5.7 represent the tip deviation caused by a "$1-cos$" upward gust as specified by CS regulations [78]. Vertical deflection is positive in the upward direction, horizontal deflection is positive in the forward direction, and twist deflection is positive in the pitch-up direction.

As can be seen from Figure 5.7, the wing tip is in stable position at the beginning of the study. The response of vertical and horizontal displacements at the wing tip is anticipated through the period of the gust maneuver, i.e., between 1 and 2 seconds. Furthermore, when there is an upward gust (vertical gust), the effective angle of attack α_{eff} increases, causing the lift and drag to increase (as shown in Figure 5.7 a-b). The result of this physical phenomenon is a backwards and upwards movements of the tip. Keep in mind that the backward and upward movements are caused by the drag force and the lift force, respectively.

On the other side, the twist deflection is unanticipated because in the case of greater effective angle of attack α_{eff} the simulation should be appearing an aerodynamic pitch-up deflection instead of a pitch-down deflection. In this case, we should return to the first nine mode shapes previously represented in Figure 5.6 in order to explain this contradiction. The first mode shape is known to generally combine an upward vertical deflection with a pitch-down twist displacement. Hence, this mode existed during the simulation. For this reason, the wing tip pitches down. Following the gust, the tip oscillates and returns to its initial position.

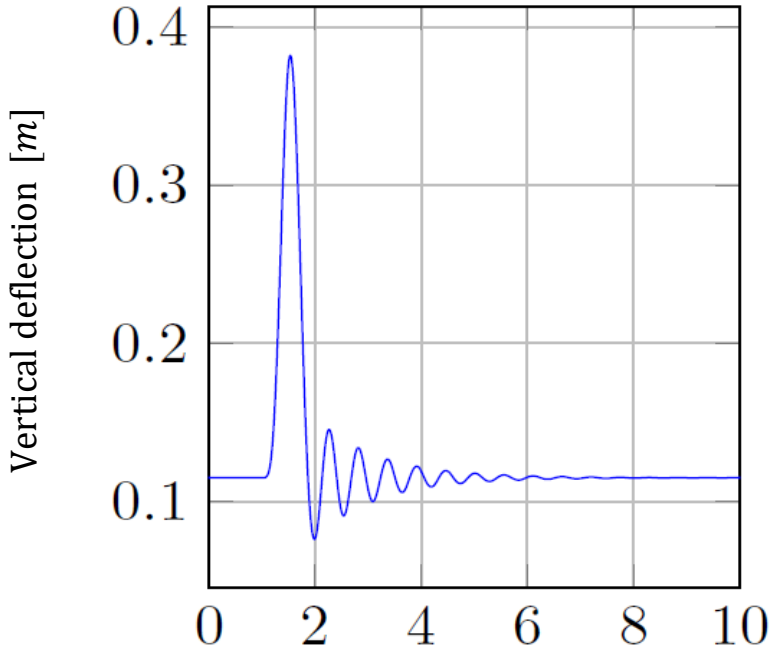
Vertical deflection [m]
0.4
0.3
0.2
0.1
0
2
4
6
8
10

(a) Time

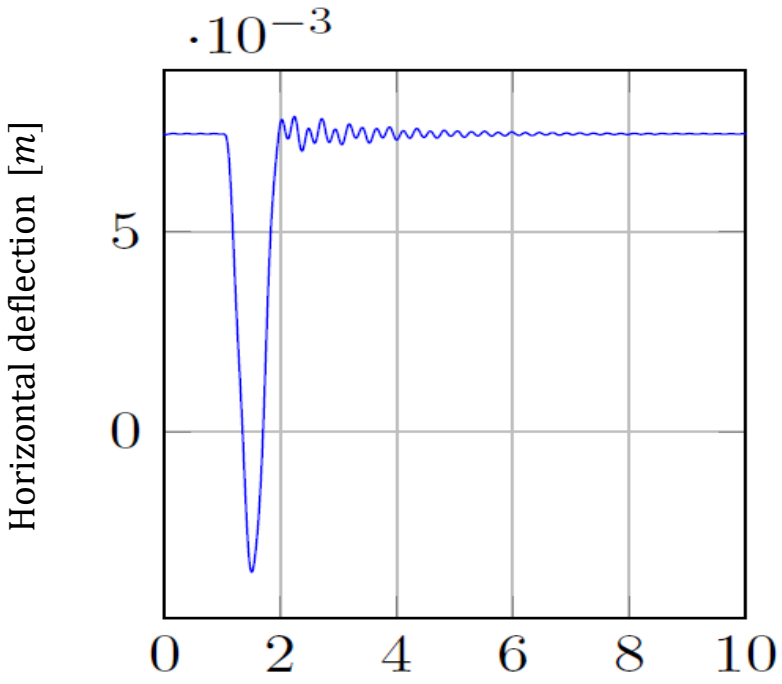
Horizontal deflection [m]
·10−3
5
0
0
2
4
6
8
10

(b) Time

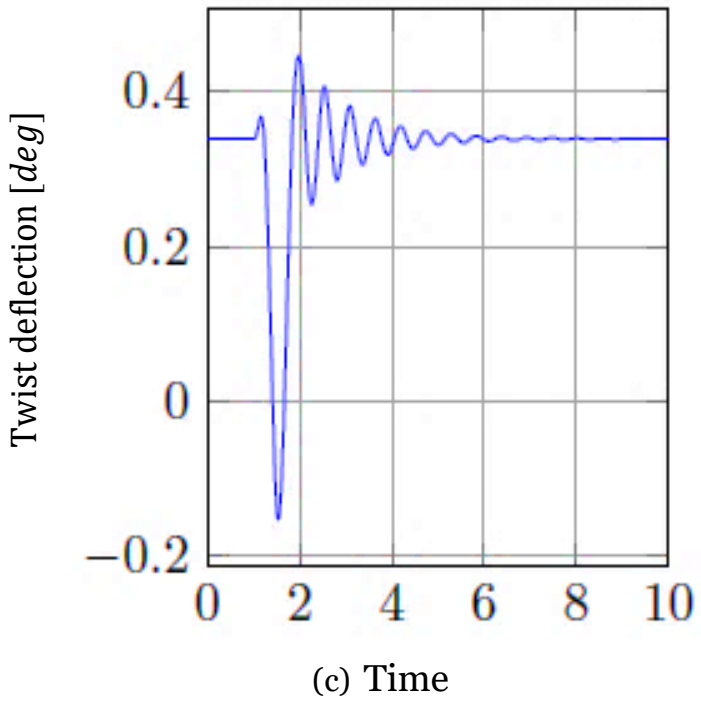

Figure 5.7: Response of Tip deflection for a forward-moving wing subjected to a "1-cos" vertical gust.

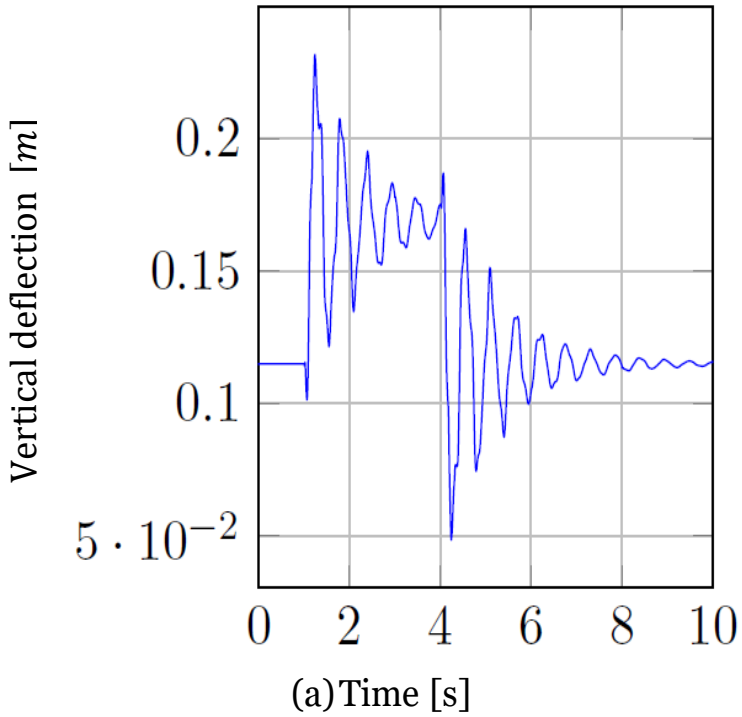

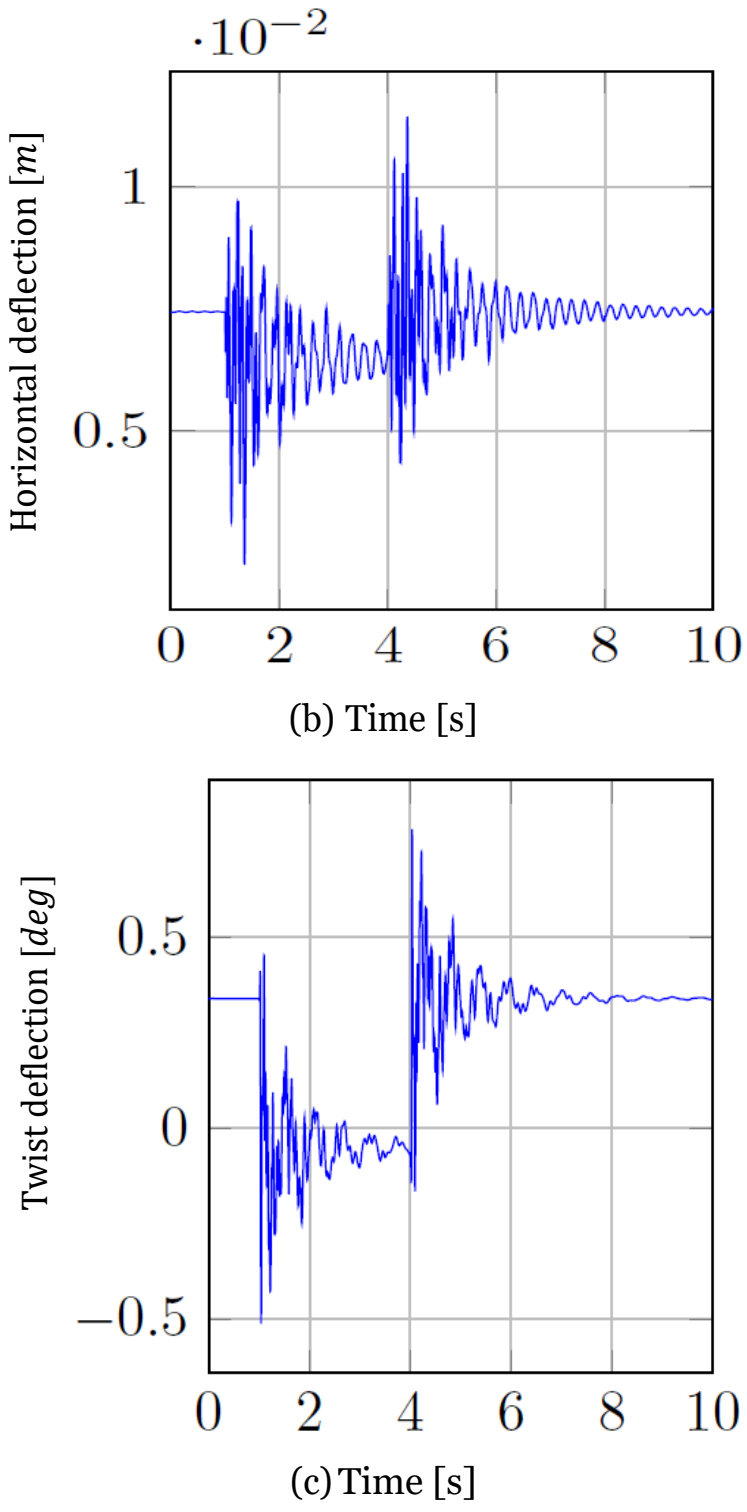

Figure 5.8: Response of Tip deflection for a forward-moving wing after a 10° downward flap deflection

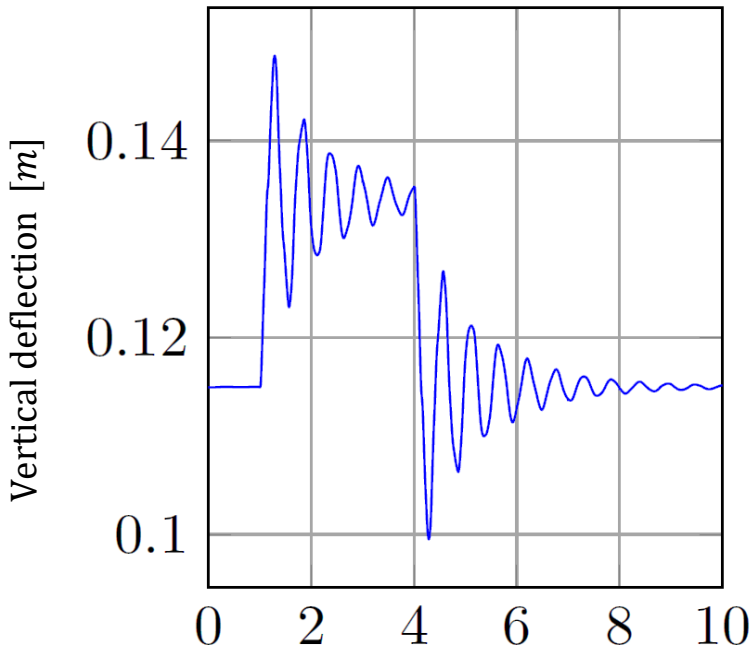

(a)Time [s]

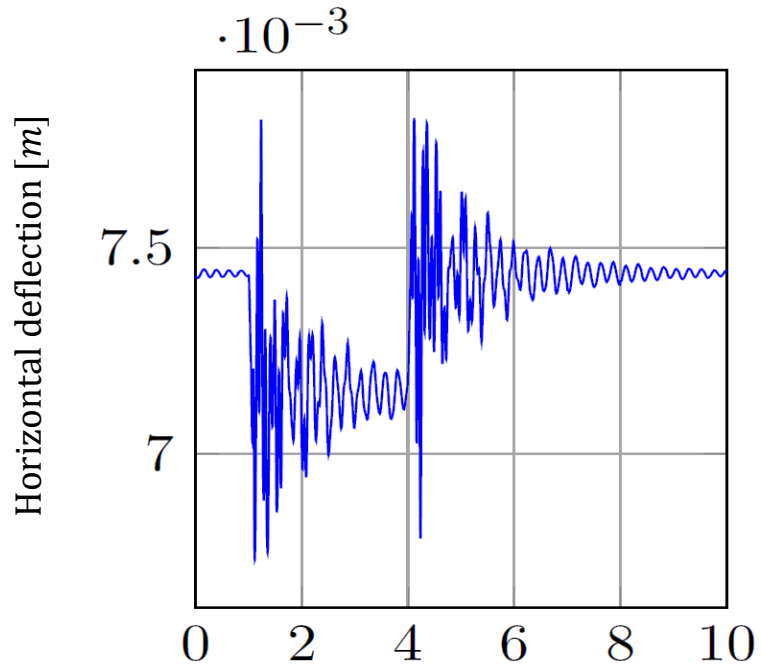

(b)Time [s]

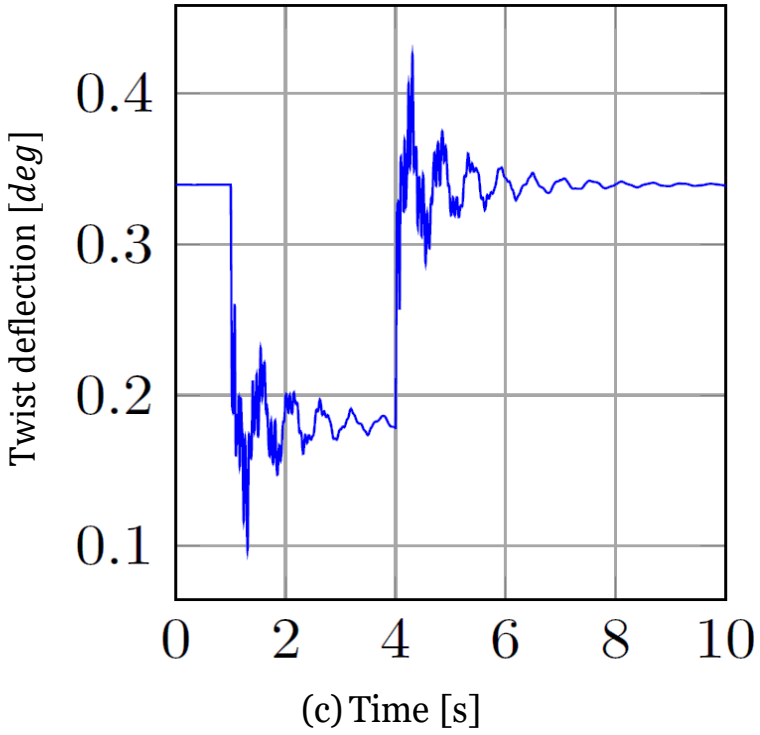

Figure 5.9: Response of Tip deflection for a forward-moving wing after a 10° downward aileron deflection.

5.3.3 Dynamic Evaluation

The model's steady-state behavior was checked in the preceding section. The following section deals with the model's transitory response. Two ways of validation will be used. Firstly, a decay envelope analysis will be used to validate the model's damping when the wing is subjected only to structural load. Moreover, the dynamic response of the wing when it is under all forces (i.e., structural and aerodynamic forces) is evaluated in order to verify the model's dynamic aeroelastic response. Finally, the dynamic response after periodic gust parameter inputs is evaluated in order to confirm the model's dynamic aeroelastic response.

5.3.3.1 Modal Damping Evaluation

The oscillatory decay that damping causes governs the deflection's transitory section. The structural modal damping ratio ζ, which is generally equal to 0.020, can be given by the operator to the model. To determine whether the decay is occurring as expected, one might examine the time history of the modal amplitudes. The decay envelope method is described and applied in this section.

The sites of local peaks can be identified during the simulation. Following that, these peaks are used to fit a curve in equation's $(5-5)$ exponential form. A and B are curve fitting constants, and q_r is the modal amplitude of mode r in this equation. Following this fit, the modal damping ratio ζ_r may be calculated using equations $(5-6)$ by using the curve fit constant B and the natural frequency of the mode ω_r

$$q_r(t) = Ae^{Bt} \tag{5-5}$$

$$\zeta_r = -\frac{B}{\omega_r} \tag{5-6}$$

Table 5.1: Modal damping ratios of the first ten modes.

Mode	All loads	Only Structural Loads
1	0.076	0.022
2	0.020	0.020
3	0.059	0.020
4	0.023	0.020
5	0.024	0.020
6	0.020	0.020
7	0.019	0.003
8	0.025	0.020
9	0.020	0.020
10	0.021	0.020

The simulation involved two alternative load conditions. All forces, including aerodynamic forces, weights, aerodynamic moments, are present in the first load scenario. The aerodynamics are nonexistent in the second loading situation. Table 5.1 presents the results. The modal damping ratio for all modes ought to be 0.020 if structural damping is the only source of damping. This is only accurate, as shown in the table, when aerodynamic forces are not present and only structural damping exists. The dynamic analyses are carried out as planned because all modes in this load example have a damping ratio of 0.020.

Figure 5.10, which displays the first mode with structural loads, serves as an illustration of such a decay envelope analysis. As can be seen, all local peaks are nicely captured by the decay envelope, and the modal damping ratio is 0.02. Obviously, the only origin of damping is structural. Along with structural damping, aerodynamic damping also contributes significantly to damping. An augmentation in damping is observed while using a quasi-steady aerodynamic model. This is the case because the lift force, which acts in the opposite

direction of the plunge motion, increases as the effective angle of attack α_{eff} rises. The decay study in Figure 5.11 shows this impact to be present. This figure depicts the first plunge mode, which is subject to structural and aerodynamic loads. However, due to aerodynamic damping, the modal damping ratio is approximately four times higher than with merely structural damping. The decay envelope once again perfectly captures all local peaks.

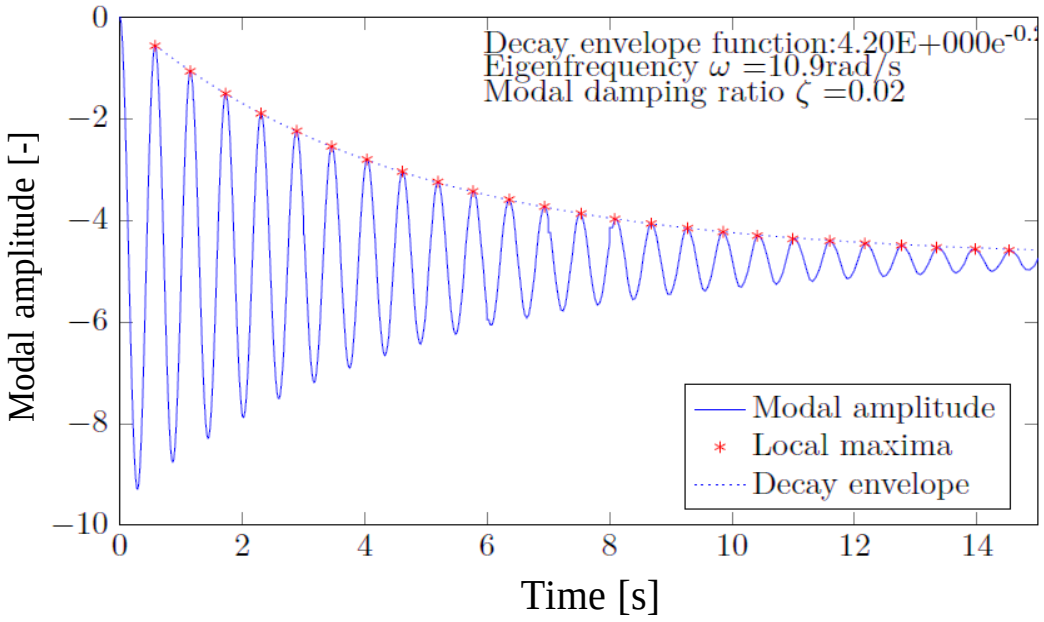

Figure 5.10: Modal damping $\zeta = 0.02$ for the 1st mode with structural loads.

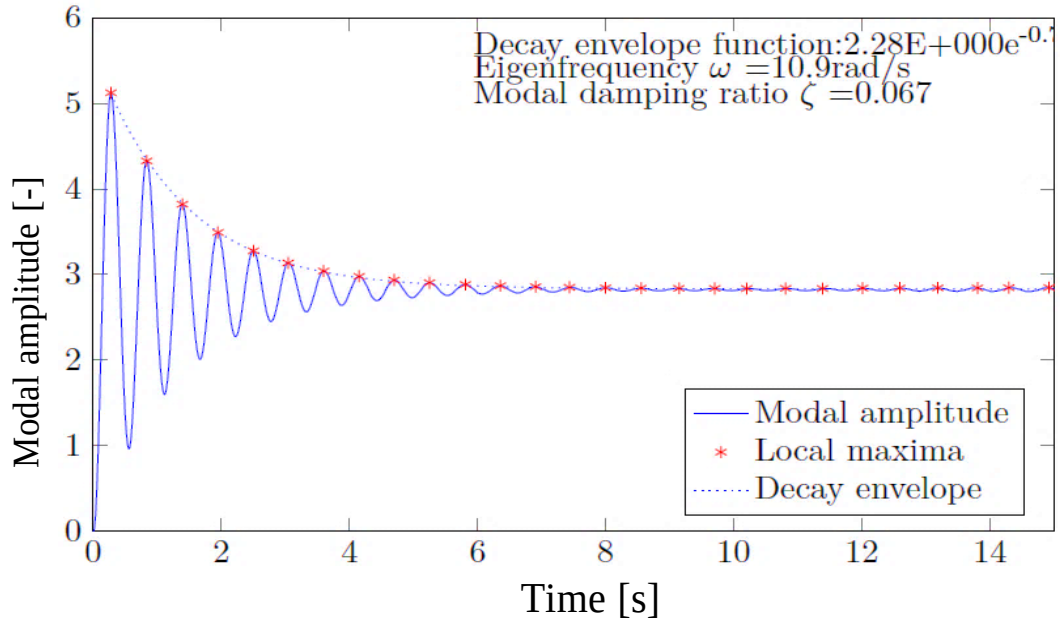

Figure 5.11: Modal damping for the 1st mode $\zeta = 0.067$ with structural load and aerodynamic forces.

5.3.3.2 Periodic Excitation with Gusts

The suitable technique to confirm the model's dynamic behavior is to look at the dynamic response to periodic gusts with different frequencies. It is envisaged that the frequency of a specific mode will dominate the reaction if the frequency of a gust corresponds with that mode's frequency [53].

In various simulations, a sinusoidal gust is encountered by a wing in steady state. It can determine the range of the mode amplitude according to a specific mode by subtracting the maximum from the minimum mode amplitude from the reaction that follows. Figure 5.12 displays the investigation's findings. These graphs represent the modes amplitude range versus the gust frequencies. The natural frequencies of the modes are indicated by the red lines. The dynamic behavior of the model is confirmed since the mode amplitude ranges are highest once the gust frequency and the mode's natural frequency correspond.

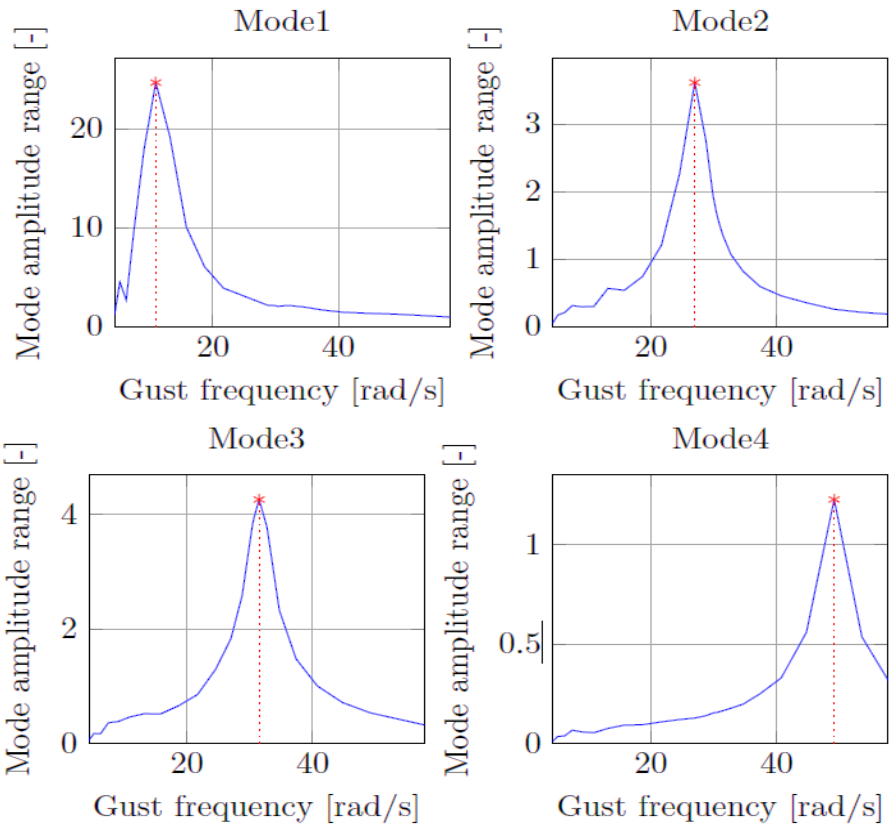

Figure 5.12: Amplitudes curves of modes 1-4 caused by period excitation using gusts.

5.4 Summary

This chapter demonstrated the application of the multiple disciplines used to build an aeroelastic wing model, as explained in chapter 2. It was clarified that the model consists of separately movable, massless elements that construct a flexible wing over a rigid wing basis. A state-space system governs the flexible wing's deformation **POM**. This system is used to capture and determine the deformation of the wing based on the input data, which represents the aerodynamic, gravitational, and moment loads. The Simscape Multibody toolbox used to illustrate this topic was thoroughly covered.

Also, the wing model was carefully checked because it led to the aeroservoelasticity theory. This theory is a critical component of aeroelastic flight mechanics and is the most significant contribution of this study.

A qualitative examination shows that the wing responds as one would expect to wind gusts and control inputs. After that, it was demonstrated that the stable deformation model was accurate because it properly matched analytical calculations. Additionally, the wing's dynamical reaction was confirmed. First, decay envelope analysis demonstrated that, in the absence of aerodynamic forces, the damping of the wing conforms to the structural damping ratios given. The second finding was that wing deflection is greatest when gust frequencies are equal to the inherent frequencies of the modes. This can be verified by periodic excitation with gusts.

In all of the checks of the wing model, satisfactory results were found, which was a good way to end the process.

Chapter 6: Conclusions and Recommendations

6.1 General conclusions

Several investigations were done into how aeroelasticity influenced the flight mechanics of the wing model. The design of a model that could simulate the dynamic aeroelastic and aeroservoelastic feedback of a flexible moving wing was the main objective of the latest studies.

The considered aeroelastic model was extensively verified, lending confidence to the model's conclusions. Regrettably, validation data utilized to calculate the dynamic behavior of an aeroelastic wing are rare. There are still no complete benchmarks or confirmation standards for aeroservoelasticity in general [58]. The majority of validation data available in the literature is mostly for flutter analysis, which this design is not improved for (see section 2.2.2).

The following is the research problem that was mentioned in Chapter 1.

Is it possible to quickly and accurately predict and calculate the load on a flexible aircraft wing in the subsonic flying range by combining the modal superpositioning method and quasi-steady aerodynamics in a partitioned way through a multibody system environment called " Simscape Multibody"?

Positively, the aforementioned issue is being addressed. The aeroelastic wing model was created using the modal superposition method. It was observed that the validity of the modal model could be improved at a low computational cost. This is achievable because a modal analysis is used to determine the structural behavior at the pre-processing stage. Since

the creation of a quantitative evaluation is impossible due to the lack of validation data, only this qualitative assessment can be made.

Finally, the addition of wing flexibility affects a number of flight mechanics factors. This is evident even for relatively inflexible aircraft, for which flexibility is typically ignored. Most flight mechanic aspects of more flexible designs are influenced by aeroelasticity. Aeroservoelasticity should be taken into account in flight mechanics models to provide correct findings, especially at the initial design stage.

6.2 Recommendations

Much effort has gone into the latest research. Nevertheless, the study is not complete, and various recommendations for future steps that might be taken can be suggested.

Firstly, the aeroelastic wing model can still be improved by including the thrust force created by the engine for the sake of obtaining more results about the effect of the thrust engine on the wing's response.

Secondly, the goal of future research is to create an Aeroelastic Flight Mechanics Model **AFM** that is capable of predicting, capturing, and simulating the dynamic behavior of the whole aircraft.

Finally, the aeroelastic flight mechanics model mentioned above will be implemented and fitted into Multibody System Dynamics **MSD** to simulate coupled flight mechanics and aeroelasticity fields. Finally, for an airplane, the qualitative behavior may be examined, and the stability properties and trim conditions will be examined with data from the theory, as in this case.

Annex A:
Aerodynamic Coefficients of The Wing Model

It's important to note that the aerodynamic information for an airfoil can vary depending on factors such as the Reynolds number, Mach number, and airfoil thickness, among others. Additionally, these values are typically obtained through wind tunnel testing or computational fluid dynamics **CFD** simulations, and may not be exact for every implementation of the NACA 0009 airfoil.

The aerodynamic lift, drag and moment coefficients for the considered model are presented in this annex. The airfoil NACA0009 has been believed to be the airfoil of the extruded wing. This airfoil produces no aerodynamic moment due to its symmetrical form. All this data was extracted from Airfoil tools database and a DATCOM model of the considered airfoil.

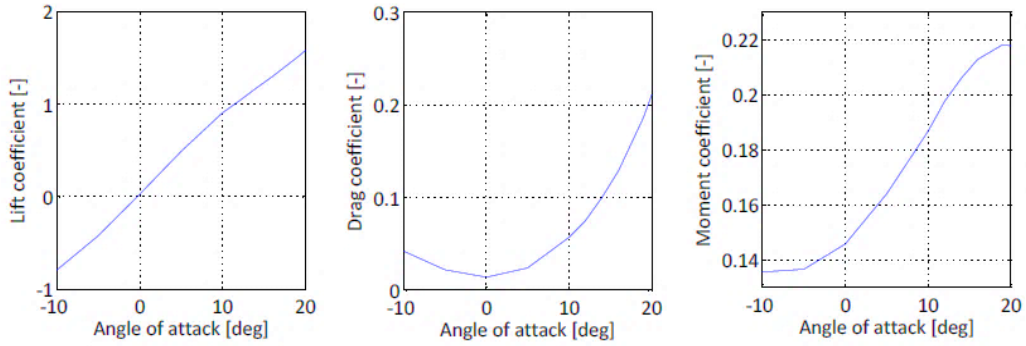

Figure A.1: Aerodynamic coefficients for the considered airfoil.

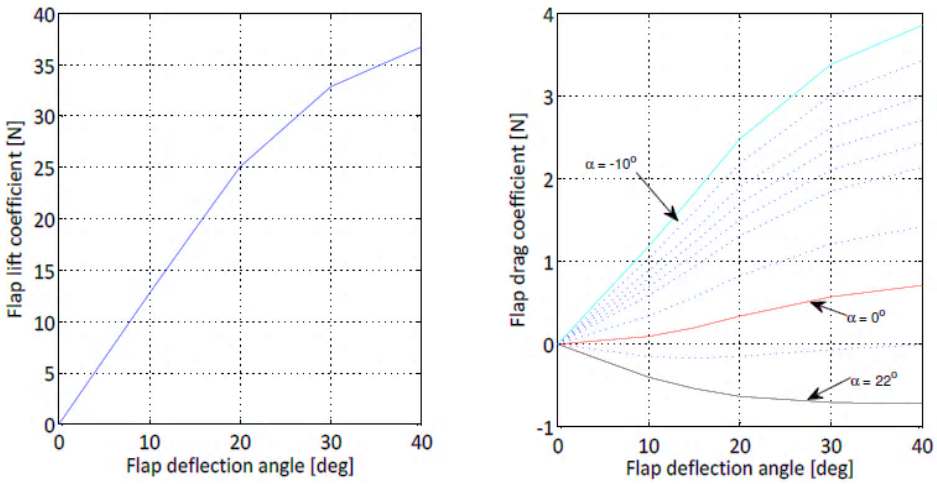

Figure A.2: Aerodynamic forces coefficients of control surface: Flap element.

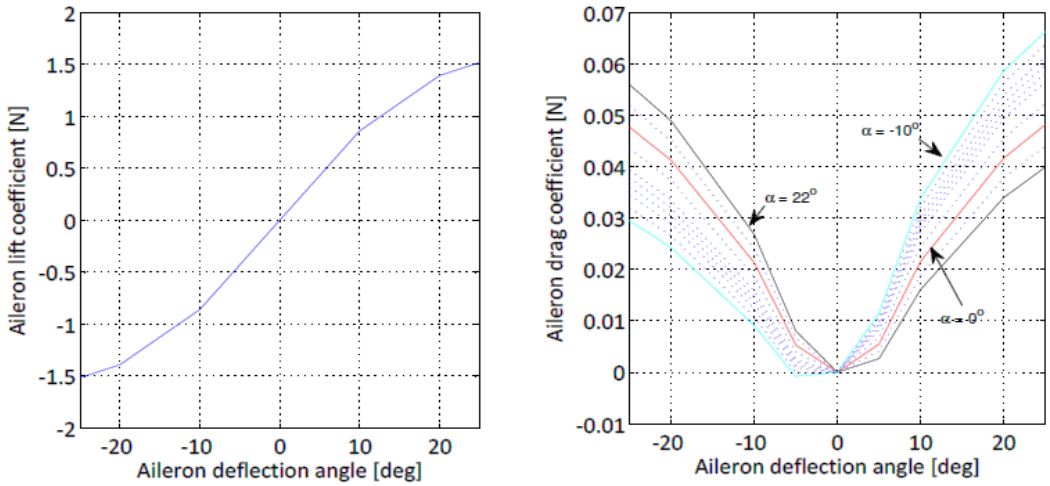

Figure A.3: Aerodynamic forces coefficients of control surface: Aileron element.

Annex B:

Structural Data Tables

The general structural deflections of the wing are depicted in this annex. This information is obtained from modal superposition analysis. Geometrical data of the considered wing also are presented in this annex.

Mode shapes of the studied wing:

The obtained modes of the deformable massless sections of the considered wing are established in the following tables B.1, B.2 at 9 extended wing sections.

Geometrical data of the wing:

This section presents the geometrical details of the wing. Figure B.1 presents the important parameters that define the airfoil NACA0009. It should be note that all these parameters are situated relative to the leading edge at a distance that is a fraction of the local chord. The geometrical and inertial parameters of the wing are shown in Table B.3 and Table B.4, respectively. Table B.5, representents the location of flap and aileron.

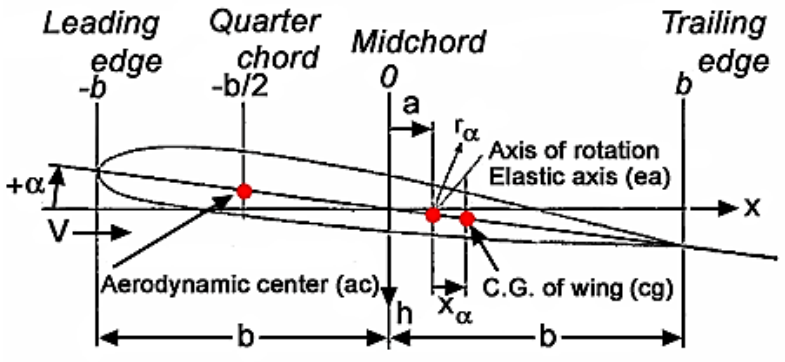

Figure B.1: Airfoil NACA0009 coordinates.

Table B.1: Deformation of massless sections for mode shapes 1,2 and 3.

	First mode – 1.685 Hz			Second mode – 4.305 Hz			Third mode - 5.024 Hz		
η	$h\,[m]$	$g\,[m]$	$\xi\,[rad]$	$h\,[m]$	$g\,[m]$	$\xi\,[rad]$	$h\,[m]$	$g\,[m]$	$\xi\,[rad]$
0.000	0.000	0.000	0.000	0.000	0.000	0.000	0.000	0.000	0.000
0.125	-1.02e-5	-1.59e-8	-2.07e-4	-3.64e-5	-1.27e-5	-5.98e-3	-6.81e-5	4.61e-5	-1.95e-2
0.250	-5.51e-5	-3.95e-8	-6.29e-4	-2.05e-4	-4.06e-5	-2.09e-3	-1.92e-4	2.43e-4	-3.71e-2
0.375	-8.43e-5	-1.24e-7	-9.73e-4	-3.95e-4	-7.95e-5	-3.08e-4	-3.93e-4	2.03e-5	8.99e-3
0.500	-1.64e-4	-2.27e-7	-1.65e-3	-9.04e-4	-2.16e-4	-4.05e-4	-4.94e-3	3.45e-6	8.52e-2
0.625	-1.95e-3	-3.74e-6	-1.95e-3	-1.13e-3	-2.26e-4	-3.48e-3	-8.19e-2	4.26e-5	1.46e-2
0.750	-3.78e-2	-397e-5	-3.12e-3	-1.23e-3	-4.02e-4	-2.46e-4	-9.45e-2	5.24e-5	2.05e-2
0.875	-6.15e-2	-4.46e-5	-3.02e-2	-1.91e-3	-3.76e-3	-4.06e-2	-2.04e-2	7.05e-5	3.12e-2
1.000	-7.02e-2	-5.34e-4	-3.75e-2	-1.75e-2	-5.90e-3	-2.99e-2	-2.23e-2	8.79e-5	2.61e-2

Table B.2: Deformation of massless sections for mode shapes 4, 5 and 6.

	Fourth mode – 7.844 Hz			Five mode – 11.137 Hz			Six mode - 12.453 Hz		
η	$h\,[m]$	$g\,[m]$	$\xi\,[rad]$	$h\,[m]$	$g\,[m]$	$\xi\,[rad]$	$h\,[m]$	$g\,[m]$	$\xi\,[rad]$
0.000	0.000	0.000	0.000	0.000	0.000	0.000	0.000	0.000	0.000
0.125	-3.44e-5	5.21e-5	4.23e-2	0.76e-3	2.10e-4	4.13e-2	6.13e-4	-6.23e-5	3.13e-3
0.250	-9.02e-4	0.98e-4	7.98e-2	3.23e-3	3.23e-4	8.48e-2	2.55e-3	-3.16e-4	4.45e-2
0.375	-2.34e-4	1.95e-4	1.13e-1	4.77e-3	2.23e-3	5.16e-1	3.37e-3	-2.88e-4	5.16e-2
0.500	-1.24e-3	2.87e-4	2.54e-1	6.84e-3	1.55e-3	3.45e-1	2.48e-3	-4.55e-3	6.77e-2
0.625	-1.23e-3	3.45e-4	2.79e-1	8.65e-3	2.75e-3	4.23e-1	2.55e-4	-7.88e-3	2.16e-2
0.750	2.42e-4	3.77e-4	3.56e-1	8.77e-3	3.33e-3	3.86e-1	1.98e-3	-8.23e-3	1.36e-1
0.875	2.21e-3	3.65e-4	3.78e-1	5.23e-3	3.13e-3	2.52e-1	1.16e-3	-9.13e-3	1.75e-1
1.000	3.56e-3	2.66e-4	4.03e-1	2.14e-3	2.79e-3	1.16e-1	1.11e-2	-984e-3	1.97e-1

Table B.3: Dimensional characteristics of the considered wing.

Geometrical param.	Dimension	Geometrical param.	Dimension
Semispan $[m]$	17.9	Adjusting angle $[deg]$	6
Root chord $[m]$	7.0	Twist angle of the wing $[deg]$	2
Taper [-]	0.229	Place of elastic axis $[chords]$	0.33
Leading edge sweep angle $[deg]$	26	Place of aerodynamic center $[chords]$	0.25
Dihedral angle $[deg]$	5.1	Place of center of gravity $[chords]$	0.43

Table B.4: Physical properties that describe the wing resistance to rotational motion.

Section	Mass [kg]	Roll moment [kgm^2]	Pitch moment [kgm^2]	Yaw moment [kgm^2]
1	3624	1280	4978	6013
2	3235	1125	3723	4315
3	2795	0738	2075	2998
4	2310	0570	1195	2115
5	1927	0498	8745	1288
6	1433	0337	4590	798
7	992	0255	2043	451
8	547	158	780	197

Table B.5: Location of control surfaces : Flap and Aileron.

Parameter	Control surfaces: Flap	Control surfaces: Aileron
Control surface place [-]	0.453	0.877
Location of application point [$chords$]	1.00	1.00
Location of elastic axis [$chords$]	0.33	0.33

Bibliography

[1] M. Bianchin, G. Quaranta, and P. Mantegazza, "State space reduced order models forstatic aeroelasticity and flight mechanics of flexible aircraft," in *Proceedings of the XVII Congresso Nazionale AIDAA*, (Rome, Italy), AIDAA, 2003.

[2] D. Inman, *Engineering Vibrations*. Upper Saddle River, USA: Prentice-Hall, 2nd ed., 2001.

[3] L. Cavagna, P. Masarati, and G. Quaranta, "Coupled Multibody/Computational Fluid Dynamics Simulation of Maneuvering Flexible Aircraft," *Journal of Aircraft*, vol. 48, no. 1, pp. 92–106, 2011.

[4] H. Mai, J. Neumann, and H. Hennings, "Gust Response: A Validation Experiment and Preliminary Numerical Simulations," in *Proceedings of the International Forum on Aeroelasticity and Structural Dynamics*, (Paris, France), 2011.

[5] O. Wright, "Flying-machine," 1906.

[6] M. Field, "Flight Dynamics of Flexible Aircraft with Aeroelastic and Inertial Force Interactions," pp. 1–23, 1990.

[7] Jason G., Dallas K., Steve M., "Flexible Bodies with COTS Control Design and Physical Modeling Tools", *AIAA Modeling and Simulation Technologies Conference and Exhibit*, Hilton Head, South Carolina, August 2007.

[8] Subedi, D., Tyapin, I., Hovland, G. Modeling and analysis of flexible bodies using lumped parameter method. *In 2020 IEEE 11th International Conference on Mechanical and Intelligent Manufacturing Technologies* (*ICMIMT*), Cape town, South Africa, pp. 161-166.2020.

[9] Macchelli, A., Melchiorri, C., Stramigioli, S.. Port-based modeling of a flexible link. *IEEE Transactions on Robotics*, 23(4): 650-660, 2007.

[10] Khalil, W., Gautier, M., Modeling of mechanical systems with lumped elasticity. Proceedings 2000 ICRA. Millennium Conference. *IEEE International Conference on Robotics and Automation. Symposia Proceedings* (Cat.No.00CH37065),4:3964-3969, 2000.

[11] Yushu, B., Zhihui, G., Yuchun, D., Impact vibration reduction for flexible manipulators via controllable local degrees of freedom. *Chinese Journal of Aeronautics*, 26(5): 1303-1309, 2013.

[12] Patra, S., Sarkhel, P., Hui, N.B., Banerjee, N., Modelling and simulation of a fishing rod (Flexible Link) using Simmechanics. *Journal Européen des Systèmes Automatisés*, 53(4): 451-460, 2020.

[13] Gaultier, P.E., Cleghorn, W.L., Modeling of flexible manipulator dynamics: A literature survey. *In Proc of 1st Natl App Mech and Robotics Conf*. 1989.

[14] Rückwald, T., Held, A., Seifried, R., Flexible multibody impact simulations based on the isogeometric analysis approach. *Multibody System Dynamics*, 54(1): 75-95, 2022.

[15] Held, A., Moghadasi, A., Seifried, R., DynManto: A Matlab toolbox for the simulation and analysis of multibody systems. *International Design Engineering Technical Conferences and Computers and Information in Engineering Conference*, 83914, V002T02A005, 2020.

[16] Lee, Y., Hamilton, J.F., The lumped parameter method for elastic impact problems. *Journal of Applied Mechanics*, 50(4a): 823-827, 2015.

[17] De Lannoy, S., Wing bending calculation with a single set of equations. *Wing bike-A Human Powered Hydrofoil*, 1-17, 2017.

[18] Wang, Y., Huston, R.L., A lumped parameter method in the nonlinear analysis of flexible multibody systems. *Computers and Structures*, 50(3): 421-432, 1994.

[19] Hatch, M., Vibration simulation using MATLAB and ANSYS, 2000.

[20] Jiang, Y.W., Xu, D.P., Jiang, Z.X., Kim, J.H., Hwang, S.M., Comparison of Multi-physical coupling analysis of a balanced armature receiver between the lumped parameter method and the finite element/boundary element method. *Applied Sciences*, 9(5): 839, 2019.

[21] Svoboda, F., Hromčík, M., Finite element method-based modeling of a flexible wing structure. *In 2017 21st International Conference on Process Control* (*PC*), pp. 222-227, 2017.

[22] Laiche, A., Boulahia, A., Modeling and simulation analysis of aircraft wing loads. *International Journal of Advanced Research in Engineering and Technology*, 13(5): 32-39, 2022.

[23] Lomax, Ted, L. Structural Loads Analysis for Commercial Transport Aircraft: Theory and Practice. Vol. 70, pp. 163, 1998.

[24] Venkatesan, S. P., N. Beemkumar, J. Jayaprabakar, and P. N. Kadiresh., Modelling and Analysis of Aircraft Wing with and without Winglet. International *Journal of Ambient Energy*, 42(4): pp. 363–73, 2021.

[25] João, F., Alves F., Matos. Structural Analysis and Optimization of a UAV Wing, *Wind Energy,* 23(4):1006–25, 2020.

[26] Abbas, Y., Tariq E., Abdul Aziz A., Alnazir K. and Mohammed A. Structural Analysis of a Transport Aircraft Wing, *INCAS Bulletin* 13(1): pp.3–9, 2021.

[27] Yang, J., Liu, Y., and Zhang, W., Static Aeroelastic Modeling and Rapid Analysis of Wings in Transonic Flow. 2018.

[28] Abbas, Y., Elsonni, T., Abdulmajid, A. A., Khalafallh, A., and Alnazir, M., Structural analysis of a transport aircraft wing. *INCAS Bulletin*, 13(1), pp.3–9, 2021.

[29] Atmeh, G. M., Hasan, Z., and Darwish, F., Design and Stress Analysis of a General Aviation Aircraft Wing, 2010.

[30] A. Collar, "The Expanding Domain of Aeroelasticity," *Journal of the Royal Aeronautical Society*, 1946.

[31] E. H. Dowell, R. Clark, and D. Cox, *A Modern Course in Aeroelasticity*. Dordrecht, The Netherlands: Kluwer Academic Publishers, 4th ed., 2004.

[32] P. P. Friedmann, "Renaissance of Aeroelasticity and Its Future," *Journal of Aircraft*, vol. 36, no. 1, pp. 105–121, 1999.

[33] S. Ricci and A. Scotti, "Wind Tunnel Testing of an Active Controlled Wing underGust Excitation," in *Proceedings of the 49th AIAA/ASME/ASCE/AHS/ASC Structures, Structural Dynamics, and Materials Conference*, (Schaumburg, USA), American Institute of Aeronautics and Astronautics, 2008.

[34] E. Livne, "Future of Airplane Aeroelasticity," *Journal of Aircraft*, vol. 40, no. 6, pp. 1066–1092, 2003.

[35] R. Yurkovich, D. Liu, and P. Chen, "The State-of-the-Art of Unsteady Aerodynamics for High Performance Aircraft," in *Proceedings of the 39th AIAA Aerospace Sciences Meeting & Exhibit*, (Reno, USA), 2001.

[36] E. Dowell, J. Edwards, and T. Strganac, "Nonlinear Aeroelasticity," *Journal of Aircraft*,vol. 40, no. 5, pp. 857–874, 2003.

[37] D. E. Raveh, "Computational-fluid-dynamics-based aeroelastic analysis and structural design optimization," *Computer Methods in Applied Mechanics and Engineering*, vol. 194, no. 30, pp. 3453–3471, 2005.

[38] W. R. Krüger and M. Spieck, "Aeroelastic Effects in Multibody Dynamics," *Vehicle System Dynamics*, vol. 41, no. 5, pp. 383–399, 2004.

[39] M. Spieck, W. Krüger, and J. Arnold, "Multibody Simulation of the Free-Flying ElasticAircraft," in *Proceedings of the 1st AIAA Multidisciplinary Design Optimization Specialist Conference*, (Austin, USA), American Institute of Aeronautics and Astronautics,2005.

[40] Z. Zhao and G. Ren, "Multibody dynamic approach of flight dynamics and nonlinear aeroelasticity of flexible aircraft," *AIAA journal*, vol. 49, no. 1, pp. 41–54, 2011.

[41] M. Waszak and D. Schmidt, "Flight Dynamics of Aeroelastic Vehicles," Journal of Aircraft, vol. 25, no. 6, pp. 563–571, 1988.

[42] V. Chudnovsky, A. Mukherjee, J. Wendlandt, and D. Kennedy, "Modeling Flexible Bodies in SimMechanics and Simulink," *MATLAB Digest*, May 2006.

[43] O. Wallrapp, "Flexible Bodies in Multibody System Codes," *Vehicle System Dynamics*,vol. 30, no. 3-4, pp. 237–256, 1998.

[44] G. La Rocca, *Knowledge Based Engineering Techniques to Support Aircraft Design and*

Optimization. Dissertation, Delft University of Technology, 2011.

[45] M. Karpel and Z. Sheena, "Structural Optimization for Aeroelastic Control Effective- ness," *Journal of Aircraft,* vol. 26, no. 5, pp. 493–495, 1989.

[46] M. Karpel, B. Moulin, and M. H. Love, "Modal-Based Structural Optimization with Static Aeroelastic and Stress Constraints," Journal of Aircraft, vol. 34, no. 3, pp. 433– 440, 1997.

[47] J. Banerjee, "Explicit analytical expressions for frequency equation and mode shapes of composite beams," *International Journal of Solids and Structures,* vol. 38, pp. 2415– 2426, Apr. 2001.

[48] D. E. Raveh and M. Karpel, "Structural Optimization of Flight Vehicles with Computational-Fluid-Dynamics-Based Maneuver Loads," *Journal of Aircraft,* vol. 36, no. 6, pp. 1007–1015, 1999.

[49] I. Chowdhury and S. Dasgupta, "Computation of Rayleigh Damping Coefficients for Large Systems," *The Electronic Journal of Geotechnical Engineering,* vol. 8.0, no. C, 2003.

[50] G. P. Guruswamy, D. E. MacMurdy, and R. K. Kapania, "Static Aeroelastic Analysis of Wings using Euler/Navier-Stokes Equations Coupled with Improved Wing-Box Finite Element Structures," in *AIAA/ASME/ASCE/AHS/ASC Structures, Structural Dynamics, and Materials Conference*, (Hilton Head, USA), NASA, 1994.

[51] E. Livne and T. Weisshaar, "Aeroelasticity of Nonconventional Airplane Configurations- Past and Future," *Journal of Aircraft*, vol. 40, no. 6, pp. 1047–1065, 2003.

[52] M. Goland and Y. Luke, "The Flutter of a Uniform Wing with Tip Weights," *Journal of Applied Mechanics,* vol. 15, no. 1, pp. 13–20, 1948.

[53] B. Moulin and M. Karpel, "Gust Loads Alleviation Using Special Control Surfaces*," Journal of Aircraft*, vol. 44, no. 1, pp. 17–25, 2007.

[54] M. Karpel and B. Moulin, "Aeroservoelastic Gust Response Analysis for the Design of Transport Aircrafts," in *45th AIAA/ASME/ASCE/AHS/ASC Structures, Structural Dynamics & Materials Conference*, (Palm Springs, USA), American Institute of Aeronautics and Astronautics, 2004.

[55] A. Datta and W. Johnson, "An Assessment of the State-of-the-art in Multidisciplinary Aeromechanical Analyses," tech. rep., NASA AMES Research Center, 2008.

[56] J. Anderson, *Fundamentals of Aerodynamics*. New York, USA: McGraw-Hill, 2nd ed.,2001.

[57] D. M. Schuster, D. D. Liu, and L. J. Huttsell, "Computational Aeroelasticity: Success, Progress, Challenge," *Journal of Aircraft*, vol. 40, no. 5, pp. 843–856, 2003.

[58] J. Heeg, P. Chwalowski, J. P. Florance, C. D. Wieseman, D. M. Schuster, and B. Perry III, "Overview of the Aeroelastic Prediction Workshop," in *Proceedings of the 51st AIAA Aerospace Sciences Meeting*, (Grapevine, USA), American Institute of Aeronautics and Astronautics, 2013.

[59] B. W. Van Oudheusden, "On the Quasi-Steady Analysis of One-Degree-of-Freedom Galloping with Combined Translational and Rotational Effects," *Nonlinear Dynamics,* vol. 8, no. 4, pp. 435–451, 1995.

[60] H. Haddadpour and R. D. Firouz-Abadi, "Evaluation of quasi-steady aerodynamic modeling for flutter prediction of aircraft wings in incompressible flow," Thin-Walled Structures, vol. 44, no. 9, pp. 931–936, 2006.

[61] D. H. Hodges and A. G. Pierce, *Introduction to Structural Dynamics and Aeroelasticity*. Cambridge, UK: Cambridge University Press, 2nd ed., 2011.

[62] M. Van Dyke, *An Album of Fluid Motion*. Stanford, USA: Parabolic Press Inc., 12th ed., 1982.

[63] R. Bisplinghoff, H. Ashley, and R. Halfman, *Aeroelasticity*. New York, USA: Dover Publications, 1955.

[64] R. Palacios, J. Murua, and R. Cook, "Structural and Aerodynamic Models in NonlinearFlight Dynamics of Very Flexible Aircraft," *AIAA journal*, vol. 48, no. 11, pp. 2648– 2659, 2010.

[65] C. Farhat and M. Lesoinne, "Higher-Order Staggered and Subiteration Free Algorithms for Coupled Dynamic Aeroelasticity Problems," in *Proceedings of the 36th Aerospace Sciences Meeting and Exhibit*, (Reno, USA), American Institute of Aeronautics and Astronautics, 1998.

[66] C. Michler, S. Hulshoff, E. van Brummelen, and R. de Borst, "A monolithic approach to fluid-structure interaction," *Computers & Fluids*, vol. 33, no. 5-6, pp. 839–848, 2004.

[67] J. G. Leishman and K. Q. Nguyen, "State-Space Representation of Unsteady Airfoil Behavior," *AIAA journal*, vol. 28, no. 5, pp. 836–844, 1990.

[68] P. Marzocca, L. Librescu, and D. H. Kim, "Development of an indicial function approach for the two-dimensional incompressible/compressible aerodynamic load modelling," *Journal of Aerospace Engineering*, vol. 221, no. 3, pp. 453–463, 2007.

[69] J. S. Bae, S. M. Yang, and I. Lee, "Linear and Nonlinear Aeroelastic Analysis of Fighter- Type Wing with Control Surface," Journal of Aircraft, vol. 39, no. 4, pp. 697–708, 2002.

[70] R. Milne, Dynamics of the Deformable Aeroplan. London, UK: HM Stationery Office, 1964.

[71] T. Theodorsen, "General Theory of Aerodynamic Instability and the Mechanism of Flutter," tech. rep., National Advisory Committee for Aeronautics, 1935.

[72] Laiche, A., Boulahia, A. Mathematical modelling and simulation analysis of an aircraft wing using SimMechanics. *Mathematical Modelling of Engineering Problems*, Vol. 9, No. 3, pp. 796-802. 2022.

[73] Miller, S., Soares, T., Weddingen, Y., Wendlandt, J. Modeling flexible bodies with Simscape multibody software. *TECHNICAL PAPER*, The MathWorks, Inc., 2017.

[74] David Balbuena. Simscape Multibody Reduced Order Flexible Cylinder. (2022). (https://github.com/mathworks/Simscape-Multibody-Reduced-Order-Flexible-Cylinder/releases/tag/1.0.0), GitHub. Retrieved November 11, 2022.

[75] Dan, D. Analytical Modeling of Aircraft Wing Loads Using MATLAB and Symbolic Math Toolbox.

https://www.mathworks.com/company/newsletters/articles/analytical-modeling-of-aircraft-wing-loads-using-matlab-and-symbolic-math-toolbox.html

[76] S. Kuzmina, F. Ishmuratov, M. Zichenkov, and V. Chedrik, "Analytical-Experimental Study on Using Different Control Surfaces to Alleviate Dynamic Loads," in *47th*

AIAA/ASME/ASCE/AHS/ASC Structures, Structural Dynamics, and Materials Conference, no. May, (Reston, Virigina), American Institute of Aeronautics and Astronautics, 2006.

[77] European Aviation Safety Agency, "CS23: Certification Specifications for Normal, Utility, Aerobatic, and Commuter Category Aeroplanes," Tech. Rep. July, 2012.

[78] European Aviation Safety Agency, "CS25: Certification Specifications and Acceptable Means of Compliance for Large Aeroplanes," 201.

Abstract

In space vehicle structure design, the purpose on reducing weight is to minimize the gap of frequency concept between flight mechanics motion and structural vibration. Therefore, aircrafts are becoming more and more flexible. This require calling for a flight mechanics model that includes aeroelasticity. The development try of such a model is the subject of this research. The aim of this last is eventually to be used for disturbances and manoeuvre load prediction in the beginning design phase. This in order to avoid unstable flight conditions, moreover, the flight mechanics model may be also used to design active load alleviation systems to decrease loads on the wing structure.

Various approaches and contributions were involved in the model of aeroelastic flight mechanics of which one can cite Modal approach in a linear time-invariant state-space system for Aeroelasticity, Summation of Forces (with multibody system dynamics) for Load Prediction in aerodynamics and Conventional Serial Staggered Partitioned approach for Fluid-Structure interaction. The totality of the multibody system dynamics model is designed on the basis of user input, so, it can be included in a design optimization framework. This gives us the ability to do various supplemental analyses.

Finally, several conclusions are reached. The response of static and dynamic behavior is checked, so it's likely that it can be applied to other classical, low aspect-ratio aircraft operating in the subsonic flying range.

Key words: Aeroelasticity, Dynamic modeling, Mode-superposition, Vibration, Quasi-steady models, Lumped-parameter method, Finite element method, Multibody system dynamics, Simscape Multibody.